GOLD NANOPARTICLE BASED COMPOSITES AS SENSORS AND ACTUATORS

A THESIS SUBMITTED IN PARTIAL FULFILMENT OF THE REQUIREMENTS FOR THE AWARD OF THE DEGREE OF

DOCTOR OF PHILOSOPHY

By

BISWA RANJAN PANDA

DEPARTMENT OF CHEMISTRY
INDIAN INSTITUTE OF TECHNOLOGY GUWAHATI
GUWAHATI - 781039, INDIA

APRIL 2008

Dedicated to

My JNV Mates

DEPARTMENT OF CHEMISTRY

INDIAN INSTITUTE OF TECHNOLOGY GUWAHATI, INDIA

STATEMENT

I hereby declare that the matter embodied in this thesis is the result of investigations carried out by me in the Deparment of Chemistry, Indian Institute of Technology Guwahati, India under the supervision of Dr. Arun Chattopadhyay, Professor of Chemistry.

In keeping with the general practice of reporting observations, due acknowledgements have been made wherever the work described is based on the findings of other investigatios.

I. I. T. Guwahati

April, 2008

Biswa Ranjan Panda

Indian Institute of Technology Guw
Guwahati 781 039, I
Tel: (+91) 361-258 2304
Fax: (+91) 361-2690762
Email: arun@iitg.ernet.in
Date: April 11. 2008

Arun Chattopadhyay
Professor of Chemistry and
Head, Centre for Nanotechnology

CERTIFICATE

This is to certify that the thesis entitled "GOLD NANOPARTICLE BASED COMPOSITES AS SENSORS AND ACTUATORS" submitted by Mr. Biswa Ranjan Panda for the award of the degree of Doctorate of Philosophy of I. I. T. Guwahati, is based upon his work under my supervision. I certify that he has fulfilled all the requirements according to the rules of the institute, and neither this thesis nor any part of it has been submitted for any degree or any academic award anywhere before.

I. I. T. Guwahati

April, 2008

Arun Chattopadhyay

Supervisor

DEPARTMENT OF CHEMISTRY

INDIAN INSTITUTE OF TECHNOLOGY GUWAHATI, INDIA

COURSE CERTIFICATE

This to certify that Mr. Biswa Ranjan Panda has satisfactorily completed all the courses required for the Ph. D. degree programme. These courses include

CH 603	Supramolecules : Concept and Application
CH 630	A Fundamental Approach to Physical Chemistry
CH 611	Bioinorganic Chemistry
CH 632	Chemical Application of Group Theory

Mr. Biswa Ranjan Panda has successfully completed his Ph. D. qualifying examination in April 2004.

15/4/08

Prof. Abu Taleb Khan

Head, Department of Chemistry

I. I. T. Guwahati

Dr. Anil Kumar Saikia

Secretary

Departmental Post Graduate Committee

Department of Chemistry

I. I. T. Guwahati

ACKNOWLEDGEMENT

First of all my overwhelming thanks goes to my research supervisor, Prof. Arun Chattopadhyay, for his extreme patience and intellectual input throughout my work. I owe him lots of gratitude for lifting up my confidence level with his ever optimistic attitude.

My sincere thanks are due to all my doctoral committee members for their constructive criticism and valuable suggestions. I am grateful to Dr. Anumita Paul, Dr. A. Ramesh for their insightful advices.

I am obliged to all the faculty members of the Department of Chemistry, IIT Guwahati for their encouragement and the non-teaching staffs of the Department for their technical support.

I cherish my association with Debasish Da, Tridib Da, Gitanjali Didi, Sonit, Sahid, Biplab, Murgan, Kris, Chaitanya, Jashmini, Partho, Sadhu, Subhojit, Gopi, Pallab and Sivshankar. The moments I enjoyed with them will act as lubricant to glide over the crisis in the rest part of my life. I would like to accord my thanks to Utkalika family for their affection and mental support during my stay at IIT Guwahati. Among my friends I am greatly indebted to Nagu and Atul, for their contribution to shape my thesis.

Let me also say 'thank you' to the following people at IIT Guwahati, Dr. Manoranjan Kar of Centre for Nanotechnology, Mr. Chandan, and Mr. Senapati of Central Instrument Facility for providing their expertise in solving my research problems.

During the course of this work, at IIT Guwahati (August 2003 – April 2008), I was financially supported by the institute and CSIR, India. I wish to thank them in this occasion. I also acknowledge IIT Guwahati for providing the necessary facilities to complete my Ph. D. degree successfully.

I am forever indebted to my parents, whose love and blessing helped me to sail through. Finally, I would like to thank my schoolmates for being a constant source of inspiration.

Department of Chemistry
IIT Guwahati, Guwahati 781039
April 11, 2008 (Biswa Ranjan Panda)

TABLE OF CONTENTS

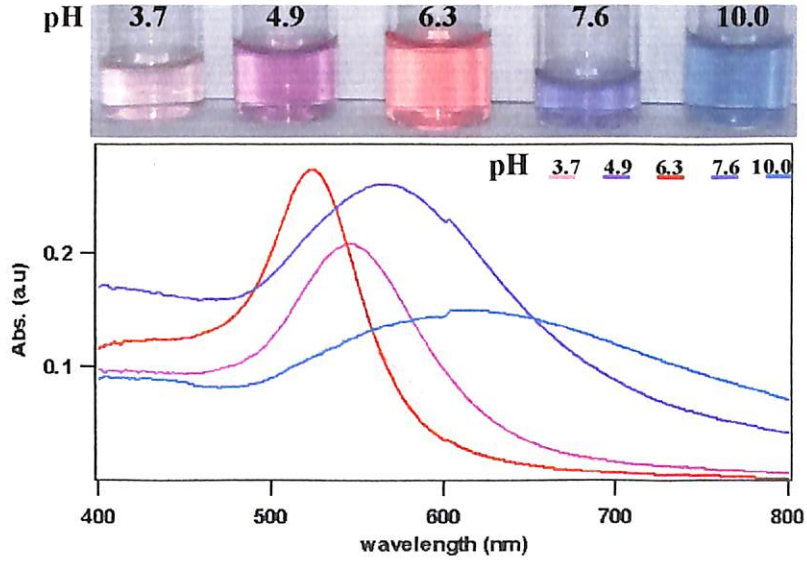

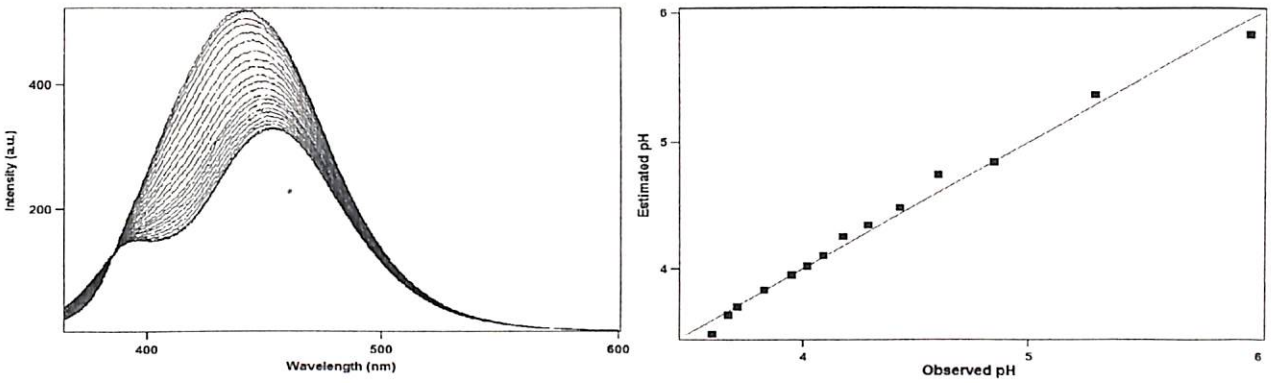

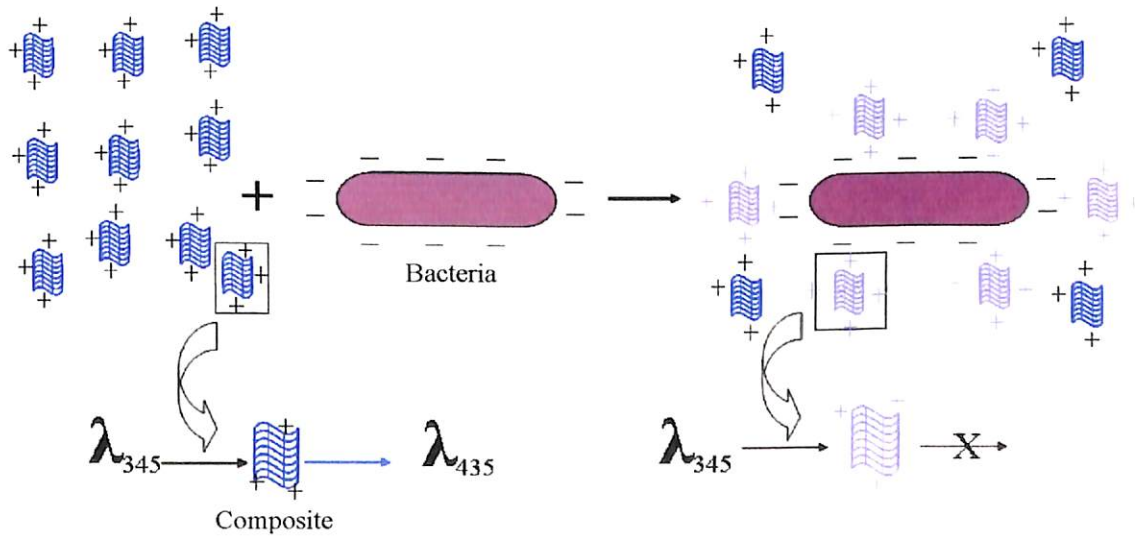

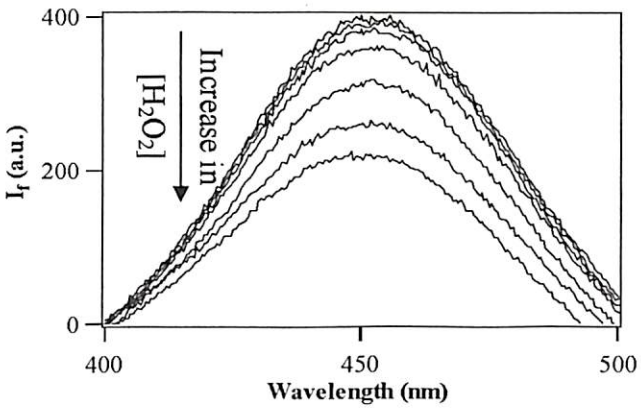

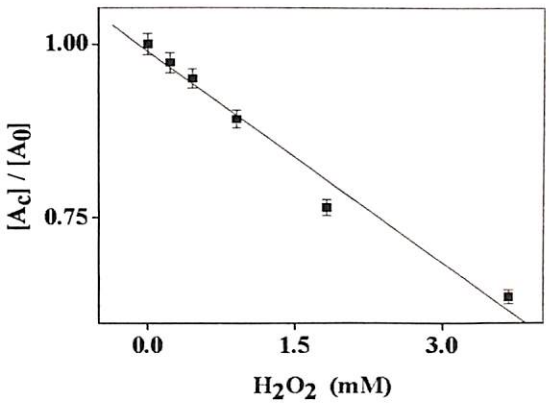

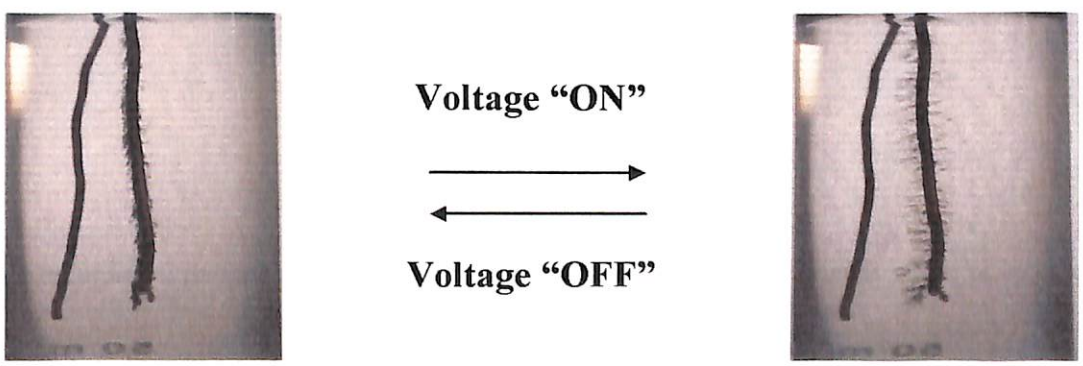

Outline of my Ph. D. thesis work.

The thesis would consist of six chapters which are described briefly in the following sections.

Chapter I.	Introduction
Chapter II.	Synthesis of Au nanoparticles at "all" pH by H_2O_2 reduction of $HAuCl_4$
Chapter III.	A Water Soluble Polythiophene-Au nanoparticle Composite for pH Sensing
Chapter IV.	Rapid and Sensitive Detection of Bacteria by a Fluorescent Au Nanoparticle – Polythiophene Composite
Chapter V.	Estimation of H_2O_2 using Fluorescence Emission of a Surfactant Stabilized Au Nanoparticle - Polythiophene composite
Chapter VI.	Electrochemical Actuation of Growing Copper Dendrimers in Water

Chapter I

This chapter will present a background of the field as well as the theme of the research works carried out in the thesis vis-à-vis the latest developments in the area.

Chapter –II

Synthesis of Au Nanoparticles at "all" pH by H_2O_2 reduction of $HAuCl_4$

In this chapter, a new method for generation of Au NPs in the pH range of 2.9 through 11.2, by the reduction of $HAuCl_4$ using H_2O_2 as the reducing agent, would be reported. The study is based on an earlier observation from the laboratory that under acidic pH H_2O_2 could reduce $HAuCl_4$. This was further extended to obtain a general method of synthesis in a wider pH range. Although, at first thought the observations is against conventional wisdom of H_2O_2 being a poor reducing agent, they can be explained using standard electrochemical potentials involved with the reaction.

Chapter - III

A Water Soluble Polythiophene-Au Nanoparticle Composite for pH Sensing

In this chapter, development of a new pH sensor based on the fluorescence properties of polythiophene - Au NP composite prepared in water is to be reported. The composite was prepared by simultaneous reduction of $HAuCl_4$ to Au NPs and polymerization of thiophene in the medium in the presence of each other only. Electron spray ionization (ESI) – mass spectrum indicated that the composite mainly

consisted of an polymer having a molecular mass of 783 amu. This means that the polymer consisted of six units of chlorothiophene and one thiophene monomer.

The polymer-nanoparticle composite, synthesized at pH 3.1 ± 0.05, when excited by light at 345 nm, exhibited a single intense emission peak with maximum at 435 nm. However, the maximum shifted gradualy to higher wavelengths with increase in pH of the solution, along with the appearance of small peak at lower wavelength. For example when the pH of the solution was increased to 6.0, the emission spectrum consisted of two peaks occurring at 390 nm and 465 nm. The results were explained by invoking the existence of two inter-convertible forms of polythiophene derivatives differing by the extent of protonation. At the lower pH values majority of the composite remained in protonated form (AH^+), having a characteristic single emission peak, while with increase in pH they were converted to a deprotonated form (A) giving rise to two emission peaks. At intermediate pH values, mixtures of the two species with concentrations corresponding to equilibria between the two forms existed. Also, the fluorescence measurements indicate that the two species were interconvertible and their concentrations could be changed by changing the pH of the medium.

Thus we have a new composite, where fluorescence of the polymer in the composite was used as a solution pH sensor.

Chapter – IV

Rapid and Sensitive Estimation of Bacteria by the Fluorescent Au Nanoparticle – Polythiophene Composite

The polythiophene-Au NP composite reported in the previous chapter was found to have its fluorescence sensitive to the presence of bacteria in aqueous solution and the change in fluorescence was maximum when the pH of the solution was kept at 3.0. For example, when the emission intensity of a 1:1 mixture of the aqueous solutions of the as-synthesized Au NP-polythiophene composite and various diluted bacterial cell suspensions were recorded, systematic decrease in the intensity was observed, with the increase in bacterial population. The decrease in fluorescence intensity of the composite with increasing bacterial concentration provided an excellent opportunity for quantitative estimation of the bacterial population. We have accounted for the decrease in emission intensity in terms of the effective concentration of the species AH^+ in the sample upon addition of bacterial cells. The relationship between the decrease in fluorescence intensity of the NP-polythiophene composite and bacterial cell concentration could be established from the well-known relationship between the intensity of fluorescence and the concentration of the fluorophore and which is can be written as follows.

$$Log\left(I_f^C - I_f^{Co}\right) = LogD + 2.3\varepsilon lx$$

where I_f^c is the intensity of steady-state fluorescence when the concentration of the fluorophore is c; x is a function of bacterial cell number and has the dimension of concentration. $D = Be^{-2.3\varepsilon lCo}$ and $B = \kappa F_\lambda I_0$

k is a proportionality constant; F_λ is the steady-state fluorescence intensity - at the emission maximum - per absorbed photon at the excitation wavelength; I_0 is the intensity of incident light, and ε is molar extinction coefficient at the excitation wavelength.

Interestingly, when the logarithm of difference in fluorescence intensities between that of the pure composite and that in the presence of different amount of bacteria was plotted against the logarithm of the number of bacterial cells a linear relationship was obtained. This was true for all four types of bacteria - *Pediococcus acidilactici* CFR K7, *Lactobacillus plantarum* MTCC 1325, *Escherichia coli* MTCC 433 and *Enterococcus faecalis* MTCC 439 - that were tested. The linear relationship being valid for all the four types of bacteria demonstrates the efficacy of the method in quantitative estimation of bacteria and the generality of the approach. Also important to mention here is that the lowest number of bacterial cells that can be estimated using the present scheme is 1000, indicating the sensitivity of the method. Remarkably, the present method allows estimation of logarithmic dilutions of bacterial cell numbers, which in the present case is on the order of 10^3-10^6 cells.

Chapter – V

Estimation of H_2O_2 using Fluorescence Emission of a Surfactant Stabilized Au Nanoparticle - Polythiophene Composite

Here we report the use of a new Au Nanoparticle- polythiophene composite in the rapid and quantitative detection of aqueous H_2O_2. The method is based on changes in the visible absorption of the Au NPs as well as fluorescence of the polythiophene in the composite, in the presence of various amount of H_2O_2. The composite was synthesized by reaction of thiophene with $HAuCl_4$ in the presence of a surfactant, sodium dodecyl sulfate (SDS).

We observed that the emission intensity of the composite decreased systematically with increase in the concentrations of H_2O_2 in the sample. In our case we studied the effect of H_2O_2, varying its concentration range from 10 mM to 0.2 mM. A plot of the area under the fluorescence curves versus the concentration of H_2O_2 indicated a linear dependence of emission on the concentration of the peroxide. It was observed that the linearity was followed when the concentrations of the H_2O_2 in the medium was below 4 mM. At concentrations above 4 mM the dependence varied randomly and is thus not reported. It's noteworthy to mention that the lowest concentration of H_2O_2 that could be measured using the change in fluorescence was 0.23 mM. This value is similar to literature values of the limits of detection of H_2O_2 using the conventional methods. The decrease in fluorescence intensity of the composite with increasing H_2O_2 concentration provides an excellent opportunity for quantitative and rather accurate estimation of the H_2O_2 concentration.

Chapter – VI

Electrochemical Actuation of Growing Copper Dendrimers in Water

This chapter reports the observation of electrochemical actuation in growing dendritic fibers made of self-assembled Cu nanostructures (of 100 nm or less in diameter) or its composite with Au NPs, on the metallic cathode of an ordinary aqueous electrochemical cell. This could be achieved when a Cu anode and another metal cathode was placed in aqueous solution of either dilute HCl or $CuSO_4$, or $CuCl_2$, or H_2O, and upon application of a D.C. voltage at 1.5-12.0 V. The actuation could be observed with an on-off cycle of the applied voltage in the above range. The phenomenon was also observed with the growth of bimetallic structures using a number of electrolytes such as $Ag(NO_3)$, $Pb(NO_3)_2$, $CoCl_2$, $NiCl_2$, $CdCl_2$, $ZnCl_2$, and $HAuCl_4$. The fibrous structures remained stretched as they grew longer with time in the presence of an applied voltage. The extent of actuation was dependent on the applied voltage, the concentration of Cu^{2+} ions in the solution, and also on ions such as Na^+, which did not get deposited at the cathode. The observed phenomena under different conditions were explained using the principles of electrocapillarity.

List of Publications

1. B. R. Panda, A. Chattopadhyay **A water-soluble polythiophene-Au nanoparticle composite for pH sensing.** *J. Colloid. Interf. Sc.* **2007**, 316, 962.

2. B. R. Panda, A. Chattopadhyay **Synthesis of Au nanoparticles at "all" pH by H_2O_2 reduction of $HAuCl_4$.** *J. Nanosci.Nanotechnol.* **2007**, 7, 1911.

3. B. R. Panda, P. N. Rao, A. Paul, A. Chattopadhyay **Electrochemical Actuation of Growing Copper Dendrimers in Water.** *J. Phys. Chem. B* **2006**, 110, 22917.

Not includes in Thesis

4. A. Nag, B. R. Panda, A. Chattopadhyay. **Performing chemical reactions in virtual capillary of surface tension-confined microfluidic devices.** *Pramana* **2005**, 65, 621.

Chapter – I

INTRODUCTION

Sensors are transducers of energy into a signal, which can be recorded for the purpose of information transfer. For example, thermometer is a well-known sensor used in our daily life, that converts the expansion and contraction of a certain volume of mercury in response to variation in temperature (the signal), to a reading on a calibrated glass tube giving information about temperature of the concerned system. The form of energy may be thermal, electrical, mechanical, chemical, optical or magnetic. Briefly speaking the sensor's physical or optical property varies in a regular fashion with respect to the changes in the input energy profile. Since all the observations are required to be compared with the existing data or need to be referred to in future its measurement in absolute or relative scale is needed. Sensors are necessary in diverse applications such as in physical and chemical analysis, molecular biotechnology, medicine, marine and environmental analysis, industrial production monitoring and bioprocess control, and the automotive industry.

While designing a sensor its sensitivity, specificity, reproducibility and versatility are the few important points those require special attention. Moreover, when the market factor comes into play accessibility is another factor that cannot be overlooked. However, it's almost impossible to design sensor that would satisfy all the above criteria. This could provide a new opportunity in designing sensors that re specific to specific applications.

In the current scenario nanoscale materials generate newer opportunities in designing sensors with significantly improved sensitivities. For example using a

nanoparticle-based assay P. Fortina et al.[1] have been able to detect attomolar concentration of proteins, a magnitude of six orders lower than concentrations detected by ELISA. D. D. Von Hoff and coworkers[2] have formulated an albumin-bound paclitaxel, an anti-cancer drug, ABI-007 of 130-nm size, to avoid solvent-related toxicities and to deliver paclitaxel to tumors via molecular pathways involving an endothelial cell-surface albumin receptor and an albumin-binding protein expressed by tumor cells and secreted into the tumor interstitium. Lewis Rothberg's lab designed a rapid sequence identification assay method for single- and double-stranded RNA on ionically coated gold nanoparticles suspended in a colloid.[3] The assay is based on either color changes or fluorescence that are sensitive to a few picomoles of target in less than 10 min, so that RNA degrdation problems could be avoided. Single-base mutations on RNA sequences can also be detected even in complex oligo-nucleotide mixtures using this method.

On the other hand, the excellent transducing ability of conjugated polymers to generate a physically measurable signal from recognized events and low cost could offer simultaneous advantages of rapidity, simplicity, specificity, detection sensitivity and affordable techniques. Polyaniline, a conducting polymers that has been widely studied for electronic and optical applications. It has a simple and reversible acid/base doping/dedoping chemistry enabling control over properties such as free-volume, solubility, electrical conductivity and optical activity[4]. A counter part of aniline in this respect is thiophene. Water soluble polythiophene(PT) derivatives have been successfully prepared, which forms complexes with DNA,[5] polypeptides,[6]

polysaccharides[7] and ATP (adenosine triphosphate).[8] Complex formation induces conformational changes in the PT backbone and subsequent change in absorption, emission, and circular dichroism (CD) spectra. These changes could be used for sensing applications. Mario Leclerc's group applied a simple electrostatic approach involving a cationic water soluble polythiophene (fluorophore), an anionic oligonucleotide (probe), and the anionic phosphate backbone of double stranded nucleic acids to detect directly and specifically identify a few hundred molecules of DNA or RNA (target) in less than 1 h, without any chemical modification of the probe or target.[5] Shinkai Seiji of Kyushu University, Japan, chose poly(3-alkoxy-4-methylthiophene) as a model conjugate polymer, which forms a supramolecular complex with the anion ATP.[8] The complexation induces a change in the π-π^* band due to conformational alternation in the PT backbone. Upon addition of increasing amount of ATP to the aqueous solution of the PT derivative, the λ_{max} shifts from 400 nm, which is characteristic absorption peak position of random coil conformation, to 538 nm which is due to π stacked aggregates of the PT structure.

Hence if schemes could be developed to systematically incorporate NPs into the conjugated polymers, with enhanced ability for transduction, mechanical flexibility, chemical stability and tunable electrical and optical properties needed for advanced and miniaturized electronic devices[9-10] of chemical, biological, and physical changes into an easily measurable electrical or optical signal, then the application potential would be versatile.

Keeping the above and future applications in view, We have developed several solution-based synthetic schemes to generate Au NPs and their composites with other metal or conducting polymer for use as chemical and biological sensors and electrochemical actuators.

In chapter II of the thesis we report the synthesis of Au NPs in the pH range of 2.9 through 11.2. The reductions of $AuCl_4^-$ by H_2O_2 at the above pH range have been explained by the standard reduction potential of H_2O_2 at various pH. However, the mechanisms of reduction depends on the pH of the solution, which are different for acidic, neutral and alkaline pH.

Chapter III comprised of the development of a method for the synthesis of Au NP-polythiophene composite, the fluorescence emission of which has been used in developing a pH sensor. Solution pH has a significant effect on chemical reactions. Hence, the measurement and control of pH is important in chemistry, biochemistry, clinical chemistry, and environmental science. Glass membrane electrodes which are based on the potentiometric techniques are the most widely employed ones for pH measurement.[11] However in recent years, a number of optical pH sensors have been developed to complement the existing glass electrodes in terms of size, costs, and response time. The optical sensors are free from electromagnetic interference and safe for in vivo pH measurements. It is noteworthy to mention that optical fibers made it easier to transport the optical beam over a long distance and remote pH sensing is now feasible. Optical pH sensors are based on pH-induced, reversible changes in

optical properties such as absorbance, reflectance, fluorescence, and refractive index.[12] Typically, sensing in an optical sensor is performed by a pH-sensitive organic dye either immobilized in a polymer matrix or by covalent linking of an organic dye to the distal end of the optical fiber. Although there is no doubt over the usefulness of these dye based techniques for biomedical, process control and environmental analysis, their sluggy response time as a result of barriers to mass transport at the polymer support, limited dynamic range and low sensitivity due to week signal and long term instability as a result of the immobilized reagent's degradation or its desorptive loss from the support[13] make them less attractive for future applications. Moreover, covalent attachment strategy involves a long, complex and tedious procedure and may lead to loss of dye sensitivity or result in poor absorption and fluorescence properties.[14] There are also some reports to broaden the dynamic range of pH measurement by using multiple pH indicators or one indicator with multiple steps of acid association (dissociation) and achieving a linear response over a broad pH range,[15] which simplifies the calibration of the sensor and is also important for constant sensitivity and precise measurement over the entire linear range. The achievements in obtaining such range are still far from perfect and still there are plenty of opportunities for development of newer pH sensors.

Recently, conducting polymers have also been used to prepare optical pH sensors. By oxidative polymerization of an appropriate monomer such as aniline and pyrrole followed by generation of conducting polymer films have suitable optical (and electrical) properties for optical pH sensing. Since the polymer film itself could act as

chromophor/fluorophor, there is no need for incorporation of another organic dye for sensing and thus the immobilization process is not required. Optical pH sensors based on polypyrrole and polyaniline have been reported by S. Demarcos et al.[16] and Z. Jin et al.[17] respectively.

Even though there are reports on immobilized fluoresceinamine for pH sensing fluorimetrically,[18] to our knowledge, a pH sensor based on water soluble poly/oligothiophene fluorophor has not previously been reported in the literature.

We have further used the composite with its fluorescence in quantitative estimation of bacteria in aqueous solution. Since bacteria are vital in recycling nutrients because of their remarkable ability to degrade a variety of organic compounds and their contribution in nitrogen fixation. Moreover the use of Lactobacillus bacteria in combination with yeasts and molds for more than thousands of years in the preparation of fermented foods such as cheese, pickles, soy sauce, sauerkraut, vinegar, wine and yoghurt and their utilization in the production of enantiomerically pure chemicals for pharmaceuticals and agrichemicals purpose requires specific detection and quantitative estimation of their population. Quantification of bacteria population not only is important for fermentation and pharmaceutical industries but also to save lives. Common infectious diseases like tetanus, typhoid fever, diphtheria, syphilis, cholera, leprosy and tuberculosis are of bacterial origin. The cause of Johne's disease, mastitis, salmonella and anthrax to farm animals are also bacterial. Hence their rapid and quantitative detection especially at low concentration is of paramount importance. The charge on bacterial cell surfaces

are known to be negative because of either teichoic acid in gram positive bacteria or the lipopolysaccharide present in the outer membrane of gram negative bacteria. This provided an opportunity to estimate bacterial concentration by interaction with positively charged polythiophene-Au NP composite. Interestingly we found that its fluorescence emission is sensitive to the presence of bacteria in aqueous solution, and the change in fluorescence was maximum when the pH of the solution was kept at 3.0. For example, when the emission intensity of a 1:1 mixture of the aqueous solutions of the as-synthesized Au NP-polythiophene composite and various diluted bacterial cell suspensions were recorded, systematic decrease in the intensity was observed, with the increase in bacterial population. The decrease in fluorescence intensity of the composite with increasing bacterial concentration provided an excellent opportunity for quantitative estimation of the bacterial population. We have accounted for the decrease in emission intensity in terms of the effective concentration of the species AH^+ in the sample upon addition of bacterial cells. The relationship between the decrease in fluorescence intensity of the NP-polythiophene composite and bacterial cell concentration could be established from the well-known relationship between the intensity of fluorescence and the concentration of the fluorophore and which is can be written as follows.[19]

$$Log\left(I_f^C - I_f^{Co}\right) = LogD + 2.3\varepsilon lx$$

where I_f^c is the intensity of steady-state fluorescence when the concentration of the fluorophore is c; x is a function of bacterial cell number and has the dimension of concentration. $D = Be^{-2.3\varepsilon lCo}$ and $B = \kappa F_\lambda I_0$

k is a proportionality constant; F_λ is the steady-state fluorescence intensity - at the emission maximum - per absorbed photon at the excitation wavelength; I_0 is the intensity of incident light, and ε is molar extinction coefficient at the excitation wavelength.

The present method allows estimation of logarithmic dilutions of bacterial cell numbers, which in the present case is on the order of 10^3-10^6 cells. The details of the estimation technique are reported in chapter IV of the thesis.

Further, when the redox reaction between thiophene and $AuCl_4^-$ was carried out in the presence of a stabilizer namely sodium dodecyl sulphate (SDS), with the intension to increase the concentration of the previously synthesized fluorescent composite, it was observed that in the solution retains the characteristic surface plasmon peak of Au NPs could be observed. Also, there was no precipitation meaning that the composite produced in the medium was stable. A small shift in its emission profile was observed. The emission spectrum of the surfactant stabilized composite was not so sensitive in acidic pH range. However when its pH was increased from ~ 3.1 (pH of the as prepared solution) to 12 or beyond, then there was a signficant improvement in its emission intensity which was also sensitive to the pH of the medium. This change in intensity is reversible and could be reverted by bringing the pH back to 3. Interestingly, when the alkalized composite was treated

with traces of H_2O_2 the emission intensity reduced significantly and irreversibly. The reduction in intensity was proportional to the concentration of H_2O_2 present in the medium and could be used for quantitative estimation of H_2O_2 concentration. The details of the procedure are described in chapter V. Since estimation of H_2O_2 is involved in the glucose estimation - where the product of oxidation of glucose is H_2O_2 – this means the present composite could also be used in future for the development of suitable glucose sensor based on its fluorescence.

Finally, we report the development of a solution based electrochemical actuator in chapter VI. In the hunt for miniaturization of electronic or optical devices the electrochemical and electromechanical properties of ionomeric polymer-metal composites,[20] ferroelectric polymers, such as PVDF,[21] ionic gels[22-23] and conductive polymers[24-26] have been explored to replicate muscle. These artificial muscles made up of either of the above materials having the unique ability to convert an electrical or chemical stimulus to mechanical displacement are termed as actuators. The idea of employing conducting polymers for actuation was proposed by Baughman et al[27] in 1990. Followed to this Pei et al[28] and Otero et al[29] demonstrated actuation of polypyrrole films upon electrochemical doping. Beside these materials Single-walled carbon nanotube (SWNT), is another potent material for MEMS/NEMS technology, which actuates[30-32] as a result of conversion of an electrical stimulus to mechanical displacement due to a novel quantum mechanical mechanism is a true replacement for Ferroelectric and Piezoelectric crystals, which are still running the market.

The actuator reported in this chapter is of the form of dendritic fibers, consisting of either of pure copper or its composite with Co, Cd, Pb, Ag, Zn, Ni, and Au. The fibers could be grown in two dimensions on a glass slide, or in the three-dimensional in a cell, consisting of self-assembled Cu or its composite structures of 100 nm or less in diameters. These fibers have diameters on the order of a micron or so and have lengths ranging from a few mm to a cm and they can be reversibly actuated by changing the applied potential. The actuation could be influenced by the concentration of ions in the solution which are deposited at the cathode or non-reactive ions like Na^+ which did not get deposited. The fibrous structures remained stretched as they grew longer with time. The observed angle of actuation with voltage is consistent with the Lippmann equation, based on electrocapillarity.[33] These are model solution based actuators which could be the foundations for the development of advanced and versatile composite actuators in solution with enormous technological applications at the microscale.

Reference and Notes

1. P. Fortina, L. J. Kricka, S. Surrey, P. Grodzinski *Trends Biotechnol.* **2005**, 23 , 168.
2. D. W. Nyman, K. J. Campbell, E. Hersh, K. Long, K. Richardson, V. Trieu, N. Desai, M. J. Hawkins, D. D. Von *J. Clin. Oncol.* **2005**, 23, 7785.
3. H. Li, L. Rothberg *Anal. Chem.* **2005**, 77, 6229.
4. J. Huang, S.Virji, B. H. Weiller, R. B. Kaner *J. Am. Chem. Soc.* **2003**, 125, 314
5. K. Dore, S. Dubus. H. Ho, I. Levesque, M. Brunette, G. Corbeil, M. Boissinot, G. Boivin, M. G. Bergeron, D. Boudreau, M. Leclerc. *J. Am.Chem. Soc.* **2004**, 126, 4240.
6. K. P. R. Nilsson, A. Herland, P. Hammarstrom, O. Inganas *Biochemistry* **2005**, 44, 3718.

7. C. Li, M. Numata, A. H. Bae, K. Sakurai, S. Shinkai *J. Am. Chem. Soc.* **2005**, 127, 4548.
8. C. Li, M. Numata, M. Takeuchi, S. Shinkai *Angew. Chem. Int. Ed.* **2005**, 44, 6371.
9. Y.R. Leroux, J. C. Lacroix, K.I. Chane-Ching, C. Fave, N. Felidj, G. Levi, J. Aubard, J.R. Krenn, A. Hohenau *J. Am. Chem. Soc.* **2005**, 127, 16022.
10. A. Holmes *Nature* **2003**, 421, 800
11. H. Galster in *pH measurement: fundamentals, Methods, Application, Instrumentation* VCH, New York, **1991**.
12. A. Song, S. Parus, R. Kopelman *Anal. Chem.* **1997**, 69, 863.
13. T. P. Jones, M. D. Porter *Anal. Chem.* **1988**, 60, 404.
14. F. Buchholz, N. Buschmann, K. Cammann *Sens. Actuator B* **1992**, 9, 41.
15. J. Lin, D. Liu *Anal. Chim. Acta* **2000**, 408, 49.
16. S. Demarcos, O. S. Wolfbeis *Anal. Chim. Acta* **1996**, 334, 149.
17. Z. Jin, Y. Su, Y. Duan *Sens. Actuator B* **2000**, 71, 118.
18. H. D. Duong, O. –J. Sohn, H. T. Lam, J. I. Rhee *Microchem J* **2006**, 84, 50.
19. B. Valeur *in Molecular Fluorescence*, WILEY-VCH, Weinheim, **2002**, pp. 50-51.
20. K. Onishi, S. Sewa, K. Asaka, N. Fujiwara, K.Oguro *Electrochim. Acta* **2000**, 46, 737.
21. K. Tashiro, H. S. Nalwa in *Ferroelectric Polymers* Dekker, New York, **1995**, pp. 63–181.
22. Y. Osada, H. Okuzaki, H. Hori *Nature* **1992**, 355, 242.
23. Z. Liu, P. Calvert *Adv. Mater.* **2000**, 12, 288.
24. M. J. Marsella, R. J. Reid *Macromolecules* **1999**, 32, 5982.
25. T. F.Otero, J. M. Sansinena *Adv. Mater.* **1998**, 10, 491.
26. K. Kaneto, M. Kaueko, Y. Min, A. G. MacDiarmid *Synth. Met.* **1995**, 71, 2211.
27. R.H. Baughman, L.W. Shaklette in *Sci. and Appl. Of Conducting Polymers* IOP Pub. Ltd. **1990**, 47.
28. E. Smela, O. Inganas, I. Lundstroem *J. Micromechanics Microengineering* **1993**, 3, 203.
29. T. F. Otero, E. Angulo, J. Rodriguez, J.C. Santamaria *J. Electroanal. Chem.* **1992**, 341, 369.
30. R. H. Baughman, C. Cui, A. A. Zakhidov, Z. Iqbal, J. N. Barisci, G. M. Spinks, G. G. Wallace, A. Mazzoldi, d. De Rossi, A. G. Rinzler, O. Jaschinski, S. Roth, M. Kertesz *Science* **1999**, 284, 1340

31. G. M. Spinks, G. G. Wallace, R. H. Baughman, L. Dai in *Electroactive Polymer Actuators as Artificial Muscles*, SPIE, Bellingham, WA, **2001**, pp. 223.
32. G. M. Spinks, G.G. Wallace, L. S. Fifield, R. L. Dalton, A. Mazzoldi, D. De Rossi, I. I.Khayrullin, R. H. Baughman *Adv. Mater*. **2002**, 14, 1728.
33. J O'M Bockris, A. K. N. Reddy in *Modern Electrochemistry*, **1st** edition, Plenum Publishing Corporation, New York, **1973**, Vol. **2**, Chap. 7, p.702

Chapter – II

Synthesis of Au Nanoparticles at "all" pH by H_2O_2 Reduction of $HAuCl_4$

Introduction

The ultimate miniaturization dreamed by Feynman and the intriguing optical, catalytic and electronic properties exhibited by the nanosized colloidal particles due to their "size effect" have influenced the recent developments in material science significantly. As a consequence there have been increased efforts in combining the knowledge of chemistry, physics and biology for engineering novel materials that are expected to contribute in overcoming challenges in the fields of electronics, energy, environment and healthcare. Naturally, chemists are interested in contributing towards this endeavor by synthesizing new and advanced materials with wide ranging compositions from highly conducting metal to soggy insulator with control features on a nanometer scale, as demanded by the applications. Understandably synthesis of metallic, semiconductor and composite nanoparticles (NPs) under a variety of experimental conditions such as polar and non polar solvents, acidic and alkaline pH, *in vivo* and *in vitro* conditions, have received added attention as these particles have wide application potential in photonics,[2] optoelectronics,[3] information storage,[4] catalysis,[5,6] biolabeling,[7] and magnetic ferrofluids.[8] Among the inorganic NPs of interests a large number of methods have been developed for size, shape, and capping-agent selective[9-11] synthesis of Au NPs, since its optical, catalytic, electrical properties are influenced by a marginal alteration in it size, shape and composition.[12-14] Moreover easy adsorption of proteins, DNA, RNA molecules on gold surface and its biocompatibility permits the use of colloidal Au NPs in bio-labeling, and drug-delivery.[15–20] Further, for structure generation in two and three-dimensions[21-22] Au

NPs have either been generated or immobilized on various substrate surfaces using primarily chemical, physical, and electrochemical methods.[23-24] It is interesting to note that even though there are a large number of methods available for the generation of Au NPs under different experimental conditions, there is no single or simple scheme to generate Au NPs at various pH, especially with the use of a single reducing agent. This is important considering the application potential of Au NPs with respect to their formation, functionalization or composite preparation under different pH conditions.

Herein we report the generation of Au NPs, in the pH range of 2.9 to 11.2, by the reduction of $HAuCl_4$ using H_2O_2 as the sole reducing agent. Even though it is commonly believed that H_2O_2 is a typical oxidizing agent and it can reduce $HAuCl_4$ only under alkaline condition, we found that Au NPs could be generated in the pH range mentioned above. Our study is based on an earlier observation that under acidic pH condition H_2O_2 could reduce $HAuCl_4$.[25,26] We set out to find a general method of synthesizing Au NPs in aqueous solution from $HAuCl_4$ precursor using H_2O_2 as the reducing agent. The method is primarily based on addition of H_2O_2 to an aqueous $HAuCl_4$ solution, where the pH of the starting solution was adjusted by using either HCl or NaOH as per the requirement. In all cases the solution turned colored in a matter of about 2 min. Ultraviolet – visible (UV-Vis) spectra of the product solution in acidic pH consisted of peaks characteristic of Au NPs, occurring around 540 nm.[27,28] On the other hand the spectra of Au NPs solution above pH 8.0 consisted of a broad peak having maximum absorption above 600 nm, which increased with the increase in pH. Transmission electron microscopic (TEM) observations indicated

the formation of primarily spherical NPs with typical average size of about 5–10 nm when the initial pH was in the acidic range. On the other hand the Au NPs generated under alkaline condition were of larger size and non-spherical in shape. X-ray diffraction measurements showed the growth of lattices along (111), (200), and (220) planes under all pH conditions.

Experimental Section

In a typical experiment, 8.5 mM sodium dodecyl sulphate (SDS, from Merck) solution was prepared in 10 mL Milli-Q filtered water. 50 μL of 1.7×10^{-2} M of $HAuCl_4$ (diluted from original 17% w/v in dilute HCl solution as purchased from Aldrich) was added to the above solution such that the final $HAuCl_4$ concentration was 8.5×10^{-5} M. This resulted in a solution of pH about 3.5. To the above solution 200 μL of H_2O_2 [38% w/v, Merck] was added at a time. The result was an intense pink colored solution with a pH of 3.3.

In order to perform the reaction at different pH, the initial SDS containing $HAuCl_4$ solution was treated either with HCl (taken from stock solution) or with NaOH (taken from stock solution), as appropriate, to obtain a particular pH of the resulting solution. 200 μL of H_2O_2 (38% w/v, Merck) was then added to each of the solution prepared at different initial pH values. In all the cases the solution turned colored in about 2 min of the addition of H_2O_2. We also observed that in all the reactions the pH of the final product solution reduced in comparison to the initial solution (solution before the addition of H_2O_2). UV-Vis spectra, of the resulting

solutions taken in cuvettes, were recorded as such by using a Perkin-Elmer Lambda 25 spectrophotometer. Transmission electron microscopic pictures were recorded after evaporation of a drop of the solution in carbon-coated copper grid using a JEOL electron microscope (Model 1200EX) operated at 120 kV accelerating voltage. X-ray diffraction measurements were performed by evaporating a part of the solution on a microscope glass slide and then recording in a Seifert powder X-ray diffractometer (Model 3003TT).

Results and discussion

When H_2O_2 was added to a solution containing $HAuCl_4$ and SDS, having pH of the solution adjusted to a predetermined value, coloration occurred typically within about 2 min of addition. The color of the solution was stable for more than a month without any observable change or precipitation. Also, the color was stable even in the absence of SDS at least for a few days. An important question that arises out of the use of commercial H_2O_2 is whether the stabilizer used can also reduce $HAuCl_4$ or not. In order to find out the answer, 200 μL of H_2O_2, used as above, was dried by simple air evaporation after keeping the solution in a beaker. The other solution ($HAuCl_4$ and SDS in water) was then added to the beaker, which was then shaken gently for mixing. No coloration of the solution under an arbitrary pH condition was observed. This means the reduction of $HAuCl_4$, was by H_2O_2 and not due to the stabilizing agent(s), to produce the NPs. Commercial H_2O_2 stabilizing agents generally contains either of boric acid, glycerol, or salicylic acid. Each of these reagents was tested independently by individually treating them with $HAuCl_4$ in SDS solution. For

example, 3 different 20 mL solutions, each containing either of 5.3×10^{-2} M salicylic acid, or 9.5×10^{-3} M of boric acid or 2.6×10^{-2} M glycerol, were prepared. To each of these solutions, $HAuCl_4$ was added such that the final concentration of $HAuCl_4$ in each of them was 8.5×10^{-5} M. No coloration was observed immediately; however there was a faint pink colour in the case of glycerol after two days of keeping the solution and in other two reagents the color appeared brown after two days. Thus it is safe to assume that H_2O_2 is the primary reagent that leads to the formation of NPs upon treatment with $HAuCl_4$. Figure 2.1(A) shows the photographs of five resultant solutions of $HAuCl_4$ (in SDS) when treated with H_2O_2 at five different initial pH values such that the final pH values of the solutions were 3.7, 4.9, 6.3, 7.6, and 10.0, respectively. We had observed a difference in the pH of the solution before and after addition of H_2O_2 (and after coloration) in a way that the final solution always had a lower pH value than that of the solution before addition of H_2O_2. As can be seen from the pictures, different initial pH resulted in different colored solution with lower pH generating more pinkish colour, whereas at higher pH the solution tend to be violet or blue. UV-Vis absorption spectra of the corresponding solutions shown in Figure 2.1(B) indicate that the color of the solutions is possibly due to the formation of Au NPs as the spectra are due to that of characteristic surface plasmon resonance (SPR) of Au NPs. It is also interesting to note that the absorption maximum is strongly dependent of the pH of the solution. Ordinarily, colloidal solutions of spherical Au NPs typically give rise to a single SPR peak at ca 535 nm, the exact position being dependent on the particle sizes.

On the other hand, when asymmetric particles are formed in the solution typically two peaks are observed, one of which occur at lower wavelength (535 nm or so) due to transverse plasmon resonance excitation and a second one at a higher wavelength due to the longitudinal surface plasmon resonance. In one of the previous works from the laboratory, it was observed that shape-specific NPs could also give rise to two peaks instead of one. For example, triangular Au NPs have been shown to have two peaks one occurring at around 535 nm while the other one typically occurring at a relatively higher wavelength of about 750 nm. On the other hand, hexagonal Au NPs have their longitudinal plasmon resonance peak at a much higher wavelength of around 900–1000 nm. In the present set of experiments, there was no second peak present in the absorption spectra of Au NPs in the region of our studies (up to 1100 nm). Thus in the present situation only spherical or nearly spherical particles were probably formed.

Further investigations of the colloidal solutions by TEM revealed that at a lower pH typically uniform and small sized NPs were formed. The results are shown in Figure 2.2. As is evident from the figure, the particles formed at pH 2.9 have sizes that are typically in the range of 5–10 nm. On the other hand with the increase in pH there is an apparent increase in particle size. For example, as shown in the panels of Figure 2.2, the NPs generated at pH 7.2, and 7.6, respectively have typical particle diameters of 60–80 nm.

Mags of these figs not appropriate for conclusions sought to be drawn.

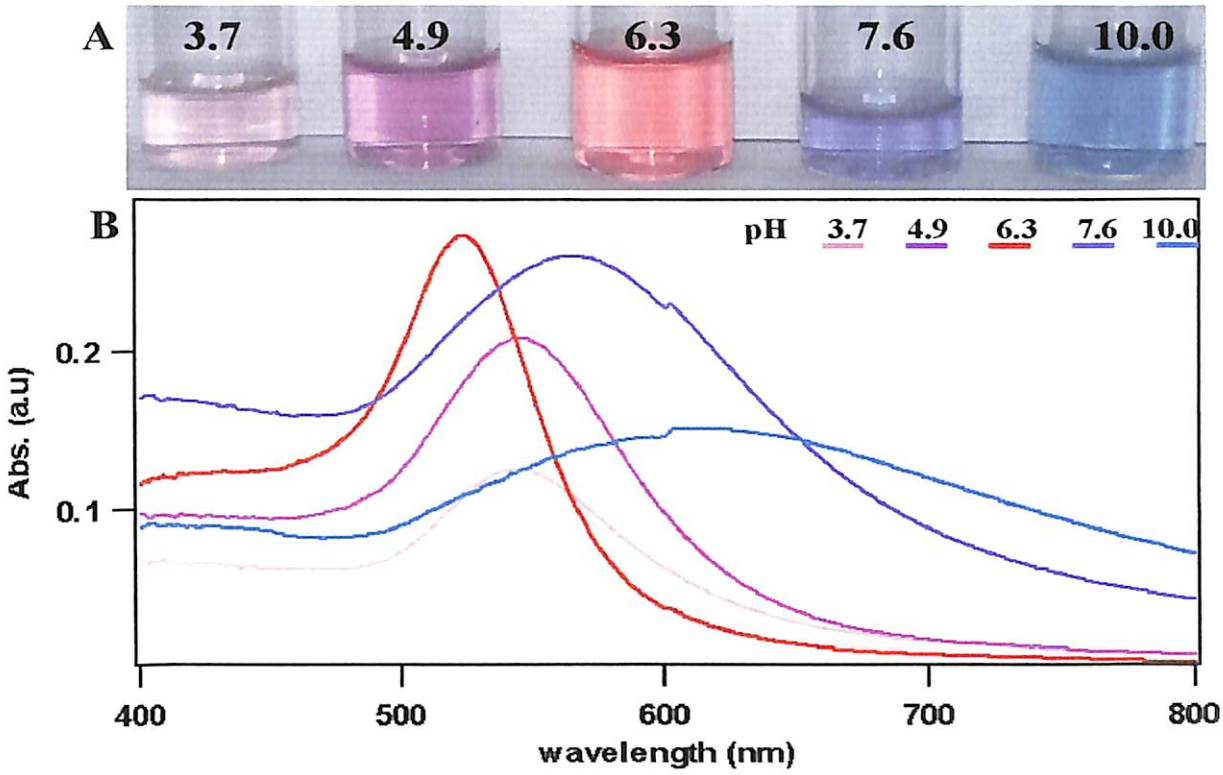

Figure 2.1 (**A**) Photographs of Au colloids synthesized using the present method at different pH. The number on the vial indicates the final pH of the solution. (**B**) UV-Visible spectra of Au colloids synthesized at different pH of the solutions.

It is also interesting to note that the NPs formed at higher pH are not exactly spherically symmetrical as can be seen in Figures 2.2B and 2.2C for NPS synthesized at pH values of 7.2 and 7.6 respectively. Also they cannot be assigned to have any well-defined geometric shape. Also shown in Figure 2.2D is the TEM of Au NPs prepared at a pH of 11.2. It is interesting to note that these particles seem to be the agglomeration of smaller particles that have individual diameters in the range of 25 – 30 nm.

SPR from aggregate or single particle?

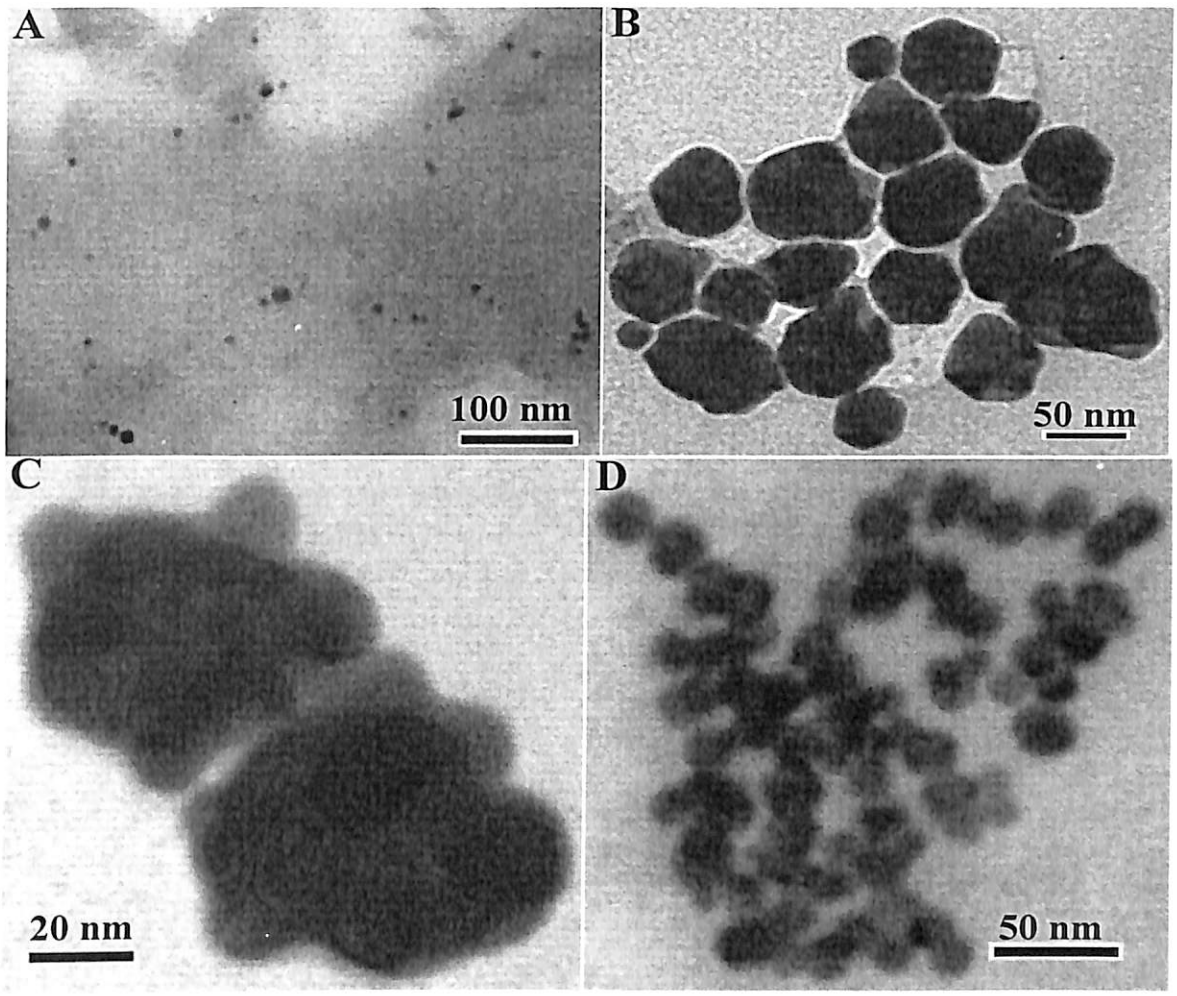

Figure 2.2 TEM of the Au NPs generated at various pH values. The Au NPs were generated at pH 2.9 (A), 7.2 (B), 7.6 (C) and 11.2 (D) respectively.

We would like to mention here that there have been reports of the role of Cl^-, Br^-, NO^-, HSO_3^- salts of Na^+, K^+ in the formation of non-spherical NPs[29] as well as the role of hydroxide[30] ions in the formation of irregularly shaped particles and their corresponding assembly. In the present case a host of factors like pH at which the particles are formed, the presence of ions such as Na^+, OH^-, Cl^- and the presence of stabilizing agent probably contribute towards the sizes and shapes of particles formed.

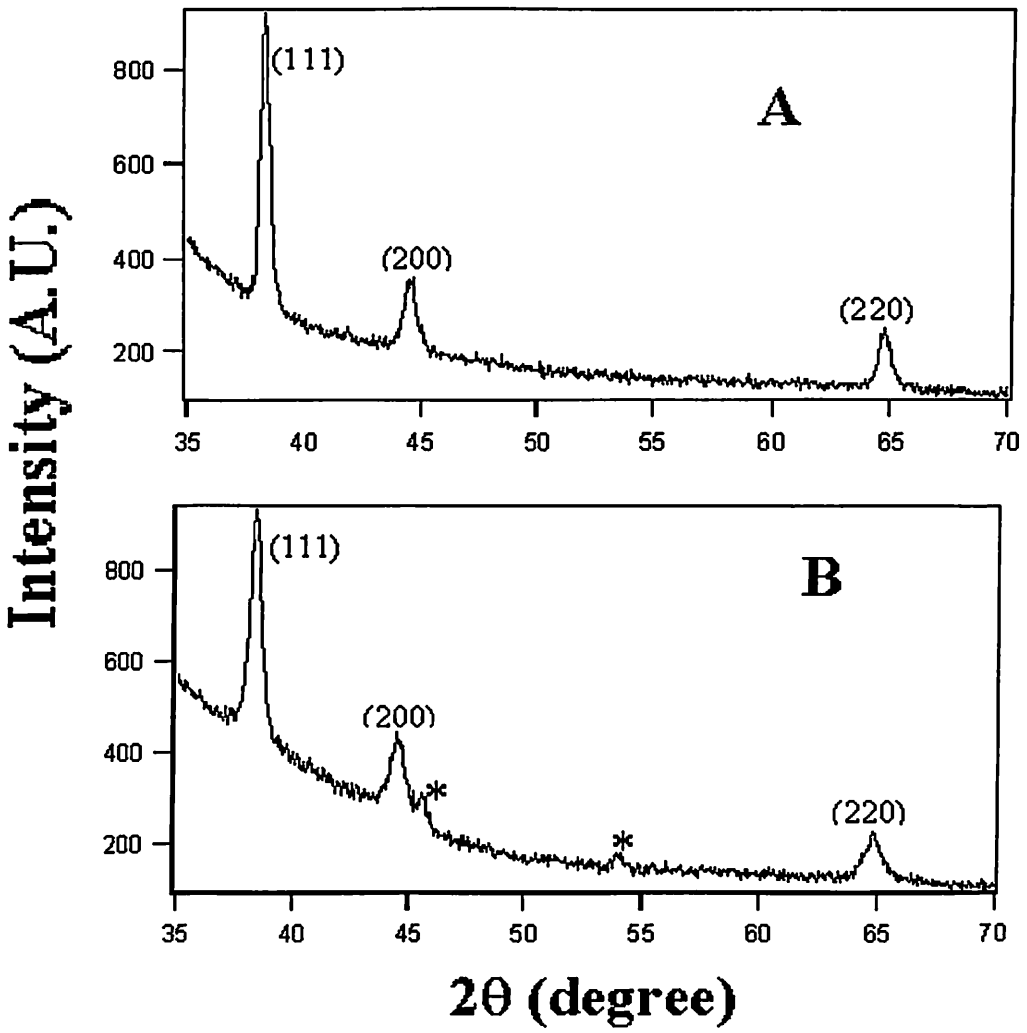

Figure 2.3 (A) is the XRD patterns obtained from the Au NP solution prepared at pH 3.1. On the other hand the XRD patterns in Figure 3(B) is due to Au NPs prepared at pH 9.8. Both the figures clearly show that the particles formed have growth in all three lattice planes namely (111), (200), and (220) of Au nanocrystals as the XRD patterns have peaks at 38.5°, 44.5°, and 64.5° characteristic of growth of all the above three planes of Au respectively.

Figure 2.3 shows the powder XRD patterns of some of these NPs generated at two different pH values and recorded after evaporation of drops of NPs solution on glass slides. Figure 2.3A is the XRD patterns obtained from the Au NP solution prepared at pH 3.1. On the other hand the XRD patterns in Figure 2.3B is due to Au NPs prepared at pH 9.8. Both the Figures clearly show that the particles formed have growth in all three lattice planes namely (111), (200) and (220) of Au nanocrystals as the XRD patterns have peaks at 38.50, 44.50 and 64.50 characteristic of growth of all the above three planes of Au respectively.[31] This also support that the particles generated under the present conditions are three dimensional in nature and no disc or such shapes were obtained. It is important to make an observation here with respect to the XRD patterns in Figure 2.3(B), which is due to the Au NPs generated under alkaline pH. In addition to three prominent peaks due to the three planes of Au NPs, there are two small peaks occurring at 45.5° and 54°. The peaks are due to the lattice planes (220) and (311) respectively of NaCl possibly formed by the reaction of NaOH with HCl present in the medium. This is especially the case for the NPs grown under alkaline conditions, as we have observed that in acidic conditions the Au NPs generated had peaks only due to Au and no other impurity.

consistent with solubility of NaCl ?

A fascinating and often intriguing question arises when H_2O_2 is used as the reducing agent especially while reducing a species such as Au^{3+} to Au. One would normally be quick to dismiss the possibility of reduction of Au^{3+} to Au under acidic condition as the standard reduction potential of $Au^{3+} \rightarrow Au$ is 1.498 V, while that of

H_2O_2 to H_2O under acidic condition is 1.776 V. This makes it apparently improbable to reduce Au^{3+} to Au by H_2O_2. However, if one considers that in the present set of experiments $HAuCl_4$ was used as the precursor for Au generation, then the situation becomes different. Consideration of the standard electrochemical potentials of the following reactions would help to understand the reductions of $HAuCl_4$ by H_2O_2 under all pH conditions.[32]

Reaction		E^0(V)	
$AuCl^-_4 + 3e$	$= Au + 4Cl^-$	+1.002	(2.1)
H_2O_2	$= O_2 + 2H^+ + 2e$	−0.695	(2.2)
$H_2O_2 + 2OH^-$	$= O_2 + 2H_2O + 2e$	+0.146	(2.3)
$H_2O_2 + 2H^+ + 2e$	$= 2H_2O$	+1.776	(2.4)

As is evident from the above, reaction (2.1) and reaction (2.2) can be combined resulting in the reduction of $AuCl^-_4$ to Au by H_2O_2. In other words, the following reaction is thermodynamically favorable in acidic conditions.

$$2AuCl_4^- + 3H_2O_2 \rightarrow 2Au + 8Cl^- + 3O_2 + 6H^+ \qquad (2.5)$$

The standard redox potential of the net reaction is +0.307 V. The same reaction would occur even in neural pH. On the other hand, under alkaline condition the reduction is even more favored as the net standard redox potential is +1.148 V. The reaction that takes place under alkaline condition is a combination of reactions (2.1) and (2.3) above. The overall reaction under alkaline condition would be as follows.

$$2AuCl_4^- + 3H_2O_2 + 6OH^- \rightarrow 2Au + 8Cl^- + 3O_2 + 6H_2O \quad (2.6)$$

Thus reduction of $HAuCl_4$ under all pH conditions is possible although the exact mechanism of reduction involved may be different, depending on the pH of reaction medium.

In brief, herein we have reported the generation of Au NPs from $HAuCl_4$ by using H_2O_2 as the reducing agent in aqueous solution. The UV-Vis absorption spectra of the NPs formed at various pH consisted of single peaks characteristic of transverse plasmon resonance and were different depending on pH with peak shifting towards higher wavelength as the pH was increased. TEM pictures indicated that at lower pH conditions the particles were generally spherical and small in sizes. The particles generated at higher pH tend to be larger and sometimes agglomerated to form large structures.

Reference and Notes

1. R. Feynman *California Institute of Technology Journal of Engineering and Science* **1960**, 4, 23.
2. S. A. Maier, M. L. Brongersma, P. G. Kik, S. Meltzer, A. A. G. Requicha, H. A. Atwater *Adv. Mater.* **2001**,13, 1501.
3. T. Miyasaka, T. N. Murakami *Appl. Phys. Lett.* **2004**, 85, 3932.
4. S. Kolliopoulou, P. Dimitrakis, P. Normand, Hao-Li Zhang, N. Cant, S. D. Evans, S. Paul, C. Pearson, A. Molloy, M. C. Petty, D. Tsoukalas *J. Appl.Phys.* **2003**, 94, 5234.
5. J. Liu, Y. Chi, H. Lin, C. Mou, B. Wan *Catalysis Today* **2004**, 93-95, 141.
6. B. L. V. Prasad, S. I.Stoeva, C. M. Sorensen, V. Zaikovski, K. J. Klabunde *J. Am. Chem. Soc.* **2003**, 125, 10488.
7. M., Jr. Bruchez, M.Moronne, P. Gin, S. Weiss, A. P. Alivisatos *Science* **1998**, 281, 2013.

8. K.S. Suslick, M. Fang, T.Hyeon *J. Am. Chem. Soc.* **1996**, 118, 11960.
9. U. Schlotterbeck, C. Aymonier, R. Thomann, H. Hofmeister, M. Tromp, W. Richtering, S. Mecking *Adv. Funct. Mater.* **2004**, 14, 999.
10. B. Pal, T. Torimoto, K. Iwasaki, , T. Shibayama, H. Takahashi, B. Ohtani *J.Phys.Chem. B* **2004**, 108, 18670.
11. M. J. Hosteler, J. E. Wingate, C. –J. Zhong, J. E. Harris, R. W. Vachet, M. R. Clark, J. D. Londono, S. J. Green, J. J. Stokes, G. D. Wignall, G. L. Glish, M. D. Porter, N. D. Evance, R. W. Murray *Langmuir* **1998**, 14, 17.
12. T. R. Tshikhudo, Z. Wang, M. Brust *Materials Science and Technology* **2004**, 20, 980.
13. T. K. Sarma, A. Chattopadhyay *Langmuir* **2004**, 20, 3520.
14. S. Kan, T. Mokari, E. Rothenberg, U. Banin *Nature Mater.* **2003**, 2, 155.
15. K. I. Bolotin, F. Kuemmeth, A. N. Pasupathy, D. C. Ralph *Appl. Phys. Lett.* **2004**, 84, 3154.
16. S. I. Khondaker, Z. Yao *Appl. Phys. Lett.* **2002**, 81, 4613.
17. J. J. Storhoff, C. A. Mirkin *Chem. Rev.* **1999**, 99, 1849.
18. R. Elghanian, J. J. Storhoff, R. C. Mucic, R. L. Letsinger, C. A. Mirkin *Science* **1997**, 277, 1078.
19. T. A. Taton, R. L. Letsinger, C. A. Mirkin *Science* **2000**, 289, 1757.
20. G. F. Paciotti, L. Myer, D. Weinreich, D. Goia, N. Pavel, R. E. McLaughlin, L. Tamarkin *Drug Delivery* **2004**, 11, 169.
21. L. Motte, F. Billoudet, E. Lacaze, J. Douin, M. P. Pileni *J. Phys. Chem. B* **1997**, 101, 138.
22. S. Chen *Adv. Mater.* **2000**, 12, 186.
23. S. Paul, C. Pearson, A. Molloy, M. A. Cousins, M. Green, S. Kolliopoulou, P. Dimitrakis, P. Normand, D. Tsoukalas, M. C. Petty *Nano Lett.* **2003**, 3, 533.
24. S. Shih, W. Su, Y. Lin, C. Wu, C. Chen *Langmuir* **2002**, 18, 3332.
25. Vogel's Qualitative Inorganic Analysis 6th Ed. Orient Longman (**1987**), p 253.
26. T. K.Sarma, D. Chowdhury, A. Paul, A. Chattopadhyay *Chem.Commun.* **2002**, 10, 1048.
27. L. M. Liz-Marzan *Langmuir* **2006**, 22, 32.
28. P. Mulvaney *J. Phys. Chem. B* **2001**, 105, 3441.
29. A. Filankembo, M. P. Pileni *J. Phys. Chem. B* **2000**,104, 5865.
30. K. K. Caswell, C. M. Bender, C. J. Murphy *Nano lett.* **2003**, 3, 667.

31. S. Chen, Y. Liu, G. Wu *Nanotechnology*., **2005**, 16, 2360.

32. R. C. Weast, D. R. Lide, M. J. Astle, W. H. Beyer in *CRC Handbook of Chem. & Phys.* 70th Ed. CRC Press, Boca Raton, Florida (**1989 - 1990**) p D-151 – D-153.

CHAPTER – III

A water - Soluble Polythiophene – Au Nanoparticle Composite for pH Sensing

Introduction

Since the report of electrical conductivity in doped polyacetylene by Chiang et al. in 1977[1] the field of conjugate polymers has been developing at a galloping pace. The appealing applications and recent availability of a broad range of high-purity polymers has brought a rejuvenation in the field of semiconductor devices, which include transistors,[2-7] photodiodes[8,9] and LEDs.[10-14] The potential for commercialization of some of these semiconductor devices is perceived to be high, because of their low cost for development and manufacturing. Not only is the low-manufacturing cost but also the mechanical flexibility, chemical stability and tunable electrical and optical properties of these π-conjugated polymers that have generated immense academic and industrial interest for further development of advanced and miniaturized electronic devices.[15,16] These polymers, when appropriately functionalized, can detect, transduce, and possibly amplify chemical, biological, and physical changes into optical or electrical signals, which make them important for futuristic devices.

On the other hand, inorganic metal and semiconducting nanocrystals (NCs) offer unique advantages, over other conventional materials, for their use as optical sensors owing to their size-controllable properties and environmental and photo stabilities.[17] The high oscillator strengths of the metal nanoparticles (NPs) and the continuous absorption spectra and emissivity of semiconductor NCs have been attractive options for NP based solutions and solid-state devices, where the optical properties of the NCs would act as probes for diverse applications such as colorimetric DNA and nucleic acid assays,[18,19] molecular markers for extracellular

and intracellular events,[20] temperature,[21] and pH sensing,[17] and cell imaging and targeting,[22,23] It would be even more versatile if one could systematically incorporate metal or semiconductor NCs into the conducting polymer or vice versa so that the best of both—the extraordinary optical properties of the NCs and the optical, chemical, and electrical properties of the polymer could be combined into functional multicomponent solid-state and solution-phase devices. In this regard, our laboratory had for the first time introduced the idea of one-pot synthesis of Au NP–polyaniline composites[24] where the electrical conductivity of the polymer was significantly enhanced upon incorporation of metal NPs. Several other groups, since then, have also developed schemes for the generation of metal NP-conducting polymer composites, especially those having nanoscale dimensions.[25,26] Further, the laboratory has demonstrated that an Au NP – polyaniline composite could act as a model colorimetric glucose sensor[27] and a TiO_2 NC– polypyrrole film[28] generated at the air–water interface has superior photochemical properties.

In this chapter, a new pH sensor is introduced whose functioning is based on the fluorescence properties of a polythiophene-Au NP composite prepared in water. [29] The method depends on the generation of the composite by simultaneous reduction of $HAuCl_4$ to Au NPs and polymerization of thiophene in the medium in the presence of each other only. The composite, which was quite stable in water, had characteristic emissions which changed in the pH range of 3.0 to 6.0, thus providing a solution indicator of pH based on optical properties. The emission characteristics were reversible with respect to change in pH of the medium. Also, the presence of an isosbestic point in the emission spectra which acts as an internal standard helped in

ratiometric analysis of the pH of the medium. The mass spectra of the composite at the two extreme pH values indicated that the nature of the polymer did not change on varying the pH other than simple protonation and deprotonation. The presence of Au NP in the composite was ascertained by transmission electron microscopy (TEM) and the polymer was further characterized by FTIR spectroscopy. Based on the observations, we have calculated the pK_{eq} of the composite from the acid – base equilibria at different pH values and using this value we also demonstrate that the pH of an aqueous solution in the range of 3.0 to 6.0 could be calculated from the emission spectra of the composite in the medium.

Materials and Methods

Thiophene (>99%) and $HAuCl_4$ (17 wt% solution of $HAuCl_4$ in dilute HCl, 99.99%) used for the gold nanoparticle–polythiophene composite preparation were procured from Sigma–Aldrich. The acids (HCl, H_2SO_4, HNO_3) and alkalis (NaOH, K_2CO_3) used in the titration were procured from Merck India Ltd. Milli-Q grade water was used in all the experiments. The Au NP–polythiophene composite was synthesized as follows. A homogeneous dispersion of 30.0 mM thiophene in water was prepared by sonicating the requisite amount of thiophene in 10.0 ml water at 35.0 KHz and at room temperature (~25° C), in a closed glass vial. This was followed by addition of 40.0 µl of 1.72×10^{-2} M $HAuCl_4$ (prepared from the 17 wt % solution of $HAuCl_4$ as procured from Sigma–Aldrich). The above mixture was kept in a mechanical shaker operating at 100 rpm and 25 °C. It was observed that a dark purple colored solution

was produced in 2 h, the UV–visible spectrum of which consisted of a peak at 540 nm, which is indicative of the formation of Au NPs in the medium.[30] The shaker was further kept on for a day, which led to a colorless solution, in addition to the formation of a dark-colored precipitate. The solution was separated from the precipitate by decantation. Energy dispersive X-ray spectroscopy of the precipitate indicated the presence of a significant amount of Au. The solution as such was stable for weeks without any further change in color or absorption and emission spectra.

TEM pictures were recorded after evaporation of a drop of the parent solution on a carbon-coated copper grid using a JEOL electron microscope (Model 1200EX) operating at 120 keV accelerating voltage. All the pH measurements were made using a pH meter made by WTW, Germany, of Model Inolab pH 720 after proper calibration with WTW technical buffer solutions at room temperature (~25° C).

In order to perform acid–base titration and emission measurements at different pH, 40.0 ml of the parent solution, collected from a few identically prepared composite sets, was first neutralized with NaOH (aq). This was followed by titration with a known strength of HCl (aq). After each addition, pH of the resulting solution was measured along with measurement of emission spectrum of the same. The emission spectra were measured using a Varian (CARY-Eclipse) fluorescence spectrophotometer at room temperature. In order to perform the pH titration in the reverse order NaOH was added to the solution (from acidic pH to neutral pH). This was followed by measurements of both the resulting pH and the emission spectrum as before. The acid as well as alkali was added using a micropipette.

Result and Discussion

In the present set of experiments thiophene was polymerized by oxidative coupling with $HAuCl_4$,[31,32] by a method similar to polymerization by Fe(III) compounds.[33,34] Since the standard reduction potential of $AuCl_4^-$ to Au^0 ($E^0 = 1.002$ V)[35] is greater than that of Fe^{3+} to Fe^{2+} ($E^0 = 0.771$ V)[35] reduction, the process is expected to be more facile. The chemical reaction involving the composite formation could be described by the following processes (Equation (3.1) and Scheme 3.1):

$$AuCl_4^- + 3e = Au + 4Cl^-, \qquad (E^0 = 1.002\ V) \qquad (3.1)$$

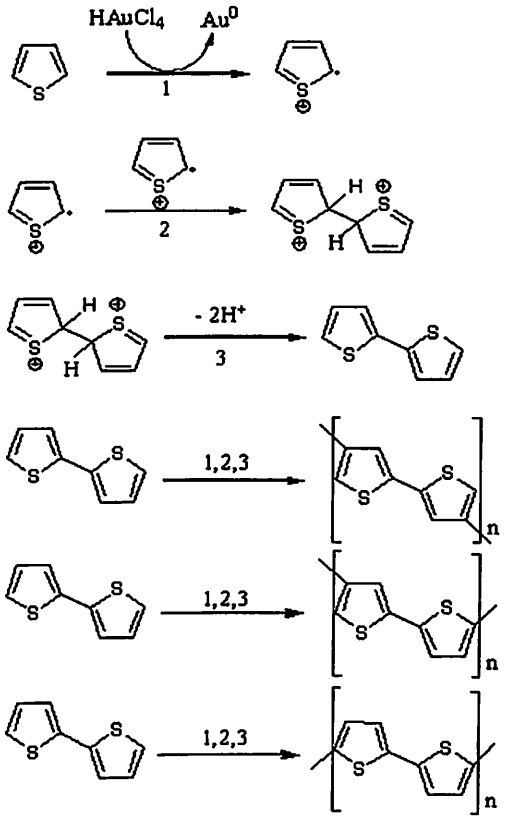

Scheme 3.1 Where n ≥ 1 (continued)

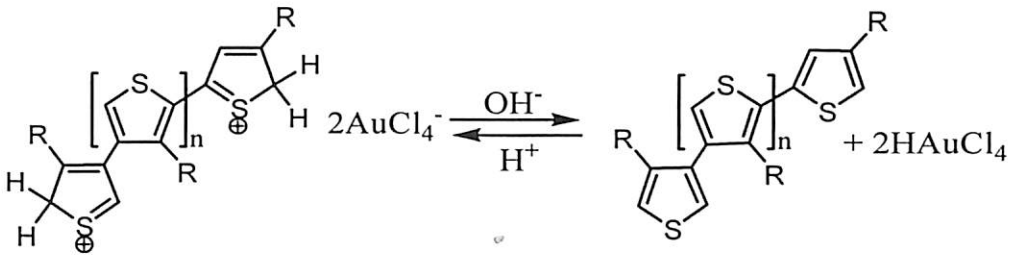

Scheme 3.1 Where n ≥ 1 and R = H or Cl

It is plausible that the sulfur groups of the polymer[36] help in the formation of a stable composite where there is no phase separation between the NPs and the polymer (which has been observed herein).

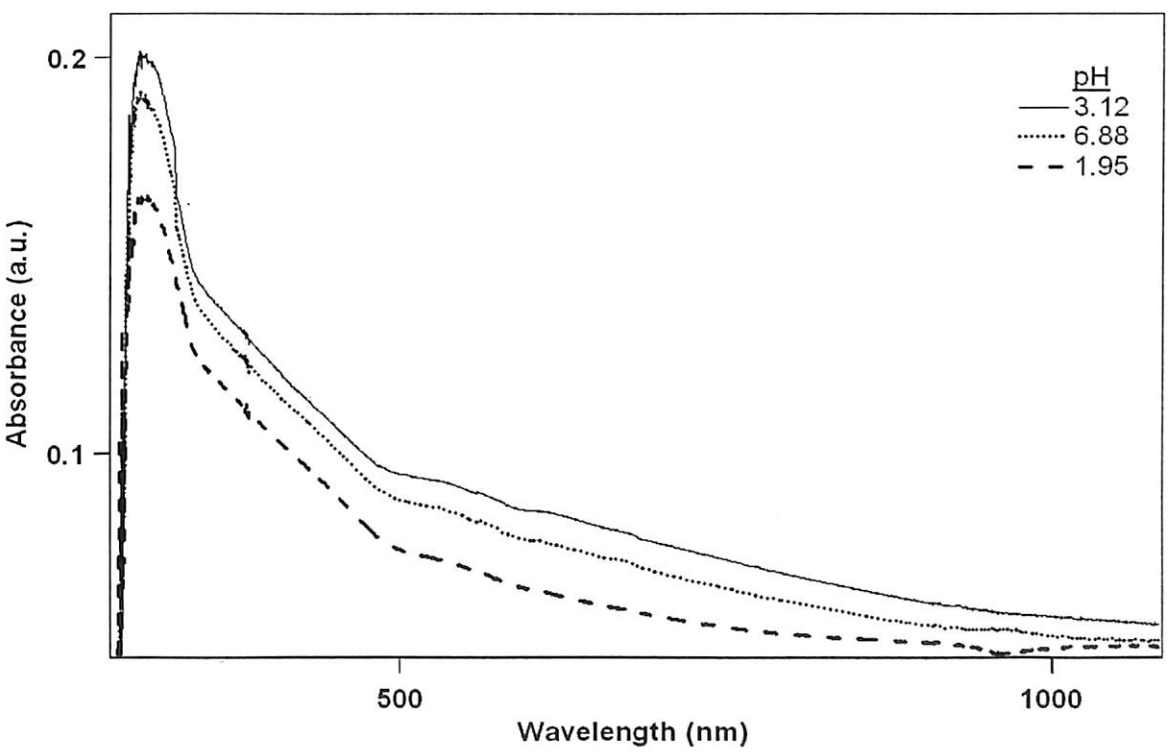

Figure 3.1 UV–vis spectra of the composite solution at the pH values of 1.95, 3.12 and 6.88.

A judicious choice of the ratio of $HAuCl_4$ and thiophene concentration in water produced a colorless solution, in addition to a dark precipitate. The solution was

separated from the precipitate by decantation. The solution was stable for weeks without any further precipitaion, change in color, or absorption and emission spectra. We also observed that changing the pH of the solution by treatment with acid (HCl) or base (NaOH) in the working range did not change the absorption spectrum. For example, as shown in Figure 3.1, absorption curves were similar in shape. The spectrum is a characteristic of the polymer as the characteristic peak of the surface plasmon resonance (SPR) of Au NPs was absent in the medium.

It is interesting to mention here that although the final solution (in addition to the dark precipitate) had no characteristic peak of the presence of Au NPs in the medium, the same reaction mixture during synthesis indicated the formation of Au NPs. For example, when the UV-vis spectrum of the mixture of thiophene and $HAuCl_4$ was recorded after 2 h from the initial mixing, the solution had a peak at 540 nm (Figure 3.2), which is indicative of the formation of Au NPs during the initial stages of synthesis. On the other hand, the absence of the SPR peak for Au NPs in the working solution could be due to two reasons. First of all, since there was a large amount of precipitate, it is plausible that the remaining amount of Au NPs in the solution was too low to provide any detectable absorption. It might also be due to delocalization of SPR within the polythiophene matrix or change in the dielectric constant due to change in the environment, such that it is not feasible to excite optically as has been reported earlier.[37]

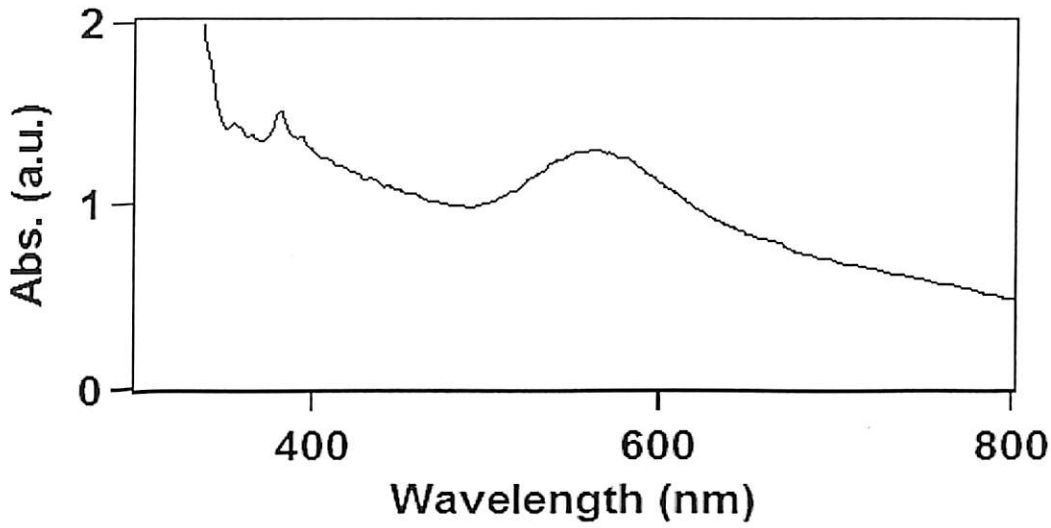

Figure 3.2 UV–vis spectra of $HAuCl_4$ and thiophene mixture in water after 2 h of shaking.

In fact, a transmission electron microscopic (TEM) picture (Fig. 3.3A) of a drop cast (clear) solution indicated the formation of small spherical Au NPs with typical sizes in the range of 5–10 nm, where the NPs could be observed being embedded in the polymer. Selected area electron diffraction (SAED) pattern of the NPs is shown in figure 3.3B.

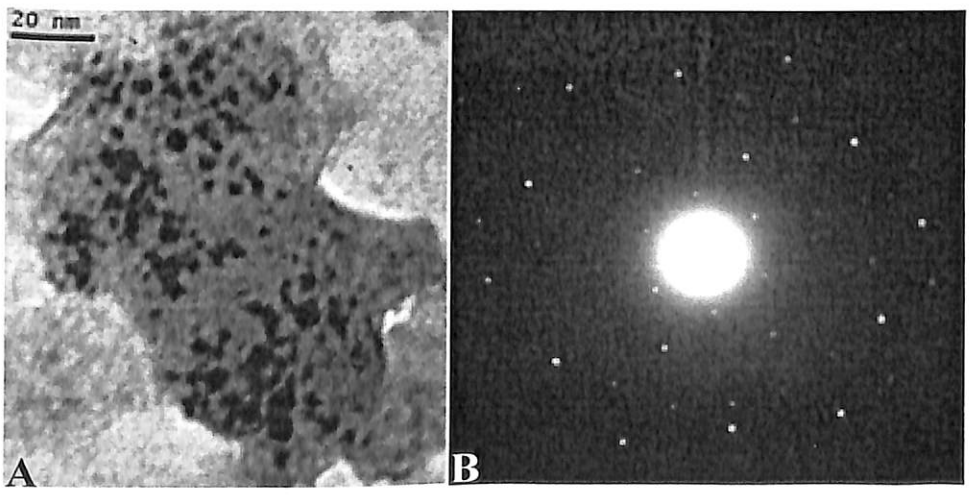

Figure 3.3 Transmission electron micrograph of a drop cast solution of the composite (**A**) and corresponding selected area electron diffraction patterns (**B**).

As is clear from the figure Au NPs were present in the solution. The TEM picture also reveals the presence of polymer in the solution embedding the NPs.

Further, FTIR spectrum of the composite (Figure 3.4A) consisted of peaks at 3137 cm^{-1} attributed to C–H stretching and the peak at 1400 possibly due to C=C stretching vibration of thiophene. [38,39] The peaks below 1000 cm^{-1} were of poor quality and hence we also recorded the FTIR spectrum of the precipitate (Figure 3.4B), which was produced simultaneously under the same conditions. Here the peak at 790 cm^{-1} appeared prominently, thus indicating the formation of 2,5-disubstituted thiophene derivatives. In addition, characteristic frequencies of C=C stretching vibrations of extensively conjugated polythiphenes appeared at 1384, 1440, and 1457 cm^{-1}.

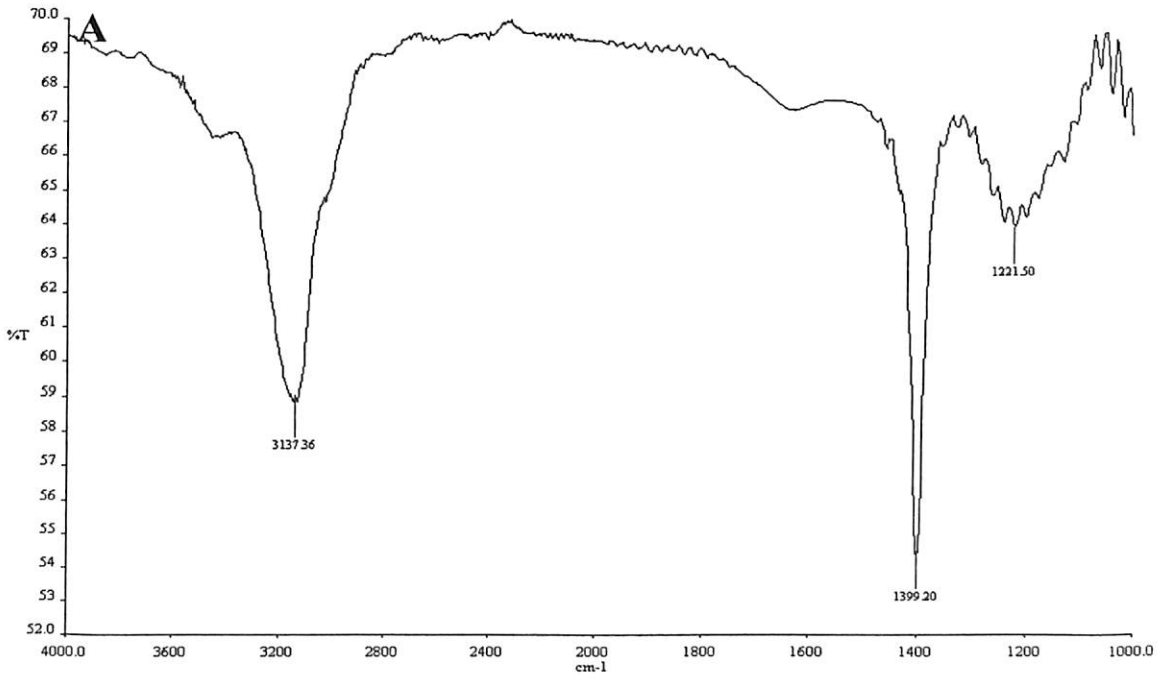

Figure 3.4(A) FTIR spectrum of the composite.

Figure 3.4 (B) FTIR spectrum of the precipitate produced simultaneously with the composite.

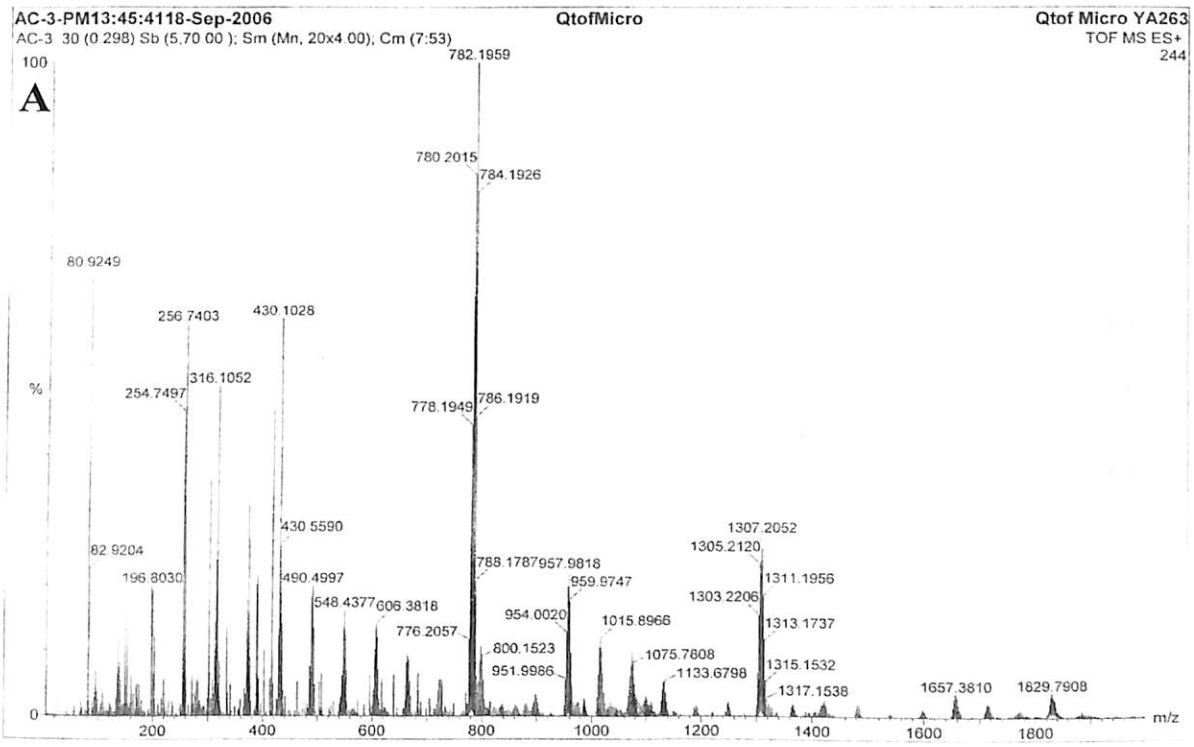

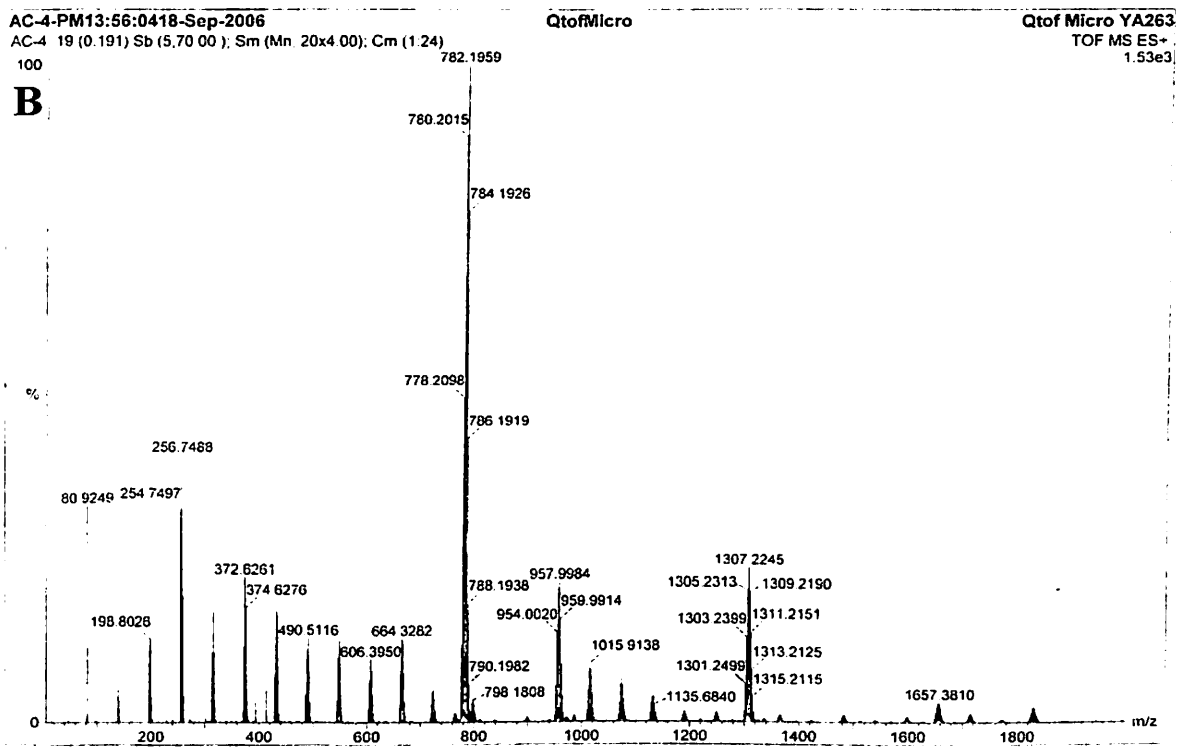

Figure 3.5 Electrospray ionization mass spectra of the composite recorded for the solutions kept at pH 1.95 (**A**) and at pH 6.88 (**B**).

In brief 2,5-disubstituted polythiopene derivatives were formed in both the precipitate and the dispersion. Electron spray ionization (ESI)– mass spectra of the composite recorded at pH 1.95 and 6.88 were found to be the same, thus indicating that the basic nature of the polymer did not change upon change in the pH of the solution (Figure 3.5a and 3.5b). In other words, addition of acid and base to the solution did not lead to further chemical reaction other than simple protonation and deprotonation.

A careful analysis of the mass spectra indicated the formation of polymers consisting of different units of chlorothiophene (mass fragment of ~ 116.5a.m.u.).

This is clear from the difference in mass of alternate peaks in both the spectra. However, the pattern did not indicate the formation of a single polymer as the peaks were of comparable intensity. In other words, it is possible that a large number of polymers (and oligomers) of different molecular weights were formed in the mixture with Chlorothiophene as one of the common units. The formation of Chlorothiophene as a monomer can be understood from the presence of $HAuCl_4$ reacting with thiophene in the course of redox reaction in the presence of additional HCl.

Further, when the as-prepared composite solution was excited at 345 nm a strong emission with a peak at 435 nm could be observed. The pH of the solution was measured to be 3.00± 0.05. Interestingly, when the pH of the solution was changed by addition of an appropriate amount of NaOH or HCl the emission peak position changed. Figure 3.6 shows the emission of the composite solution in the pH range of 6.75 to 2.98. As is clear from the figure, the emission spectra at low pH consisted of a single peak at 435 nm. The peak gradually shifted to higher wavelength, with increase in pH of the solution, with the appearance of another peak at still lower wavelength. For example, at pH 5.00 there are two emission peaks—one with a relatively weaker intensity at 390 nm and another one of stronger intensity with a peak at 465 nm. It is also clear from the figure that the shift of emission maximum is gradual with respect to changes in pH of the solution, thus providing an ideal substrate for in situ measurements of pH in the specified range. It may also be noted here that the changes in the spectral characteristics are completely reversible upon change of pH (Figure 3.7).

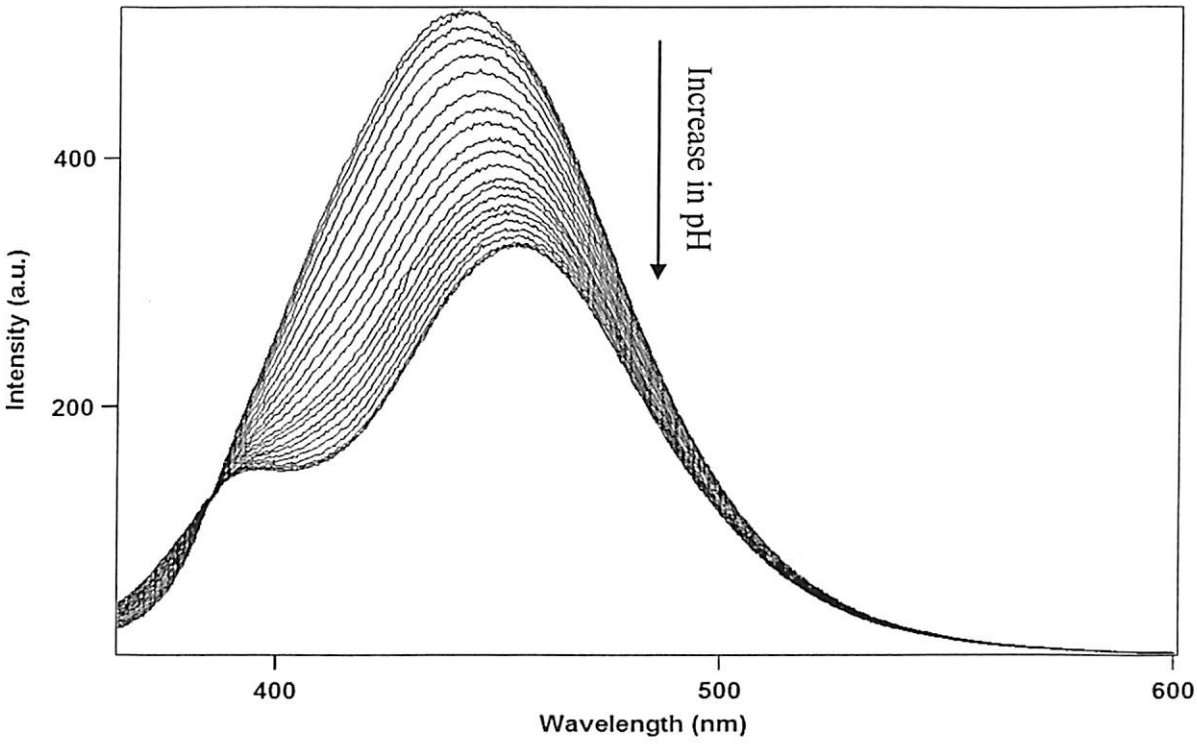

Figure 3.6 Photoemission spectra of the composite at various pH values. On moving from bottom to top the pH at which spectra are recorded are 6.75, 5.96,5.29, 4.85, 4.60, 4.43, 4.29, 4.18, 4.09, 4.02, 3.95, 3.83, 3.71, 3.68, 3.60, 3.53,3.45, 3.35, 3.26, 3.17, 3.10, 3.04, and 2.98. These pH values were obtained by addition of HCl of known strength to the solution. The excitation wavelength was fixed at 345 nm.

Furthermore, it is noteworthy that in the set of emission spectra of the composite (Figure 3.6) the emission intensity at 383.5 nm remains constant (similar to the isosbestic point in common emissions where two species are interconverted in the presence of a chemical stimulus), thus acting as an internal standard for the emission characteristics with respect to change in pH of the solution. This is an additional advantage in the pH measurements as the point supports in the ratiometric analysis of the pH of the solution.

We have observed that on change in pH of the solution beyond the range specified above the emission spectra of the composite did not change (except for the effect of dilution). Thus we have confined our studies in the pH range of 3.0 to 6.0. A question may be raised here with respect to the role of Au NPs in the emission spectra of the composite. Although the emission property of the composite is based on the protonation and deprotonation of the polymer chromophore, the polymer alone in the dispersible form, as the case here, may be difficult to synthesize as well as stabilize in aqueous dispersions.

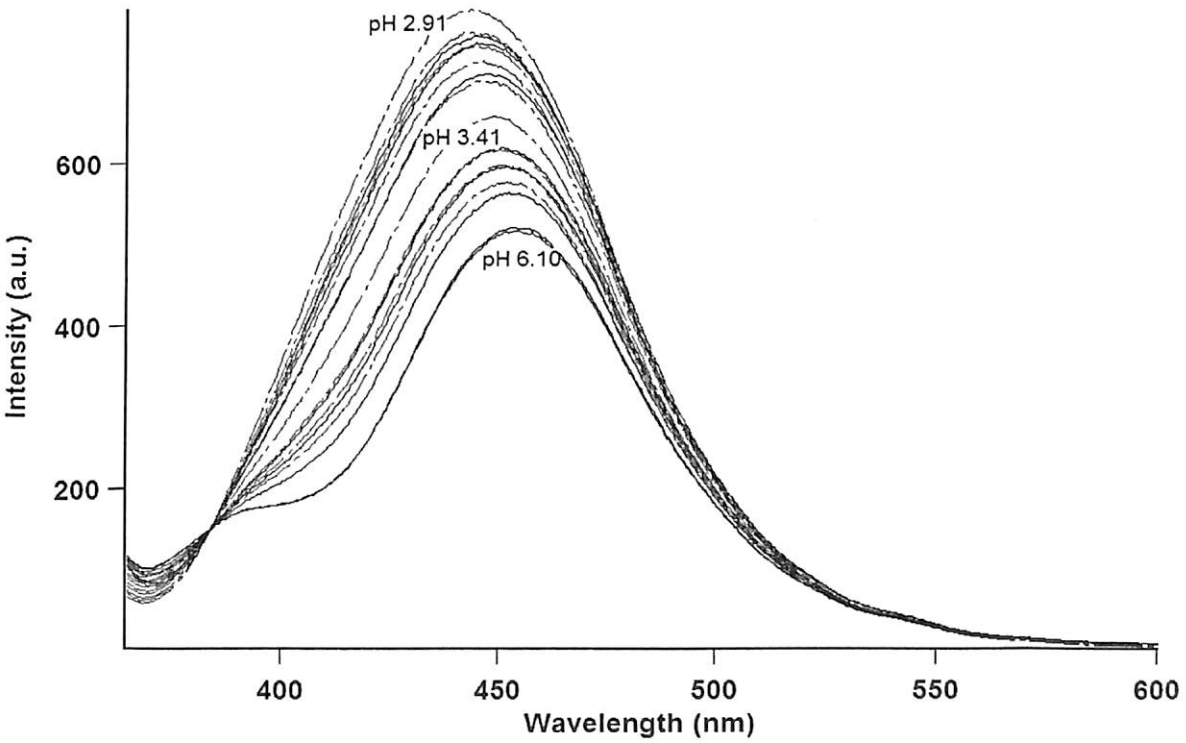

Figure 3.7 A demonstration of the reversibility of the acid-base titrated emission spectra of the composite. Spectra in black (read from top to bottom) were recorded at observed solution pH values of 2.99, 3.12, 3.32, 3.77, 3.93, 4.21, 5.46 and 6.10 respectively. This was achieved by addition of specific amount of NaOH solution of known strength to the as-prepared solution. Similarly, spectra were recorded in the reverse pH order by addition of HCl. The spectra in blue, on reading from bottom to the top, were recorded at observed solution pH values of 4.07, 3.92, 3.80, 3.41, 3.30, 3.18, 3.11, 2.99 and 2.91 respectively. The black and

blue curves are nearly superimposed when the pH values are closure. The apparent differences in the spectra (which do not superimpose) are due to small difference in pH between them (at which the emission spectra were recorded).

Moreover the colloidal Au NPs and the polymer in the composite, prevented each other from agglomerating and helped to remain suspended in water for months. Being water dispersible, devoid of additional surfactants, and the ability to reversibly change between charged and neutral states of the active species create additional advantages for applications. The observed emission at pH 3.10 matches reasonably well with a literature report of the emissions of oligomers of thiophene.[40] Thus the chromophore involved in the emissions may well be the polymer of thiophene. The reversibility of the emission characteristics with respect to changes in pH indicates that the main process may be protonation and deprotonation of the chromophore. Then one can write the equilibrium reaction as

$$A + H^+ \rightleftharpoons AH^+$$

where A is the deprotonated polythiophene–Au NP composite and AH^+ is its protonated counterpart and the equilibrium constant (k_{eq}) for the reversible process can be expressed as

$$k_{eq} = \frac{[AH^+]}{[A][H^+]} \qquad (3.2)$$

The above protonation and deprotonation reaction in the medium was further confirmed by the observation of changes of pH of the solution on addition of acids such as HCl, H_2SO_4, and HNO_3 or bases such as NaOH and KCO_3. For example,

when the solution was neutralized by addition of NaOH and then subsequently HCl was added, the observed pH was more than the calculated pH, i.e., the amount of acid added to the solution. This indicates protonation of the chromophore. Analogous observations were made when acidic solution was titrated with NaOH. We also observed that addition of KCl or KBr (and corresponding sulphate or nitrate salts) did not affect the emission spectrum of the composite, indicating that it's $[H^+]$ or $[OH^-]$ that affected the spectra and not other ions such as Na^+, K^+, Cl^-, Br^-, SO^-_4 , NO^-_3 .

Further, we used the following procedure to calculate pK_{eq} from equation (3.2). If $[AH^+]_0$ (which is the same as $[A]_0$) represents the maximum concentration of AH^+, then at any instant of time the total concentration of A and AH^+ is $[AH^+]_0$. For the estimation of $[AH^+]_0$, first the as-prepared solution was titrated to neutral pH (7.0). Then the solution at neutral pH was titrated by addition of HCl and the corresponding pH value was measured for each addition of HCl. Here the observed pH was higher than the expected pH calculated from the added $[H^+]$. In this way, there was a point (pH 3.04) beyond which the change in the pH of the solution was equivalent to the amount of $[H^+]$ added. The $[AH^+]_0$ was then calculated from the difference in the $[H^+]$ that was actually added and the amount of $[H^+]$ that would have been required to reach pH 3.04 in the absence of the composite. Once $[AH^+]_0$ was known, the $[AH^+]/[A]$ was calculated at each observed pH during the titration. Hence pK_{eq} was calculated for each titer value (Table 3.1). The pK_{eq} was found to vary from 3.4 to 6.2. Similar results were obtained by titrating from pH 2.99 with NaOH in order to obtain $[A]_0$. The details of titration data are shown in Table 3.1.

Why is K_{eq} ~~does~~ changing with pH? It's an equ. const.

Table 3.1 Estimation of $[AH^+]_0$ and pK_{eq} of the protonation–deprotonation process involving the composite.

Obs. pH	Corresponding $[H^+]$ (x 10^{-7} M)	Expected $[H^+]$ (x 10^{-7} M)	Difference (x 10^{-5} M)	pK_{eq}
6.75	1.778	1.778	0.0	
5.96	10.96	199.64	1.89	4.91
5.29	51.29	397.01	3.46	4.54
4.85	141.25	593.90	4.53	4.24
4.60	251.19	790.29	5.39	4.09
4.43	371.53	986.19	6.15	4.00
4.29	512.86	1181.62	6.69	3.91
4.18	660.69	1376.55	7.16	3.84
4.09	812.83	1571.0	7.58	3.79
4.02	955.99	1764.97	8.10	3.76
3.95	1122.02	1958.46	8.36	3.71
3.83	1479.11	2344.02	8.65	3.61
3.71	1949.84	2727.67	7.78	3.42
3.68	2089.30	3109.45	10.20	3.59
3.60	2511.89	3678.62	11.70	3.62
3.53	2951.21	4243.64	12.90	3.64
3.45	3548.13	4990.61	14.40	3.68
3.35	4466.84	6097.60	16.30	3.75
3.26	5495.41	7188.74	16.90	3.72
3.17	6760.83	8619.52	18.60	3.81
3.10	7943.28	10023.48	20.8	4.11
3.04	9120.11	11401.39	22.0	6.25
2.98	10471.29	12753.96	22.80	

Once the pK_{eq} is known one can now go back and calculate the pH values from the observed emission spectra as described below. If one takes the best value of pK_{eq} and then knowledge of $[AH^+]/[A]$ would yield the values of pH. The $[AH^+]/[A]$ ratio can, in principle, be calculated from the following relationship:

$$I(\lambda) = I_{A_0}(\lambda)\left\{\frac{[A]}{[A_0]}\right\} + I_{(AH^+)_0}(\lambda)\left\{\frac{[AH^+]}{[AH^+]_0}\right\} \qquad (3.3)$$

where I (λ) = intensity at wavelength λ when concentration of the deprotonated species is [A]; $I_{A_0}(\lambda)$ = intensity at wavelength λ when concentration of the deprotonated species is $[A_0]$; i.e., all the species are deprotonated;

$I_{(AH^+)_0}(\lambda)$ = intensity at wavelength λ when concentration of the protonated species is $[(AH^+)_0]$; i.e., all the species are protonated.

Since $[(AH^+)_0] = [A] + [AH^+]$ always and $[A_0] = [(AH^+)_0]$, Eq. (3) can be written as

$$I(\lambda) = I_{A_0}(\lambda)\left\{\frac{[A]}{[A_0]}\right\} + I_{(AH^+)_0}(\lambda) - I_{(AH^+)_0}(\lambda)\left\{\frac{[A]}{[A_0]}\right\} \qquad (3.4)$$

$$\text{Or} \quad \left\{\frac{[A]}{[A_0]}\right\} = \frac{\{I(\lambda) - I_{(AH^+)_0}(\lambda)\}}{\{I_{(A)_0}(\lambda) - I_{(AH^+)_0}(\lambda)\}} \qquad (3.5)$$

In order to calculate $[A]/[A_0]$ corresponding to each intermediate emission spectrum, equation (3.5) was used in conjunction with emission spectra at the observed pH values. The pH values corresponding to the intermediate spectra were then estimated using equation (3.2). The pK_{eq} value used for the calculations was 3.64, the details of which are in Table 3.2.

Table 3.2 Estimation of pH of the intermediate spectra from fluorescence emission of the composite.

Obs. pH	[A]/ [A_0] (x 10^{-5} M)	[A] (x 10^{-5} M)	[AH^+] (x 10^{-5} M)	pH
6.75				
5.96	99,370	22.60	0.14	5.84
5.29	98,209	22.40	0.41	5.38
4.85	94,196	21.50	1.32	4.85
4.60	92,777	21.10	1.65	4.75
4.43	87,748	20.00	2.80	4.49
4.29	83,866	19.10	3.68	4.35
4.18	80,878	18.40	4.36	4.26
4.09	74,742	17.00	5.76	4.11
4.02	71,364	16.30	6.53	4.03
3.95	67,603	15.40	7.39	3.96
3.83	61,531	14.00	8.77	3.84
3.71	54,125	12.30	10.50	3.71
3.68	50,399	11.50	11.30	3.65
3.60	41,980	9.57	13.20	3.50
3.53	36,411	8.30	14.50	3.40
3.45	29,188	6.65	16.10	3.25
3.35	19,635	4.48	18.30	3.03
3.26	14,382	3.28	19.50	2.86
3.17	8891	2.03	20.8	2.63
3.10	3656	0.83	22.00	2.22
3.04	663	0.15	22.60	1.46

We have performed the calculations in the observed pH range of 5.96 to 3.04. We found that the using the single pK_{eq} value (of 3.64), the estimated pH values matched well in the pH range of 5.96–3.53 with the experimental observations, thus providing a good probe for the solution pH measurements. A section of the plot of the estimated pH versus observed pH is shown in Figure 3.8.

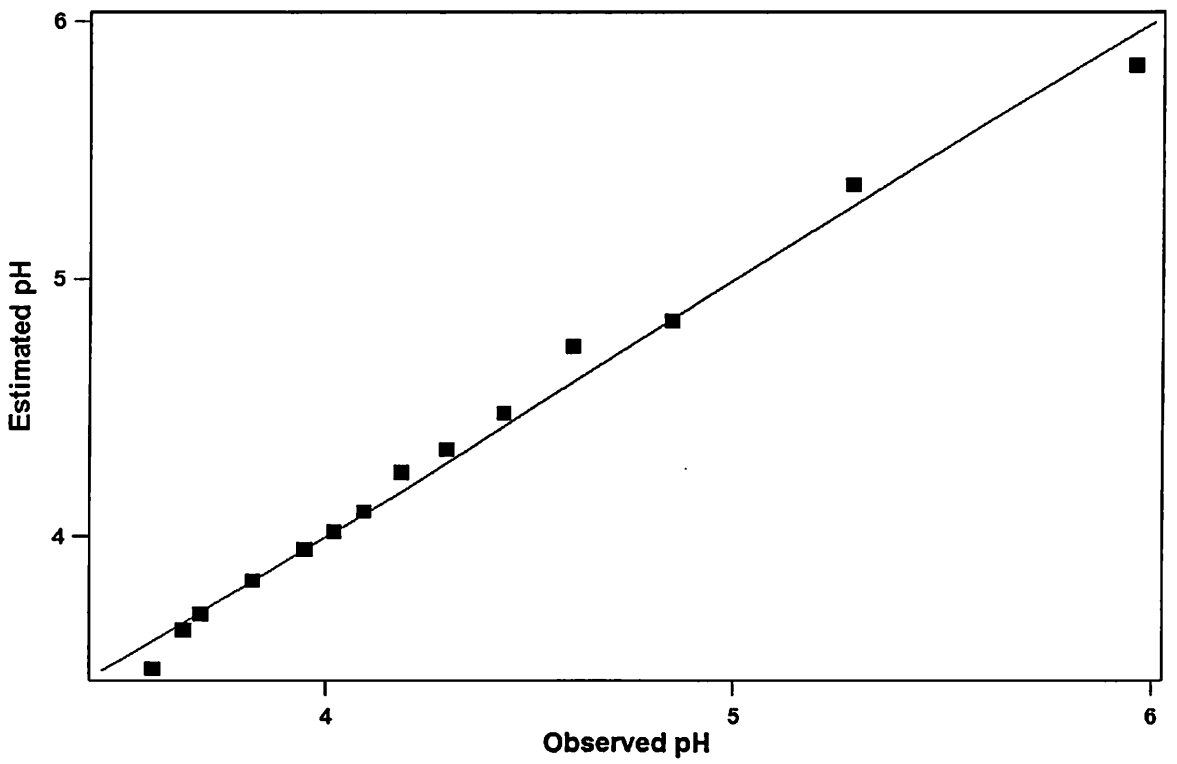

Figure 3.8 A comparison between the estimated and the observed pH.

Beyond the above pH region, the difference between the observed and the estimated pH was found to be more than 0.1 unit. This may be due to the fact that reaction between the composite and the acid or base beyond the above pH ranges can no longer be written as a simple one-proton acid base reaction. Also, the emission

characteristics of the composite may not be a simple linear dependence as written in Equations. (3.3) – (3.5). Thus we have limited the present report in that range. However, it must be noted that in the selected range the observed and estimated pH values match well. The present range as well as the errors in the estimation is better than the values reported in the literature. This makes the present method appealing and useful. We would also like to note here that we had carried out the measurements for four cycles of pH titrations and the results were reproducible, indicating the robustness of the method as well as the stability (and behavior) of the composite with respect to acid–base titrations.

In the present chapter of the thesis, we have been able to demonstrate the newly generated aqueous polythiophene–Au NP composite as a pH sensor in the range of 3.0 to 6.0. The stability of the polymer in different pH and reversibility of the cycles of operation allow the in situ measurement of pH which may otherwise not be possible. The availability of a thiophene precursor allows future systematic changes in the backbone of the polymer for generating pH sensors in even wider ranges. Also, this new composite may form the basis of sensors for ions other than $[H^+]$, provided the thiophene unit could be suitably substituted. In the present case the concept of one-pot synthesis has been applied, where the Au NPs and polymer in the composite helped in each others' stability in the medium, while the polymer acted as the sensor.

Reference and Notes

1. C. K. Chiang, C. R. Jr.Fincher, Y. W. Park, A. J. Heeger, H. Shirakawa, E. J. Louis, S. C. Gau, Alan G. MacDiarmid *Phys. Rev. Lett.* **1977**, 39, 1098.
2. F. Garnier, R. Hajlaoui, A. Yassar, P. Srivastava *Science* **1994**, 265, 1684 .

3. P. Ostoja, S. Guerri, S. Rossini, M. Servidori, C. Taliani, R. Zamboni *Synth. Met.* **1993**, 54, 447.
4. L. Torsi, A. Dodabalapur, , L. J. Rothberg, A.W. P. Fung, H. E. Katz *Science* **1996**, 272, 1462.
5. Y. Yang, A. J. Heeger *Nature* **1994**, 372, 344.
6. A. R. Brown, A. Pomp, C. M. Hart, D. M. Deleeuw *Science* **1995**, 270, 972.
7. H. Sirringhaus, N. Tessler, R. H. Friend *Science* **1998**, 280, 1741.
8. G. Yu, J. Gao, J. C. Hummelen, F. Wudl, A. J. Heeger *Science* **1995**, 270, 1789.
9. M. Granstrom, K. Petritsch, A. C. Arias, A. Lux, M. R. Andersson, R. H. Friend *Nature* **1998**, 395, 257.
10. J. H. Burroughes, D. D. C. Bradley, A. R. Brown, R. N. Marks, K. Mackay, R. H. Friend, P. L. Burns, A. B. Holmes *Nature* **1990**, 347, 539.
11. P. L. Burn, A. B. Holmes, A. Kraft, D. D. C. Bradley, A. R. Brown, R. H. Friend, R. W. Gymer *Nature* **1992**, 356, 47.
12. N. C. Greenham, S. C. Moratti, D. D. C. Bradley, R. H. Friend, A. B. Holmes *Nature* **1993**, 365, 628.
13. D. Braun, A. J. Heeger *Appl. Phys. Lett.* **1991**, 58, 1982.
14. G. Gustafsson, Y. Cao, G. M. Treacy, F. Klavetter, N. Colaneri, A. J. Heeger *Nature* **1992**, 357, 477.
15. Y.R. Leroux, J.C. Lacroix, K.I. Chane-Ching, C. Fave, N. Felidj, G. Levi, J. Aubard, J.R. Krenn, A. Hohenau *J. Am. Chem. Soc.* **2005**, 127, 16022.
16. A. Holmes *Nature* **2003**, 421, 800.
17. P.T. Snee, R.C. Somers, G. Nair, J.P. Zimmer, M.G. Bawendi, D.G. Nocera *J. Am. Chem. Soc.* **2006**, 128, 13320.
18. M.S. Han, A.K.R. Lytton-Jean, B. Oh, J. Heo, C.A. Mirkin *Angew. Chem. Int. Ed.* **2006**, 45, 1807.
19. J. Liu, Y. Lu *Angew. Chem. Int. Ed.* **2006**, 45, 90.
20. G.L. Liu, Y. Yin, S. Kunchakarra, B.Mukherjee, D. Gerion, S.D. Jett, D.G. Bear, J.W. Gray, A.P. Alivisatos, L.P. Lee, F.F. Chen *Nat. Nanotechnol.* **2006**, 1, 47.
21. D. Suzuki, H. Kawaguchi *Langmuir* **2005**, 21, 8175.
22. D.J. Bharali, D.W. Lucey, H. Jayakumar, H.E. Pudavar, P.N. Prasad *J. Am. Chem. Soc.* **2005**, 127, 11364.
23. C. Loo, A. Lowery, N. Halas, J.West, R. Drezek *Nano Lett.* **2005**, 4, 709.

24. T.K. Sarma, D. Chowdhury, A. Paul, A. Chattopadhyay *Chem. Commun.* **2002**, 10, 1048.
25. S.K. Pillalamarri, F.D. Blum, A.T. Tokuhiro, M.F. Bertino *Chem. Mater.* **2005**, 17, 5941.
26. A.P. O'Mullane, S.E. Dale, J.V. Macpherson, P.R. Unwin *Chem. Commun.* **2004**, 14, 1606.
27. G. Majumdar, M. Goswami, T.K. Sarma, A. Paul, A. Chattopadhyay *Langmuir* **2005**, 21 1663.
28. D. Chowdhury, A. Paul, A. Chattopadhyay *Langmuir* **2005**, 21, 4123.
29. I.E. Sendroiu, S.F.L. Mertens, D.J. Schiffrin *Phys. Chem. Chem. Phys.* **2006**, 8, 1430.
30. Q. Qiao, L. Su, J. Beck, J.T. McLeskey Jr. *J. Appl. Phys.* **2005**, 98, 094906.
31. J.H. Youk, J. Locklin, C. Xia, M. Park, R. Advincula *Langmuir* **2001**, 17, 4681.
32. H. Huang, X. Yang *Colloids Surf. A* **2005**, 11, 255.
33. Yu. Wang, B.L. Lucht, W.B. Euler *Polym. Prepr.* **2002**, 43, 1160.
34. C. Della Casa, F. Bertinelli, P. Costa Bizzarri, E. Salatelli *Adv. Mater.* **1995**, 7, 1005.
35. R.C.Weast, D.R. Lide, M.J. Astle,W.H. Beyer in *CRC Handbook of Chemistry and Physics,* 70th ed., CRC Press, Boca Raton, FL, **1989–1990**, pp. D-151–D-152.
36. L. Zhai, R.D. McCullouugh *J. Mater. Chem.* **2004**, 14, 141.
37. Z. Peng, L. Guo, Z. Zhang, B. Tesche, T. Wilke, D. Ogermann, S. Hu, K. Kleinermanns *Langmuir* **2006**, 22, 10915.
38. Y. Pang, H. Xu, X. Li, H. Ding, Y. Cheng, G. Shi, L. Jin *Electrochem. Commun.* **2006**, 8, 1757.
39. Z. Zhang, F. Wang, F. Chen, G. Shi *Mater. Lett.* **2006**, 60, 1039.
40. Y. Choi, S. Tepavcevic, Z. Xu, L. Hanley *Chem. Mater.* **2004**, 16, 1924.

CHAPTER – IV

Rapid and Sensitive Detection of Bacteria by a Fluorescent Au Nanoparticle – Polythiophene Composite

Introduction

Bacterial contamination is a major health hazard especially in the context of food safety, environmental monitoring and pharmaceutical industry. It assumes even greater significance in case of pathogens as the presence of even a single cell may lead to serious health risk.[1] Thus, rapid quantification of bacteria is imperative for clinical diagnosis, food safety, therapeutic strategies, and for reducing potential infections. Conventional microbiological methods for estimating low numbers of bacterial cells mostly encompass enrichment of the target bacteria in the sample.[2] Most of these methods are arduous, time-consuming and require prior knowledge of the bacterial species to select an appropriate growth medium. On the contrary, molecular methods based on biorecognition events such as immunoassays and polymerase chain reaction are capable of achieving high sensitivity and specificity, circumventing additional culturing of bacterial cells.[3,4] However, like the conventional microbiological techniques, a priori knowledge of appropriate surface antigens and target genes are required to detect the bacterial cells.

Recently, many attempts have been made to augment the sensitivity of bacterial estimation without the need for target amplification and enrichment. A number of immunoassays have been developed based on bioconjugated nanoparticles, kinetic exclusion assays and on-chip microfluidic platforms.[5-7] However, majority of these methods require sophisticated instrumentation, which makes the process cost prohibitive. Ideally, analytical tools meant for estimation of bacterial cells should be designed to achieve rapid and high sensitivity with minimal sample manipulations. A reasonable solution from the point of sensitivity and speed is the use of fluorescence,[8]

which is non-invasive, with an obvious advantage of zero background interference and is hence extremely sensitive towards its microenvironment. In the present chapter, we describe a new bacterial quantification scheme based on reduction of the fluorescence emission intensity of a polymer nanocomposite by the bacterial cells. The synthesis of the composite and its use in pH sensing has been described in Chapter III. The salient features of our method include (1) its ease of operation with minimal sample manipulation steps; (2) high sensitivity and quantitative data acquisition; and (3) its generality of detection of different bacterial cells. Our results show that the composite could estimate as low as 1000 bacterial cells suspended in saline solution.

Materials and Methods

A homogeneous mixture of thiophene (99+%, Sigma-Aldrich) of 30 mM strength was prepared by sonicating, the requisite amount of thiophene in 10 mL water, at 35 KHz and room temperature (~ 28° C). This was followed by addition of 50 µL of 1.72 X 10^{-2} M $HAuCl_4$ (prepared from 17 wt % solution of $HAuCl_4$ in dilute HCl; 99.99%, Sigma-Aldrich). The above mixture was incubated in a mechanical shaker operating at 100 rpm and 25° C for a day. Initially, the solution was dark purple in color, which upon further shaking turned light yellow to a colorless solution of pH ~ 3.0, in addition to a small amount of a dark precipitate. The solution was decanted and then used for the experiments with a series of diluted bacterial suspension

The bacterial strains used in the present investigation included gram-positive lactic acid bacteria (LAB): *Pediococcus acidilactici* K7, *Lactobacillus plantarum*

MTCC 1325 and *Enterococcus faecalis* MTCC 439 and gram-negative strain of *Escherichia coli* MTCC 433. LABs were propagated in de Man Rogosa and Sharpe (MRS) medium under static condition at 37°C. *E.coli* and *E. faecalis* were propagated in nutrient broth (NB) and brain-heart infusion broth (BHI), respectively, in a shaking incubator at 37°C.

The four bacterial strains were grown for 12 h in the appropriate media and specified conditions as mentioned before. An aliquot of the culture was serially diluted and plated on respective agar-based medium to determine the bacterial colony forming units (CFU). Cells were harvested from the remaining culture broth by centrifugation at 8,000 rpm for 5 min. The cells were washed twice with 0.85% saline solution to remove residual media components and then diluted 10, 50, 100, 500, 1000 and 10000 times in 0.85% saline solution. The bacterial cell suspensions and Au NP-polythiophene composite were mixed in a ratio of 1:1 (v/v) and the emission spectra of the samples were recorded in a fluorescence spectrophotometer (Cary Eclipse, Varian Inc., USA) at an excitation wavelength of 345 nm. Additional experiments were performed with neutralized Au NP- composite, wherein diluted cells of *P. acidilactici* CFR K7 (10, 100 and 1000 dilutions) were taken. The fluorescence intensity of the polymer composite was measured as mentioned before following treatment with the bacterial cells. The intensities at the maximum emission wavelength (435 nm) and at various bacterial concentrations, were used to obtain the plot shown in Figure 4.1.

Quantitative analysis of bacteria-AuNP polythiophene composite was studied by dynamic light scattering particle size analyzer (LB-550, Horiba, Japan). A 10 mL saline suspension of *P. acidilactici* CFR K7 cells in the range of 10^5 and 10^4 CFU were mixed with equal volume of Au NP polythiophene composite solution. The particle distribution size for polymer composite, bacterial cells as well as their mixture was then analyzed.

For TEM analysis 5.0 μL aliquot of the Au NP- polythiophene composite, cell suspension of strain *P. acidilactici* CFR K7 and a mixture of bacteria- Au NP-polythiophene composite were deposited on three separate carbon-coated copper TEM grids followed by air-drying. Images of the samples were recorded in a TEM (JEM-2100, JOEL, Japan) operating at an accelerating voltage of 80 keV.

Results and Discussion

The polymer nanocomposite used herein comprised of Au NPs and chlorinated polythiophene, which has been developed recently in our laboratory.[9] The water dispersible composite exhibits intense fluorescence that depends on the pH of the solution. A single intense emission peak is obtained with maximum at 435 nm, when the polymer-nanocomposite solution at pH 3.0 is excited at 345 nm. This emission is due to the protonated form of the composite (AH^+). On the other hand, when the pH of the solution is increased to 6.0, the emission spectrum consists of two weaker peaks occurring at 390 nm and 465 nm. These peaks are due to completely deprotonated form of the composite (A). At intermediate pH values, mixtures of the two species with concentrations corresponding to equilibria between the two forms exist. Interestingly, we observed that the fluorescence of the composite was highly sensitive

to the presence of bacteria in the medium and the change in fluorescence was maximum when the pH of the solution was kept at 3.0. For example, when the emission intensity of a 1:1 mixture of the aqueous solution of the Au NP-polythiophene composite and the various diluted bacterial cell suspensions were recorded, systematic decrease in the intensity was observed, with the increase in bacterial population. The decrease in fluorescence intensity of the composite with increasing bacterial concentration provided an excellent opportunity for quantitative and rather accurate estimation of the bacterial concentration. We have accounted for the decrease in emission intensity in terms of the effective concentration of the species AH^+ in the sample upon addition of bacterial cells. The relationship between the decrease in fluorescence intensity of the NP-polythiophene composite and bacterial cell concentration could be established from the well-known relationship between the intensity of fluorescence and the concentration of the fluorescent species and which is derived below.

The dependence of intensity of steady-state fluorescence, I_f^c , and the concentration of the species, c can be written as,[10]

$$I_f^c = k F_\lambda I_0 \left\{1 - e^{-2.3\varepsilon lc}\right\} \qquad (4.1)$$

Here k is a proportionality constant; F_λ is the steady-state fluorescence intensity - at the emission maximum - per absorbed photon at the excitation wavelength; I_0 is the intensity of incident light, and ε is molar extinction coefficient at the excitation

wavelength. When the sample is excited at a fixed wavelength keeping all other optical configurations unchanged, the above equation can be further simplified into

$$I_f^c = B\left\{1 - e^{-2.3\varepsilon lc}\right\} \qquad (4.2)$$

Where $B = \kappa F_\lambda I_0$

For the pure composite sample, with concentration C_0, Equation (4.2) can be written as,

$$I_f^{Co} = B\left\{1 - e^{-2.3\varepsilon lCo}\right\} \qquad (4.3)$$

In the presence of the bacterial cells, when the effective concentration of the fluorescent species decreased due to sequestration by bacterial cells, the eqⁿ (4.3) can be written as

$$I_f^C = B\left\{1 - e^{-2.3\varepsilon l(Co-x)}\right\} \qquad (4.4)$$

Where x is a function of bacterial cell number and has the dimension of concentration and c is the concentration of the remaining fluorophores unaffected by the presence of bacteria. Equations (4.3) and (4.4) can be combined and restated as

$$Log\left(I_f^C - I_f^{Co}\right) = LogD + 2.3\varepsilon lx \qquad (4.5)$$

where $D = Be^{-2.3\varepsilon lCo}$

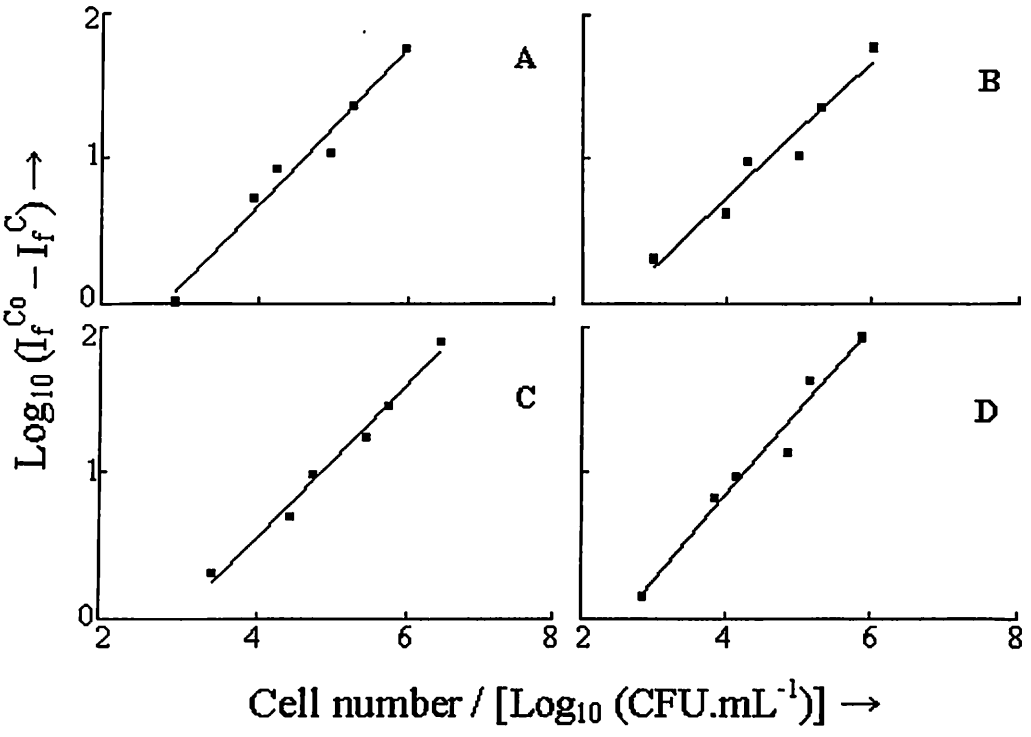

Figure 4.1 Decrease in fluorescence intensity of Au NP-polythiophene composite as a function of bacterial cell number. **A**: Treatment with *Pediococcus acidilactici* CFR K7; **B**: Treatment with *Lactobacillus plantarum* MTCC 1325; **C**: Treatment with *Escherichia coli* MTCC 433; **D**: Treatment with *Enterococcus faecalis* MTCC 439. The excitation wavelength was set at 345 nm and the emission maximum was observed at 435 nm.

Interestingly, when the logarithm of difference in fluorescence intensities between that of the pure composite and that in the presence of different amount of bacteria was plotted against the logarithm of the number of bacterial cells a linear relationship was obtained. This was true for all four types of bacteria - *Pediococcus acidilactici* CFR K7, *Lactobacillus plantarum* MTCC 1325, *Escherichia coli* MTCC 433 and *Enterococcus faecalis* MTCC 439 - that were tested. The results are shown in figure 4.1.

Clearly, the linear relationship being valid for all the four types of bacteria – three of which are gram positive and the other one being gram negative bacteria demonstrates the efficacy of the method in quantitative estimation of bacteria and the generality of the approach. It is important to mention here that in all cases of measurements the bacteria were suspended in saline and then mixed with composite in a 1:1 ratio and the pH of the solution was set at 3.0. When a calibration curve (Figure 4.2) was obtained from the fluorescence of the composite at various dilutions, the emission intensity was linear with concentration indicating that mere dilution of the composite did not lead to any structural or fluorescence change of the species. Hence, the change in fluorescence was exclusively due to interaction between the composite and the bacteria. Presumably there was no equilibrium between the bacterial cells and the composite as observed in normal quenching process.

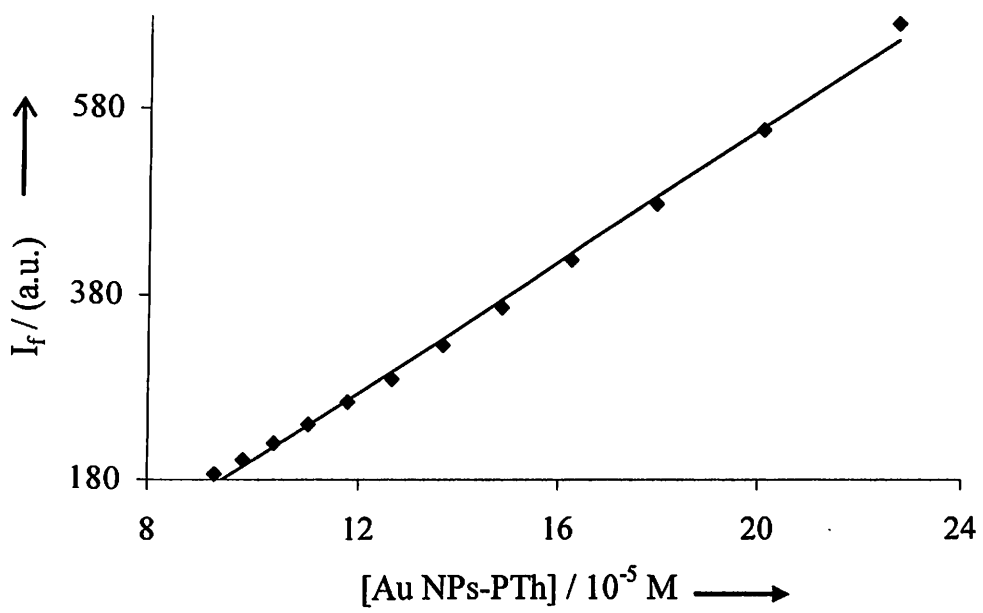

Figure 4.2 Calibration curve indicating fluorescence intensity as a function of molar concentration of the Au nanoparticle-polythiophene (AuNP-PTh) composite solution.

Also important to mention here is that the lowest number of bacterial cells that can be estimated using the present scheme is 1000, indicating the sensitivity of the method. Remarkably, the present method allows estimation of logarithmic dilutions of bacterial cell numbers, which in the present case is in the order of 10^3-10^6 cells. Furthermore, based on the above results the equation (4.5) could be rewritten as,

$$Log\left(I_f^{Co} - I_f^{C}\right) = LogD + 2.3\varepsilon l K_b Log_{10} N_b \qquad (4.6)$$

Here, K_b is a phenomenological constant having the dimension of concentration and N_b is the number of bacteria present in the medium. From the slopes of the graphs in Figure 4.1, the values of K_b for the four bacterial species were found to be 3.30×10^{-4} ML^{-1} for *P. acidilactici* CFR K7, 2.86×10^{-4} ML^{-1} for *L. plantarum* M1325, 3.15×10^{-4} ML^{-1} for *E. coli* M433 and 3.47×10^{-4} ML^{-1} for *E. faecalis* M439 species respectively. The nearly equal values of K_b for all the species indicate that the interaction between the bacteria and the composite is non-specific. However, the quantitative nature of the interaction is startling and thus provides a good mean for their accurate estimation.

The Au NP-polythiophene composite, at pH 3.0, is in the completely protonated form (AH^+) and bacterial cell surfaces are known to be negatively charged possibly due to the presence of either teichoic acid in gram positive bacteria[11] or the outer membrane lipopolysaccharide present in gram negative bacteria.[12] It is plausible that the positively charged composite interacts with the negatively charged cell surfaces of the bacteria leading to the reduction of fluorescence intensity of the composite. Interestingly, when extracted bacterial cell surface proteins were added to

the composite solution, no change in fluorescence could be observed (data not shown), thus indicating that cellular macromolecules other than protein may be involved in the interaction. This could be similar to the interaction between chitosan - a known antimicrobial agent - and the bacteria where the cell surfaces of the bacteria get attached to the positively charged chitosan leading to annihilation of the bacteria.[13] However, the role of Au NPs present in the composite in the attachment of the bacteria cannot be completely ruled out, for which further investigations are required. A schematic representation of the charge-based interaction between the composite and the bacterial cells leading to loss of total fluorescence is shown in scheme 4.1.

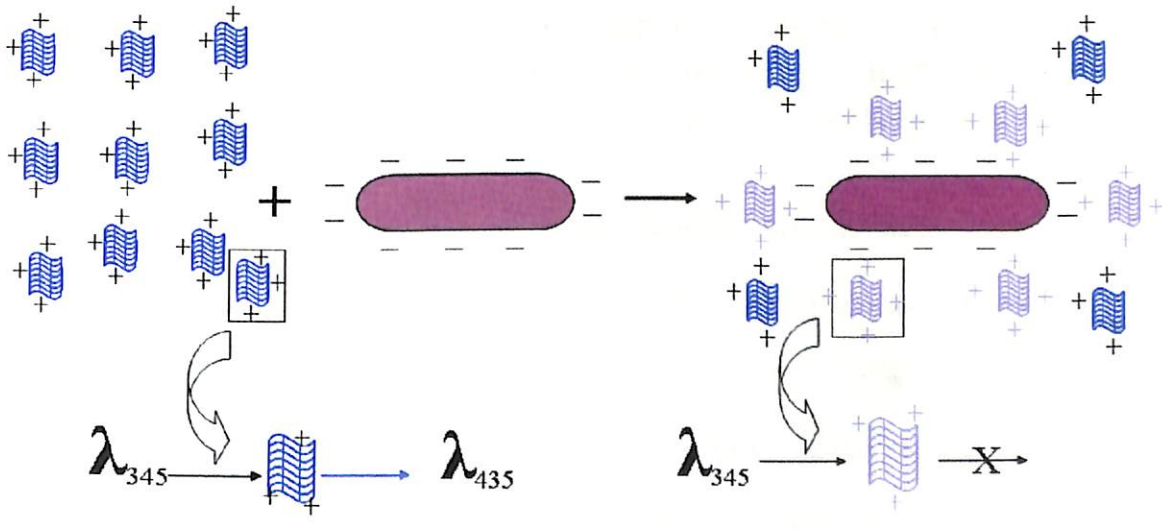

Scheme 4.1 A schematic representation of interaction between positively charged composite and bacteria leading to loss of fluorescence.

The interaction between the bacteria and the composite was further probed using transmission electron microscopy (TEM). Investigation of drop-coated composite on a TEM grid revealed the presence of small NPs of Au, with diameters in the range of 5-10 nm, interspersed uniformly in the polymers that were fibrilar in shape (Figure 4.3A).

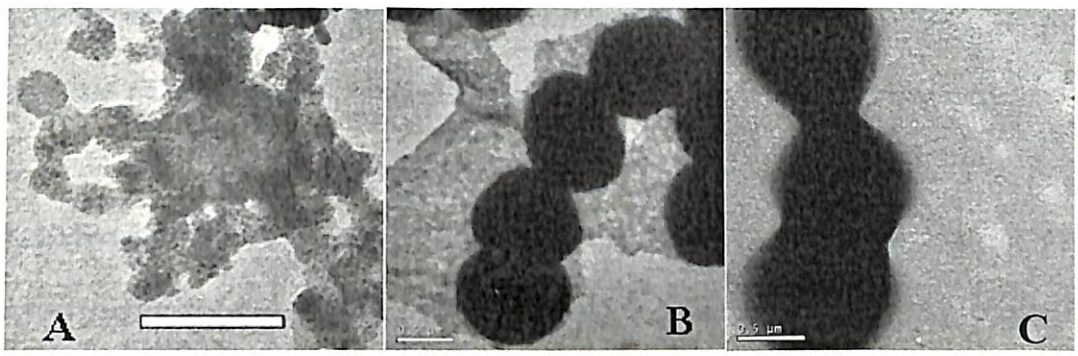

Figure 4.3 TEM image of Au NP – polythiophene composite (A); Au NP – polythiophene composite and *Pediococcus acidilactici* CFR K7 strain mixed together (B); *Pediococcus acidilactici* CFR K7 strain only (C). The scale bar is 100 nm in (A), 0.5 μm in (B) and (C).

When the bacteria-treated composite solution was similarly observed through TEM (Figure 4.3B) then bacteria (cells of P. acidilactici CFR K7) being attached to the composite could be observed. Interestingly, there was neither any indication of the bacteria being lysed nor was there any significant deformation of the bacteria upon attachment with the composite. A micrograph of bacteria, as shown in Figure 4.3C compares well with those attached to the composite.

The quantitative attachment of the polymer species onto bacterial cell surface was ascertained by dynamic light scattering experiments wherein the particle size distribution of the polymer composite, bacterial cells alone and a mixture of cells and the composite were analysed (Figure 4.4). It is clear from Figure 4.4A that the majority of the composite particles were submicron in size with a large number of particles being in the range of 100-300 nm in sizes, whereas the bacterial cells displayed an average size of about 3-4 μm (Figure 4.4B). When the composite and the bacterial cells (10^4 CFU) were mixed together the particle size distribution characteristic for the smaller sized composite diminished indicating preferential attachment of the smaller size composite species to bacterial cells (Figure 4.4C). Also, the overall relative particle size distribution at above 3 μm increased indicating the formation of composite-bacteria particles, in addition to the presence of free composite particles. The propensity of this diminution of particle size distribution for the composite was even more pronounced when a higher number of bacterial cells (10^5 CFU) were added to the composite solution (Figure 4.4D). Here, the relative number of particles above 4 μm was also significant. Collectively, the results clearly indicate a quantitative interaction between the polymer composite and the bacterial cells and demonstrate the preferential attachment of smaller size polymer species onto the bacterial cell surface. Thus, selection of smaller size Au NP-polythiophene composite can possibly enhance the sensitivity of bacterial quantitation. On the other hand, relatively larger size particles (composite) were also attached to the bacteria especially when the concentration of the bacteria was higher. However, the change in fluorescence intensity seems to be independent of the size distribution of the

composite as several samples prepared under identical conditions produced small differences in particle size distribution and also that did not seem to affect the present way of estimating bacterial concentrations.

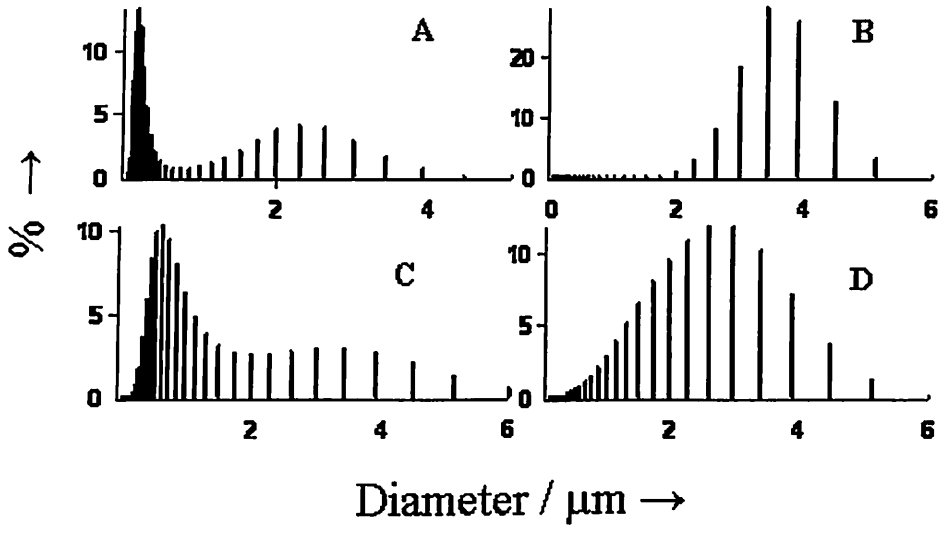

Figure 4.4 Particle size distributions of Au NP-polythiophene composite (A), cells of *Pediococcus acidilactici* CFR K7 (10^5 cells) (B) and a mixture of the composite and bacterial cells (C and D). Bacterial cell numbers are 10^4 in C and 10^5 in D respectively.

Sensing and quantification of bacterial cells is not only technologically challenging but also scientifically intriguing. While it is important to find routine and facile methods of estimating bacteria in a laboratory or industrial setup, understanding the modus operandi of such methods is equally important to innovate and formulate sensing platforms which would be amicable for automation and serve as the next generation gold-standards in rapid microbiological methods. In the present case, a new composite of mono-chlorinated polythiophene-Au NP that is highly fluorescent, while being dispersed in aqueous solution as small particles, has been found useful in

measuring bacterial cells with high accuracy over a wide range of concentrations and also to be able to estimate reasonably smaller number of bacteria. The method allows quantification of different kinds of bacteria too, opening the possibility of wider applications. It is interesting to observe that interaction between the bacteria and the composite appears to be independent of size (molecular weight) of the polymer. This possibly indicates that the interaction of bacteria with the composite leads to the quenching of the fluorescence from the electronic excited state, which possibly is a unit smaller than the size of the polymer. This is important in a sense that in future if systematic changes in the backbone of the polymer could be made and thus the nature of emission as well as interaction could be controlled then sensing of individual bacterial species as well as their detection in a quick and precise manner could be carried out. This requires clear understanding of the interaction between the composite and the bacteria, which is our future goal.

How ? Interaction is electro-static.

Reference and Notes

1. J. P. Nataro, J. B. Kaper *Clin. Microbiol. Rev.* **1998**, 11, 142.
2. A. K. Deisingh, M. Thompson *J. Appl. Microbiol.* **2004**, 96, 419.
3. T. Geng, M. T. Morgan, A. K. Bhunia *Appl. Envir. Microbiol.* **2004**, 70, 6138.
4. K. Matsuda, H. Tsuji, T. Asahara, Y. Kado, K. Nomoto *Appl. Envir. Microbiol.* **2007**, 73, 32.
5. X. Zhao, L. R. Hilliard, S. J. Mechery, Y. Wang, R. P. Bagwe S. Jin, W. Tan *Proc. Natl. Acad. Sci.* **2004**, 101, 15027.
6. F. Su, Y. Endo, H. Saiki, X. Xing, N. Ohmura *Biosens. Bioelectron.* **2007**, 22, 2500.
7. D. A. Boehm, P. A. Gottlieb, S. Z. Hua *Sensors and Actuators B* **2007**, 126, 508.
8. S. Rossetti, M. C. Tomei, L. L. Blackall, V. Tandoi *Lett. Appl. Microbiol.* **2007**, 44, 643.
9. B. R. Panda, A. Chattopadhyay *J. Coll. Inetrf. Sci.* **2007**, 316, 962.

10. B. Valeur in *Molecular Fluorescence*, WILEY-VCH, Weinheim, **2002**, pp. 50-51.
11. V. Berry, A. Gole, S. Kundu, C. J. Murphy,R. F. Saraf *J.Am.Chem.Soc.* **2005**, 127, 17600.
12. W.W. Wilson, M.M. Wade, S.C. Holman, F.R. Champlin *J. Microbiol. Methods* **2001**, 43, 153-164.
13. Y.Hu, Y. Du, J. Yang, Y. Tang, J. Li, X.Wang *Polymer* **2007**, 48, 3098-3106

CHAPTER – V

Estimation of H_2O_2 using Fluorescence Emission of a Surfactant Stabilized Au Nanoparticle-Polythiophene Composite

Introduction

Estimation of H_2O_2 concentration with high precision is not only important in chemistry but also in many biological phenomena. For example, H_2O_2 plays an important role in plant metabolism. Gene encoding antioxidant enzymes are regulated by H_2O_2. Besides this, expression of genes encoding proteins that are potentially involved in programmed cell death (PCD), as well as signaling proteins such as calmodulin, protein kinases and transcription factors (TFs) are also modulated by the peroxide in plant cells. Moreover H_2O_2 is known to inactivate K^+ channels, to cause cytosolic alkalinisation and to activate plasma membrane Ca^{2+} channels. Further, a number of enzymes are known to release H_2O_2 from specific substrates. So, a reliable and simple method for H_2O_2 assay is of considerably significance from the points of view of analytical biochemistry and clinical diagnostics.

Classical inorganic chemistry technique based estimation of H_2O_2 is performed either by titrating against KMnO4 or iodometrically.[1] However the problems with accuracy in the estimation using permanganometry method, especially in the presence of an oxidizing competitor and the sensitivity and time consuming titration based methods, call for a simple, specific and ultra sensitive technique. The established technique for glucose estimation in biological samples is by oxidizing the substrate with the enzyme glucose oxidase, followed by quantitative electrochemical estimation of the product hydrogen peroxide (H_2O_2). The same strategy is also followed for clinical and commercial glucose estimation purposes. Additionally, for micro quantities of H_2O_2 estimation in biological samples a large number of published

methods utilize the principle of coupled oxidation, where catalase or peroxidase combines with liberated H_2O_2 to form a complex that brings about the oxidation of substances such as nirite,[2] ethanol,[3] cytochrome c,[4] or manganous ions in the presence of p-cresol.[5] The extent of these oxidations may be measured by manometric, colorimetric or spectrometric means, having the advantage of greater sensitivity. In this context Andreae[6] and subsequently Perschke and Broada[7] utilized fluorescent scopoletin (6-methyl-hydroxy-1,2-benzopyrone), which gets oxidized stochiometricaly (1:1) by H_2O_2 to a nonfluorescent compound. Further, a few reducing substances such as ascorbic acid, glutathione and manganous ions competitively inhibit the oxidation of scopoletin, thus making the process less general. On the other hand, esculetin - a phenolic coumarine derivative - is more readily oxidized and does not suffer from the interference of ascorbic acid. However, the weak fluorescence and the catalytic effect of phenolic oxidase on its oxidation make it unsuitable for an exclusive replacement of scopoletin. Keston and Brandt[8] used diacetyldichloro- fluorescin - a stable nonfluorescent reagent - as a replacement for scopoletin, which after activation by alkali, becomes fluorescent when treated with peroxidase and a small amount of H_2O_2. Unfortunately, the peroxidase – fluorescent substrate/product combinations fail to assay H_2O_2 in plant extracts, which contain relatively high levels of endogenous substrates for peroxidase. The difficulty in purification of these interfering compounds makes it less attractive to use the present methods of estimation of H_2O_2. Interestingly, H_2O_2 forms a yellow colored complex on reaction with titanium(IV) that absorbs at 410 nm in acidic solution.[9,10] Patterson

et al.[11] discovered that a complex of Ti(IV) with 4-(2-pyridylazo) resorcinol has higher sensitivity of detection of H_2O_2 over Ti(IV) alone. Recently there are significant efforts being devoted in developing nanotechnology based sensors for H_2O_2.[12-14]

In this chapter, we report a fast, easy and reliable technique to measure trace amounts of H_2O_2, based on the fluorescence emission of a new surfactant stabilized gold nanoparticle – polythiophene composite (Au NP - PTH) in aqueous solution. The composite, synthesized by the reaction of thiophene and $AuCl_4^-$, is stable and has a strong fluorescence at 450 nm when excited by light at 360 nm. The method involves treatment of the composite with different amount of the commercially available hydrogen peroxide in alkaline condition (pH > 12) and measuring the subsequent decrease of fluorescence intensity. The decrease in intensity varies linearly with the concentration of H_2O_2 thus making the measurement simple and robust. Also, the method is highly sensitive and H_2O_2 concentration as low as 0.2 mM could be estimated using the present scheme. To the best of our knowledge, this is the first report on the use of a composite of a fluorescence polymer and Au NPs in quantitative estimation of H_2O_2.

Experimental section

Materials

Sodium dodecyl sulfate (SDS, >99%), thiophene (>99%) and $HAuCl_4$ (30 wt. % $HAuCl_4$ in dilute HCl, 99.99%) were procured from Sigma–Aldrich. The alkali

(NaOH) and H_2O_2 used in the titration were procured from Merck India Ltd. Milli-Q grade water was used throughout the experiments.

Methods

The PTH – Au NPs composite was synthesized using the following method. A homogeneous mixture of thiophene of 30.0 mM strength was prepared by mixing the requisite amount of thiophene in a 10.0 ml of 8.3 mM (critical micellar concentration, CMC) SDS solution in water and at room temperature (~25 °C). This was followed by addition of 30.0 μL of 1.72×10^{-2} M $HAuCl_4$, prepared from 30 wt % $HAuCl_4$ in dilute HCl. The above mixture was then kept in a mechanical shaker operating at 150 rpm and 25° C. It was observed that a purple colored solution was produced in an hour. The shaker was kept on for a two days. TEM images were recorded, after evaporation of a drop of the as-prepared solution on a carbon-coated copper grid, using a JEOL transmission electron microscope (TEM; Model: JEM-2100) operating at 200 keV accelerating voltage. In order to perform emission measurements with different concentration of H_2O_2 at alkaline pH, 100.0 mL of the solution (pH = 3.1), collected from a few identically prepared composite solutions, was made alkaline (pH >12) by addition of NaOH (aq). Now for every sample 1 mL of the above alkaline composite solution was diluted to 2.95 mL with Milli-Q grade water and 50 μL of H_2O_2 (concentration of which was different for different sample) was added. The composite solution was diluted (as above) in such a way that the final absorbance at 360 nm is ~ 0.2 for all samples. The resulting solution was mixed thoroughly, and the absorption and emission spectra of the same were recorded (at 15 min after

mixing) using a Perkin Elmer (Lambda 25) UV/VIS spectrometer and a Varian (CARY-Eclipse) fluorescence spectrophotometer respectively.

Results and discussion

The UV-vis absorption spectrum of the as-prepared composite consisted of a single peak at 540 nm (Figure 5.1 a), which is characteristic of the absorption due to surface plasmon resonance of Au NPs. This indicates the formation of Au NPs in the medium. It may be mentioned here that the method of synthesis of the composite here is the same as that reported in chapter III, except for the fact that here SDS was used as the stabilizer which was not the case in the previous experiments. The presence of SDS helped stabilized the composite and no precipitation was observed subsequent to the formation of the composite. As a result the intensity of the peak due to Au NP was sufficiently strong to be able to observe spectrophotometrically, which was not possible in previous experiments. In other words, the stabilized composite were well dispersed in the medium and the concentration was high enough to be able to pursue further experiments utilizing the properties of the composite. Also, important to mention here is that since the nature of the composite was similar to that reported in the previous chapter, the details of structural analysis are not addressed separately here. On the other hand, since the composite has been used for the detection of H_2O_2 its structural and optical properties are addressed comparatively before and after treatment with H_2O_2, the details of which are mentioned below.

It is important to mention here that in order to optimise the faster detection of H_2O_2 utilizing the properties of the composite, the pH of the medium had to be kept above 12.0. At lower pH the composite was found to be insensitive to the presence of H_2O_2 for 1h. Further, our observations indicate that in the presence of H_2O_2, the UV-Vis spectrum of the composite (due to Au NPs) virtually did not alter (up to 10.0 mM). For example, when the composite was treated with 0.23 mM, 0.46 mM, 0.91 mM, 1.83 mM, 3.66 mM and 7.31 mM H_2O_2, there was no change in the spectrum due to absorption of Au NPs. As an example, one spectra for the sample without the treatment of H_2O_2 (Figure 5.1a)and other two where the composite was treated with 0.23 mM (Figure 5.1b)and 7.31 mM (Figure 5.1c) peroxide respectively are shown in Figure 5.1. As is clear from the spectra there is no effect of H_2O_2 on the absorption due to SPR of Au NPs. Since, at the above concentration range of H_2O_2, since the peak at 540 remained unchanged, this indicates that there is no change in size or shape of the NPs subsequent to the interaction of the peroxide with the composite. Also, this precludes the formation of agglomeration of the NPs, as that would have given rise to broadening or red-shift of the peak, which was not the case herein.

TEM analysis of the composite as shown in Figure 5.2, indicates that the Au NPs formed in the medium were of uniform spherical sizes and the typical size distribution was 9 ± 1.5 nm. Further, when the sample was treated with alkali and the pH of the medium was set at 12.5, there was no change in particle shape or size. This is evident from the TEM image of the sample shown in Figure 5.2b. Also, there was no apparent agglomeration of the particles.

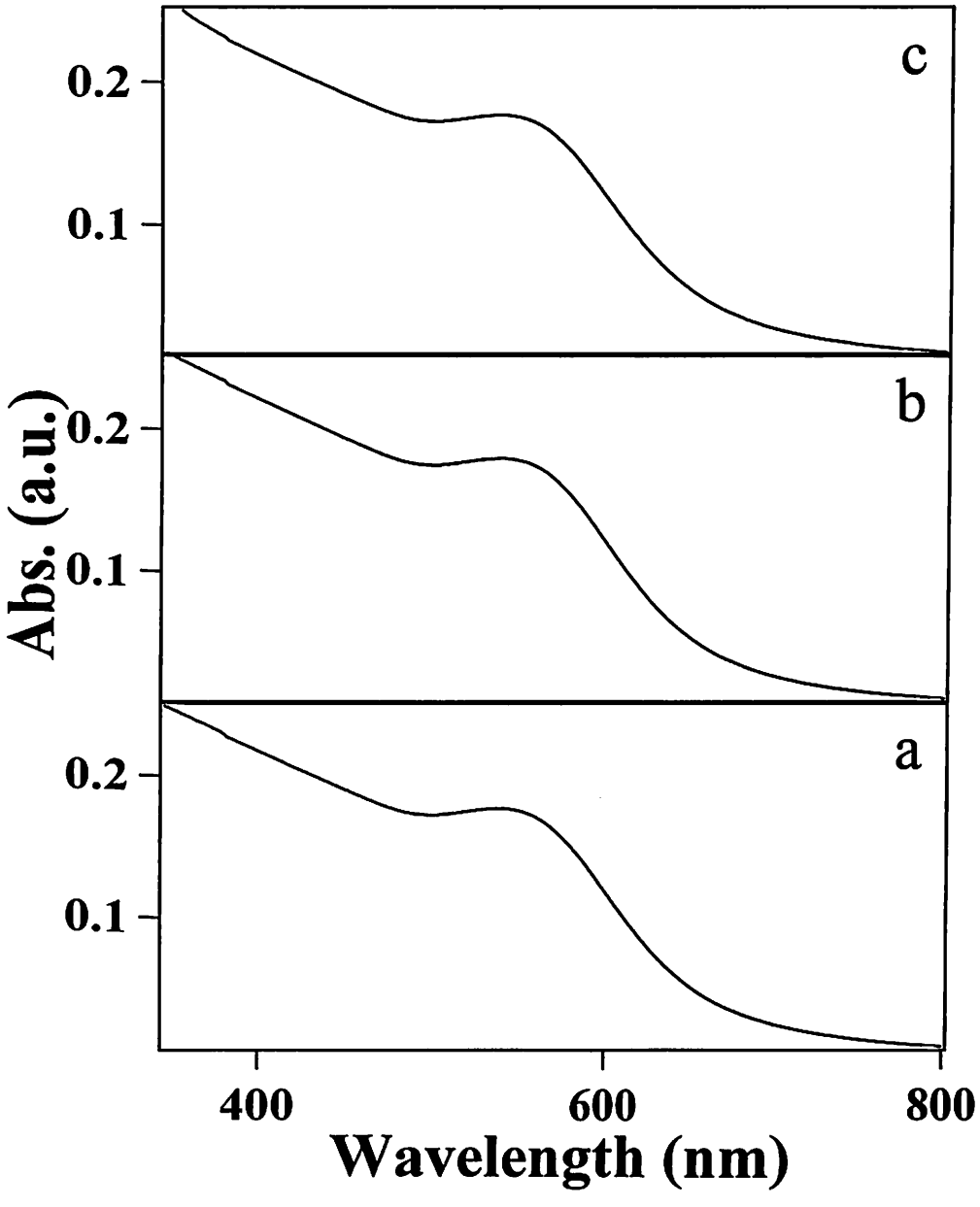

Figure 5.1 Absorption spectrum of the alkaline SDS stabilized Au NP - PTH with out H_2O_2 **(a)** and in the presence of H_2O_2 (**b** : 0.23 mM, **c** : 7.31 mM).

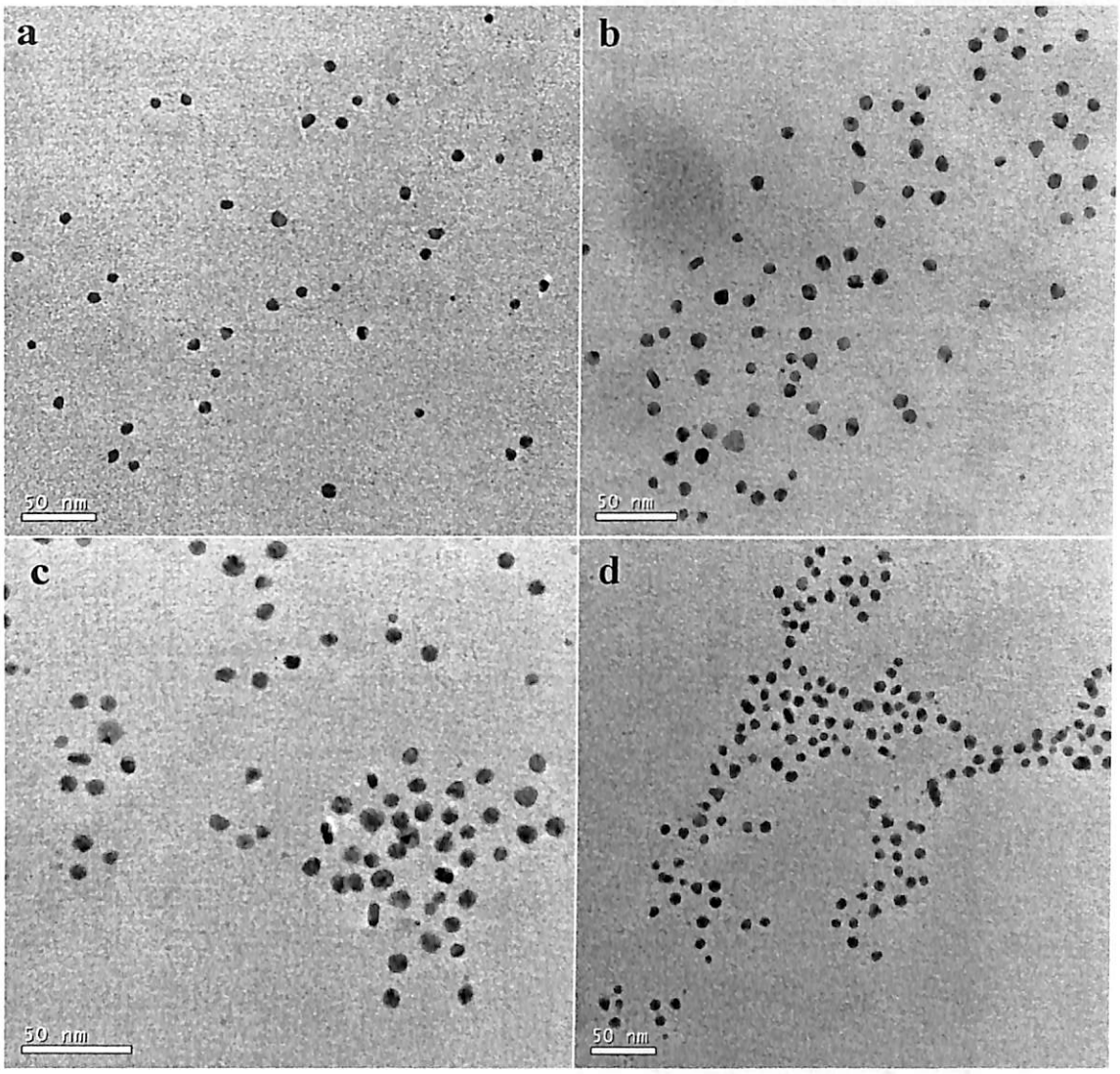

Figure 5.2 TEM images of the SDS stabilized Au NP - PTH composite sample (a) as prepared (pH ~ 3.1), (b) which made alkaline (pH ~ 12.5), and the alkaline composite in the presence of (c) 0.23 mM and (d) 7.31 mM H_2O_2.

Figures 5.2(c) and (d) are the TEM images of the samples where the composite in alkaline medium was treated with 0.23 mM and 7.31 mM H_2O_2 respectively. It's clear from the images that the size and shape of NPs were not

affected by the addition of H_2O_2. Nor there was any discernible agglomeration of the particles in the presence of peroxide. Thus addition of H_2O_2 to the samples did not affect the Au NPs present in the composite.

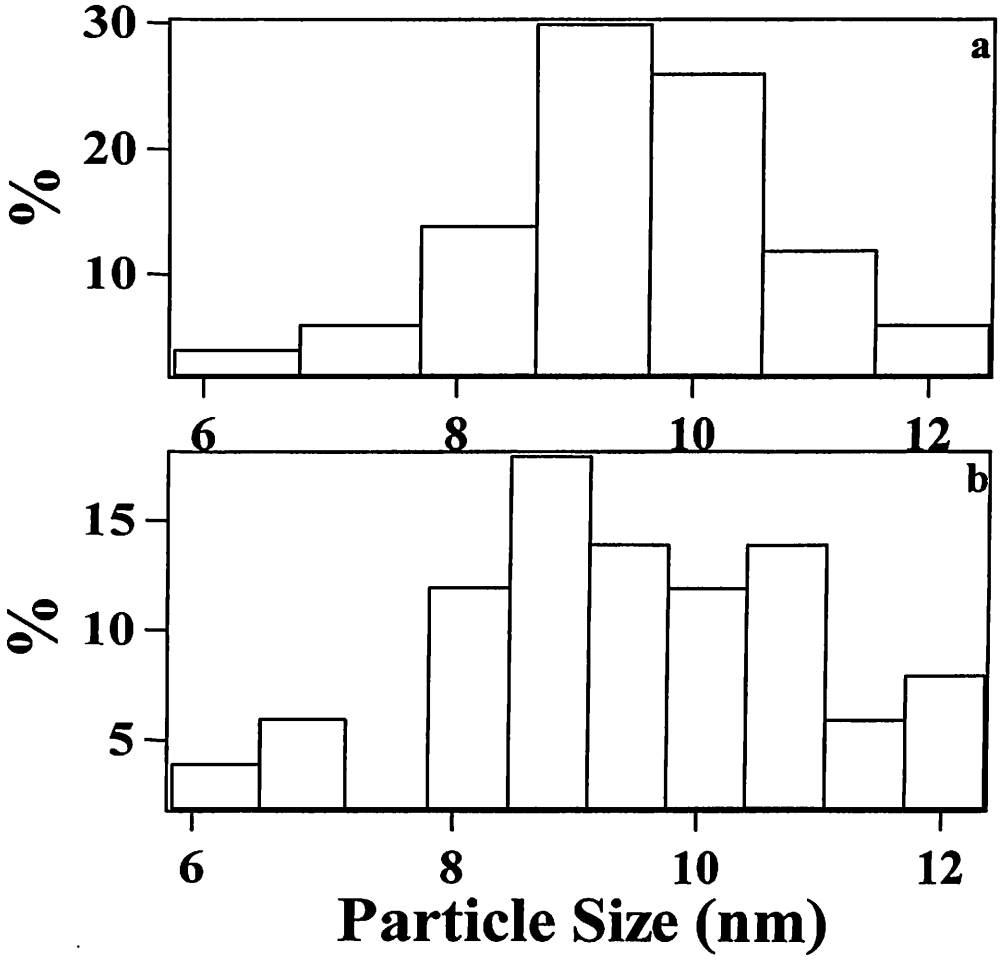

Figure 5.3 Particle size distributions of Au NPs in the composite (a) which was made alkaline (pH ~ 12.5), and (b) the alkaline composite in the presence of 0.23 mM H_2O_2.

In addition, the dynamic light scattering based particle size analysis revealed that there was not change in particle size distribution upon addition of H_2O_2. For example, as hown in Figure 5.3a, the particles produced in the medium had distributions between 6-12 nm in diameters. When 0.23 mM of H_2O_2 was added to the solution there was not much change in particle size distribution as shown in Figure 5.3b. Essentially, the addition of H_2O_2 did not have any effect on the particle size and shape of the composites especially the Au NPs.

Fluorescence spectrum of the composite consisted of a single intense emission peak with maximum at 450 nm, when excited by light of wavelength 360 nm (Figure 5.4a). The pH of the medium during the recording of the above spectrum was kept at 12.5. Unlike the absorption spectrum, the emission spectrum of the composite was found to be highly sensitive to the presence of trace amount of H_2O_2. Although, the wavelength of emission did not change, the intensity of emission decreased with the increase in the concentration of H_2O_2 in the sample. For example, in the presence of 0.23 mM, 0.46 mM, 0.91 mM, 1.83 mM, 3.66 mM, 7.31 mM of H_2O_2 emission spectral intensity of the composite decreased as shown in Figure 5.4 (b-g). A plot of the area under the fluorescence curves versus the concentration of H_2O_2 (shown in Figure 5.5) indicated a linear dependence of emission intensity on the concentration of the peroxide. It was observed that the linearity was followed when the concentrations of the H_2O_2 in the medium was below 4 mM. At concentrations above 4 mM the dependence varied randomly and is thus not reported. Furthermore, it was observed that the lowest concentration of H_2O_2 that could be measured using the

change in fluorescence was 0.23 mM. This value is similar to literature values of the limits of detection of H_2O_2 using the conventional methods. It may be mentioned here that although the pH of the medium decreased (by about 1.0) upon addition of H_2O_2 (7.31 mM) the change in fluroescene was not due to change in pH. For example, when the pH of the medium was changed by addition of HCl (by 1.0 unit) there was not change in fluorescence. In other words, the change in fluorescence was due to interaction of H_2O_2 with the composite and not due to change in the pH of the medium.

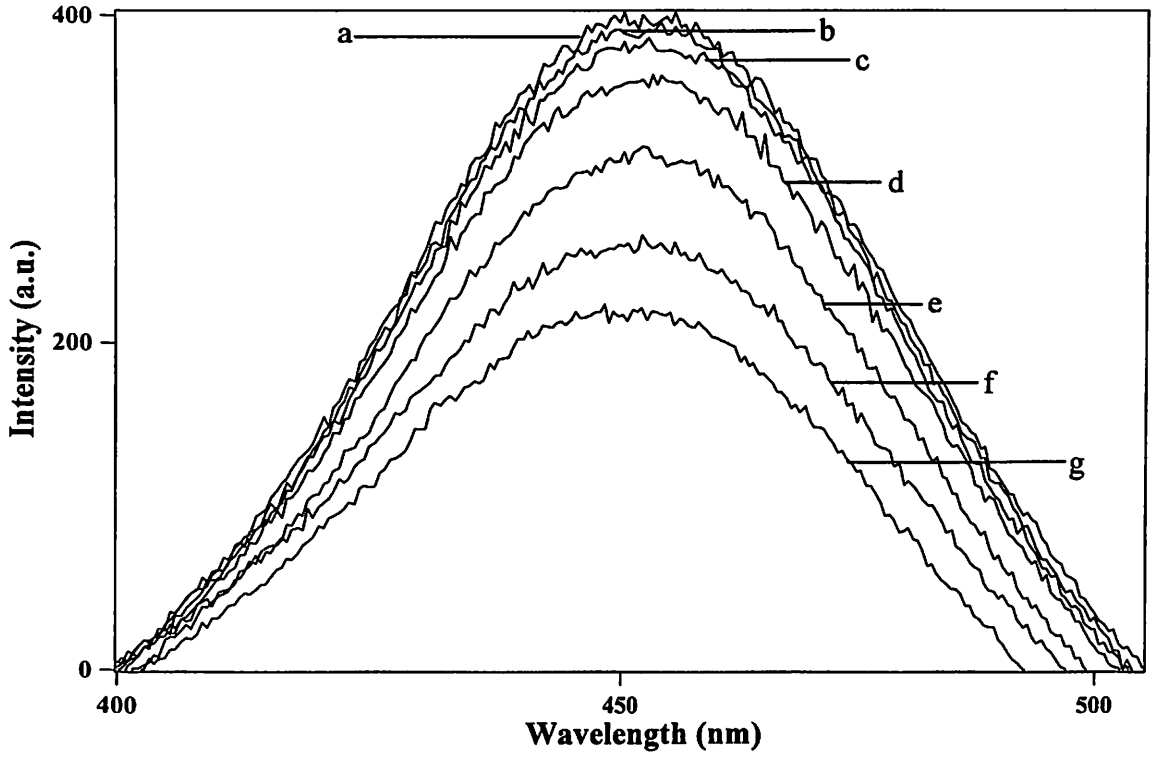

Figure 5.4 A typical emission profile of SDS stabilized Au NP-PTH with out H_2O_2 (a) and in the presence of in the presence of H_2O_2 (b : 0.23 mM, c : 0.46 mM, d : 0.91 mM, e : 1.83 mM, f : 3.66 mM, g : 7.31 mM).

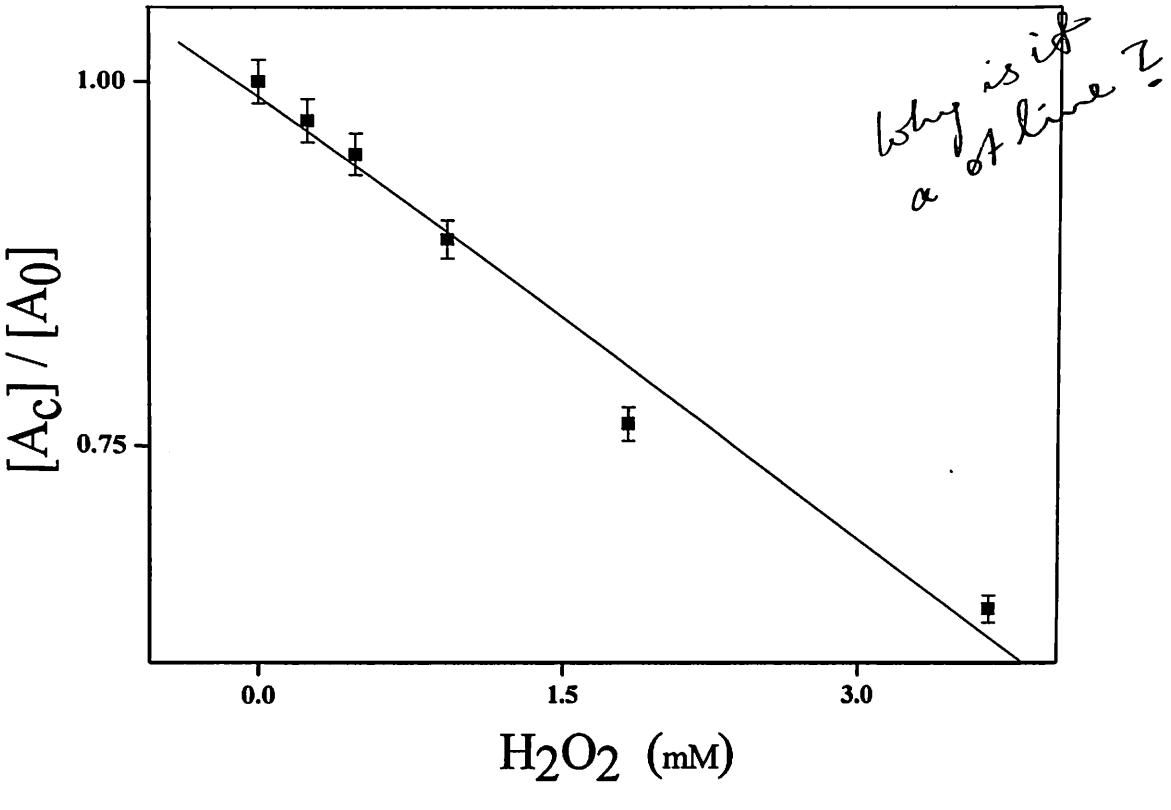

Figure 5.5 correlation between the ratio of area of H_2O_2 treated and blank (untreated) SDS stabilized Au NP-PTH sample and concentration of H_2O_2. Area calculated in the wavelength range of 405 nm to 490 nm.

A question may arise as to the origin of the change in fluorescence. As described before the presence of H_2O_2 did not alter the nature of Au NPs. Also, FTIR spectroscopic measurements indicated that there was no change in the spectral characteristics of the composite when H_2O_2 was added at pH 12.5, vis-à-vis the spectrum of the untreated composite at that pH. Of course these samples were dried at that pH and then FTIR spectra were recorded of the solid samples. Thus the FTIR spectroscopic measurements ruled out any gross change in the structure of

functional groups of the composite. It is plausible that when the composite is treated with H_2O_2 there is the loss of the bonding between Au NPs and the polymer in the composite. The bonding between the NPs and the polymer could be electrostatic in nature and that could be susceptible to replacement by H_2O_2. This may be due to the occupation of the catalytic sites on the surfaces of the NPs by H_2O_2 required for its decomposition. The loss of fluorescence is quantitative as the amount of H_2O_2 occupying the NP surfaces is fixed. Hence there is a quantitative dependence of the decrease in fluorescence intensity with the amount of H_2O_2. It is also interesting to mention here that when the composite was treated with aquaregia the SPR spectrum due to Au NPs was completely lost. On the other hand, when the sample was then treated with alkali to set the pH at 12.5 followed by treatment with H_2O_2 there was a large shift in wavelength, which appeared to be very different from the original sample. This is possibly due to interaction of H_2O_2 with the polymer. In brief, when Au NPs are bound to the polymer then catalytic decomposition of H_2O_2 by the NPs overwhelms the reaction of the peroxide with the polymer; the catalysis on the surface of the NPs leads to loss of bonding with the polymer. On the other hand, in absence of Au NPs the polymer might get easily oxidized by the peroxide and hence the large shift of emission wavelength.

In brief when the emission intensity of a 3 mL aqueous solution of the SDS stabilize Au NP – PTH composite in the presence of a series of mM concentrations of H_2O_2 were recorded, a systematic decrease in the intensity was observed, with the increase in H_2O_2 concentration in the sample. In our case we studied the effect of H_2O_2, varying its concentration range from 10 mM to 0.2 mM. The decrease in fluorescence intensity of the composite with increasing H_2O_2 concentration provides an excellent opportunity for quantitative and rather accurate estimation of the H_2O_2 concentration. It's noteworthy to mention that though the estimation technique employed here based on decrease in fluorescence, but we are considering the result over many points by calculating the area. So the result is free from the intrinsic disadvantage of methods where difference in intensity between the control and sample at a particular wavelength is generally employed.

The method developed herein could provide an easy and rapid estimation of H_2O_2 without the need for the requirement of sample preparation and other experimental setup required in electrochemical or other measurements. The method is quantitative and linear dependence of fluorescence on the concentration H_2O_2 over a wide range makes its application potential appealing. Overall, the present method takes advantage of intrinsic superiority of fluorescence based method of estimation and the properties of nanoparticles and polymer to estimate the concentration of H_2O_2, an important analyte with important industrial consequences. The present method could form the basis of a general method of testing glucose where the product of gluocose (chemically or biochemically) would be hydrogen peroxide.

High conc. of glucose upto 50 mM ?

References

1. A.I. Vogel *A Text book of Qualitative Inorganic Analysis*, 3rd Ed., Longman and Green, London, **1992**, p. 267.
2. S. Thurlow *Biochem. J.* **1925**, 19, 175.
3. D. Keilin, E. F. Hartree *Biochem. J.* **1945**, 39, 293.
4. A. M. Altschul, R. Abrams, T. R. Hagness *J. Biol. Chem.* **1940**, 136, 777.
5. R. H. Kenten, P. J. G. Mann *Biochem. J.* **1950**, 46, 67.
6. W. A. Andreae *Nature* **1955**, 175, 859.
7. H. Perschke, E. Broda *Nature* **1961**, 190, 257.
8. A. S. Keston, R. Brandt *Anal. Biochem.* **1965**, 11, 1.
9. W. M. Macnevin, P. F. Urone *Anal Chem* **1953**, 25, 1760.
10. T. Brennan, C. Frenkel *Plant Physiol.* **1977**, 59, 411.
11. B. D. Patterson, E. A. Macrae, I. B. Ferguson *Anal. Biochem.* **1984**, 139, 487.
12. M. Zayats, R. Baron, I. Popov, I. Willner, *Nano Lett.* **2005**, 5, 21.
13. H-L. Zhang, G-S. Lai, D-Y. Han, A-M. Yu *Anal. Bioanal. Chem. 2008*, 390, 971.
14. S. Liu, Z. Dai, H. Chen, H. Ju *Biosens. Bioelectron.* **2004**, 19, 963.

CHAPTER – VI

Electrochemical Actuation of Growing Copper Dendrimers in Water

Introduction

Actuators are artificial muscles having the ability to convert electrical and/or chemical energy directly into mechanical energy describing linear or angular movements because of the inherent property of its constituting materials that change in shape and dimension on exposure to a potential. So, they have wide applications in the fields of robotics, optical communication, prosthetic devices or microscopic pumps and in the miniaturization of electronic or optical devices. Ferroelectric and piezoelectric crystals are two leading member of this family, which are currently exploited for the mentioned purposes. However, the requirement of high working voltages of these materials, going to be a hindrance in their popularization. Hence increasing effort is being devoted to explore their alternatives such as gels,[1] conducting polymers[2] and carbon nanotubes.[3] Gu and co-workers[4] reported that on applying an electrical signal, sheets of vanadium oxide nanofibres contract reversibly like artificial muscles (actuators).

One of the primary focuses of nanotechnology based devices[5,6] is the fabrication and operation of nanoscale actuators, which could be controlled by internal as well as external handles. Solution - based actuators assume significance in the wake of observation of actuation of nanoscale structures with electrical[7-9] or self-generated forces[10] and of devices like the single molecule torsional pendulum made of carbon nanotubes.[11] In addition, there has been a recent surge in efforts in making polymer based actuators.[12] Also, there have been reports of observation of actuation in fluidic devices.[13] Further, autonomous movements have been induced into self-assembled structures[14] using gas bubbles generated by decomposition of H_2O_2. Although, there have been several reports of the generation of metal nanofibers,

including electrochemical generation,[15-19] there is no report of actuation of mono or bimetallic fibrous structures in aqueous solution, which are important in the generation of futuristic devices. These structures would be significant as they can be self-assembled from hybrid materials and would exhibit actuation in the presence of appropriate fields like electric, magnetic or a combination of both, because of specific molecular and ionic interactions in a solution.

In this chapter the unprecedented observation of electrochemical actuation in growing dendritic fibers[19] is reported. The dendritic structures were made of self-assembled copper nanostructures, on the cathode of an ordinary aqueous electrochemical cell, with a copper anode and any common metal cathode, upon application of a DC voltage in the range of 1.5-12.0 V, and in the presence of one of the species like dilute HCl, $CuSO_4$, $CuCl_2$, H_2O or a host of other salts. Typical scanning electron microscopic images of fibers grown identically on glass slides, exhibited dendritic fibers consisting of self-assembled Cu structures of 100 nm or less in diameter. In addition, the fibers generated in the three-dimensional cell also had similar structures and components. The presence of a non-copper metal cation in the solution resulted in bimetallic fibers consisting of Cu (from Cu^{2+} released by the anode) and the other metal from solution. The fibrous structures remained stretched as they grew longer with time. The extent of actuation was dependent on the applied voltage, the concentration of Cu^{2+} ions in the solution and also ions like Na^+ which did not get deposited at the cathode. The observed angle of actuation with voltage is consistent with the Lippmann equation, based on electrocapillarity.[20]

Materials and Methods

Silver (Ag), Aluminium (Al), Gold (Au), Copper (Cu) wires and stainless steel (SS) plates used in the experiments were obtained from commercial sources. HCl (~ 11.3 M), $CuSO_4.5H_2O$, $CuCl_2.2H_2O$, $CdCl_2$, $CoCl_2.6H_2O$, $Pb(NO_3)_2$, $AgNO_3$, $ZnCl_2$, $NiCl_2.6H_2O$ used herein were obtained from Merck (India) and $HAuCl_4$ (Hydrogen tetrachloroaurate (III), 17 wt. %,) was procured from Sigma-Aldrich. For cathode we used either commercially available Ag wire (~2 mm diameter) or Al wire (~2 mm diameter) of typically 5 cm in length or SS plate (dimension ~1 cm x 3 cm). Aqueous solution of HCl, $CuSO_4$, $CuCl_2$, $CdCl_2$, $CoCl_2$, Pb $(NO_3)_2$, $AgNO_3$, $ZnCl_2$, $NiCl_2$, $HAuCl_4$ or even milli-Q water were used as electrolytes. While the cathode metal and the electrolyte were varied, the anode was always the same in all the experiments, i.e. a Cu wire of length 5 cm and diameter 2 mm. The two electrodes were placed in the electrolyte; about 2 cm apart in a 100 mL beaker containing 100 mL of the solution and a potential difference was applied across the electrodes using an ordinary DC eliminator. When the concentration of the electrolyte was kept at or below 5.0×10^{-4} M, self-assembled dendritic fibrous structures grew on the cathode. This concentration is an upper limit for the observation of dendritic growth, above which an ordinary deposition of bulk metallic copper on the cathode was observed. Furthermore, we could observe fibrous growth of the structures in as low as 1.0×10^{-7} M concentration of the electrolyte, although it took typically 1 hr to achieve a 10 mm length fibrous structure when a potential of 12.0 V was maintained. On the other hand, under identical conditions, with higher electrolyte concentration of 1.0×10^{-4} M,

it took about 5 min to grow a fiber of similar length. In practice, there is no lower limit of concentration as we find that the fibrous growth of copper could also be obtained with only milli–Q (Millipore) grade (resistivity 18 MΩcm) water as the electrolyte and copper as the anode. However, the deposition was slow, taking about 1 hr to grow to a length of about 10 mm at an applied voltage of 12.0 V, when only 25 mL of milli-Q water was used as the electrolyte. This observation is consistent with report of similar dendritic silver growth from water using Ag as the anode.[19] It is to be noted that fibers grown at lower concentrations are thinner and more fragile than those grown at higher concentrations of the electrolyte. In addition, we find that small amounts of gaseous product evolve at the cathode (possibly H_2) and the anode (possibly O_2 and/or Cl_2). We find that gaseous evolution at the electrodes is greater at lower concentrations of electrolyte and negligible at higher concentrations of the electrolyte used in our experiments.

Composition of the dendritic fibrous structure grown in different electrolytes

Scanning electron microscopic (SEM) and Energy dispersive X-ray (EDX) analysis was pursued for the composition analysis of various fibers. The dendritic fibers were grown on a glass slide using a drop of the respective electrolyte and applying a DC voltage of 6.0 V across the electrodes immersed in the drop. Depending on the electrolyte being used, the dendritic fibers with graded composition may be grown. We have studied a variety of metal salts as electrolytes and find that only those metal cations whose standard reduction potential is less than that of water ($2H_2O + 2e^- \rightarrow H_2 + 2OH^-$, $E^o = -0.83V$) yield the bimetallic fiber. For the salts of these metals

(other than Cu^{2+}), in each case, we obtained graded bimetallic dendritic fibers (**Table 6.1**). In addition, we have collected fibers from the three-dimensionally grown fibers in regular cell and studied them under SEM. For example, the EDX analysis data of fibers grown in the presence of 10^{-4} M $CoCl_2$ at 12 V is given below (Figure 6.1).

Table 6.1 Various combination of electrodes and electrolytes used, with the compositions of the resulting dendritic structures (the slash sign means or)

Cathode (made of single metal)	**Electrolyte**	**Anode**	**Composition of the dendritic structures**
Ag /Al / Au / Stainless Steel (SS)	Dilute HCl	Cu	Only Cu
Ag /Al / Au / SS	$HAuCl_4$ in dil. HCl	Cu	Au and Cu composite
Ag /Al / Au / SS	Aqueous $CuSO_4$	Cu	Only Cu
Ag /Al / Au / SS	Aqueous $CuCl_2$	Cu	Only Cu
Ag /Al / Au / SS	Aqueous $CdCl_2$	Cu	Cd and Cu composite
Ag /Al / Au / SS	Aqueous $CoCl_2$	Cu	Co and Cu composite
Ag /Al / Au / SS	Aqueous $AgNO_3$	Cu	Ag and Cu composite
Ag /Al / Au / SS	Aqueous $ZnCl_2$	Cu	Zn and Cu composite
Ag /Al / Au / SS	Aqueous $NiCl_2$	Cu	Ni and Cu composite
Ag /Al / Au / SS	Aqueous $Pb(NO_3)_2$	Cu	Pb and Cu composite
Ag /Al / Au / SS	Water (milli-Q)	Cu	Only Cu

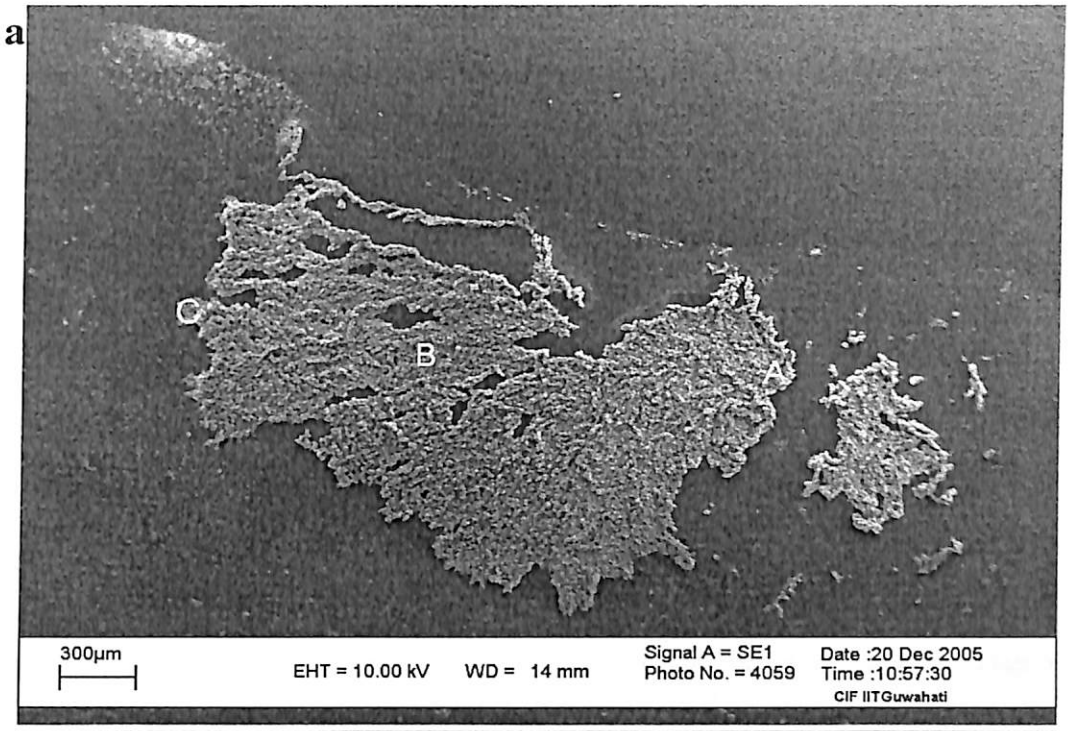

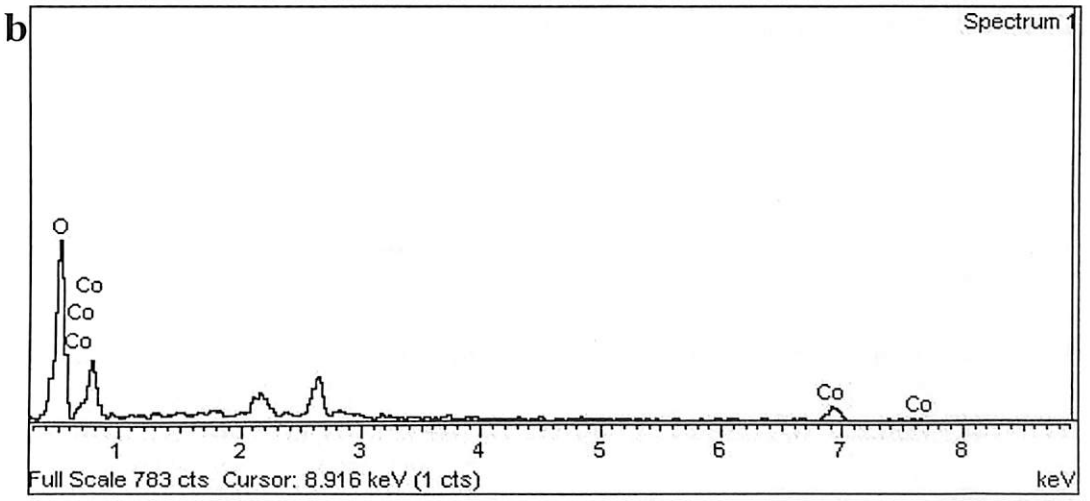

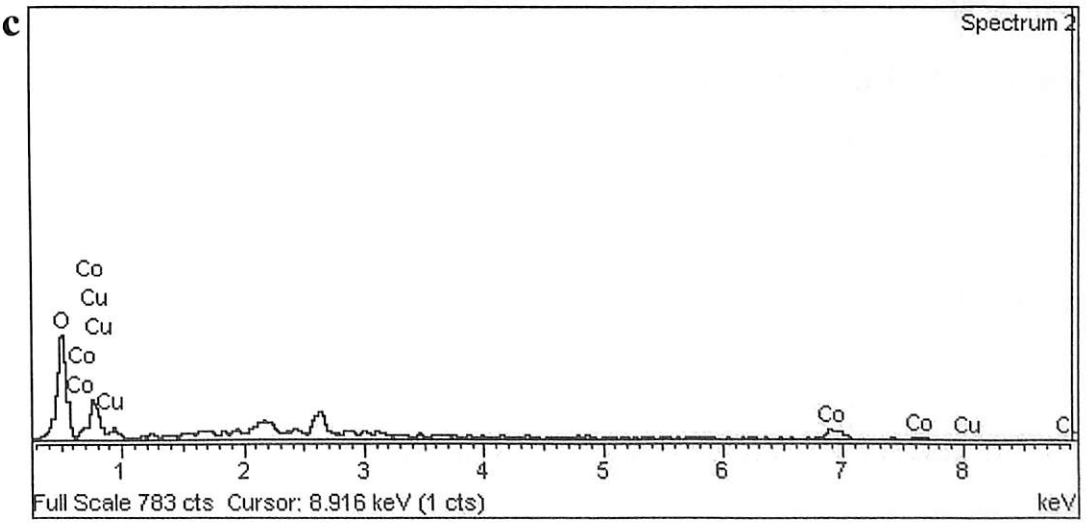

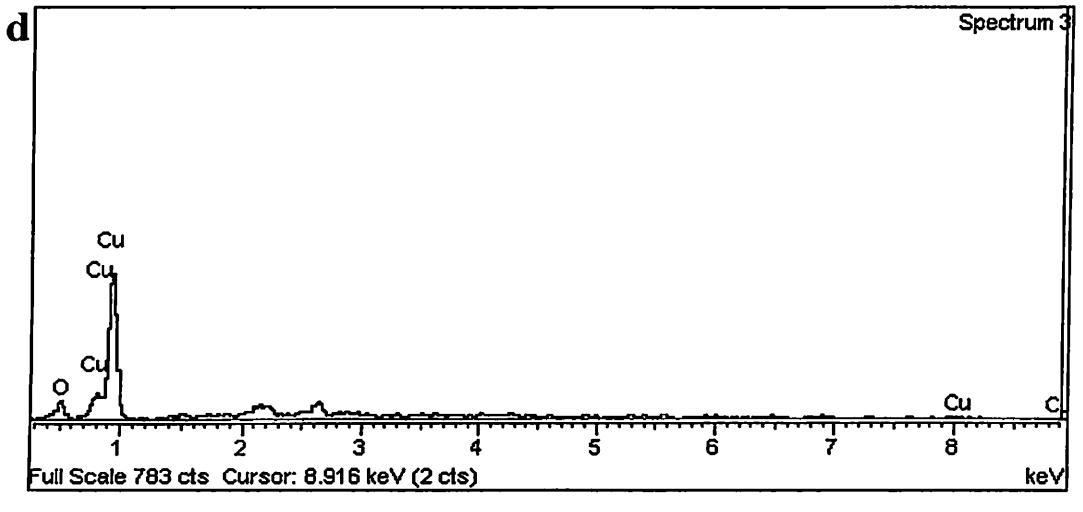

Figure 6.1(a) SEM image of bimetallic nanostructured dendrites (A – location close to the cathode, B – intermediate location, C – location far away from the cathode) on a glass slide, **(b)** EDX spectrum at location A, **(c)** EDX spectrum at location B, **(d)** EDX spectrum at location C.

Results and Discussion

When the salt concentration was kept at a value equal to or less than 5.0×10^{-4} M and copper metal anode was used dendritic fibrous structures continuously grew on the cathode. It was observed that transferring the fibers from the cell to a glass slide for microscopic studies was rather difficult. Hence the same experiment was carried out on a glass slide for the purpose of electron microscopic studies only. Scanning electron micrographs (SEM) of such structures grown identically on a glass slide with cathode and anode clamped firmly to the surface of the glass slide and using a drop of the electrolyte, such that the 'as grown' structure is preserved when recording SEM,

revealed the dendritic growth with assembly of particles that have typical dimensions in the range of 100 nm or less (Figures 6.2a). The close proximity of the glass slide in this setup interferes with appropriate and controlled actuation, possibly due to the role played by the additional interfacial forces, even though we did observed movements of the fibers at the time of the growth on the slides. Hence the actuation results were all recorded on a regular electrochemical setup. We also carried out SEM measurements of regular fibers grown on a regular cell. It is to be noted that because the dendritic structures grown in a normal electrochemical cell had to be lifted off to be observed under SEM, the overall symmetry of the dentritic structure (Figure 6.2b) could have been disturbed in the process. However in this case despite the sample handling, we found that the structures were composed of assembly of particles with dimensions typically in the range of 100 nm very similar to those in Figure 6.2a (inset). This suggests that the mechanism of growth of dentritic fibers is probably similar in the two different electrochemical cells. The actuation could be observed without any hindrance in the normal electrochemical cell as the glass walls were well separated from the growing dentrictic structures. We also mention here that the structures in the regular cell (as well as on glass slides) could be grown at any applied voltage between 1.5 V and 12.0 V and they remained stretched perpendicular to the electrode as long as the potential was applied. Although, the fibers were made up of assemblies of nanoscale structures the final diameters of the fibers were of micrometer sizes and hence the actuation of the fibers could easily be observed by naked eye.

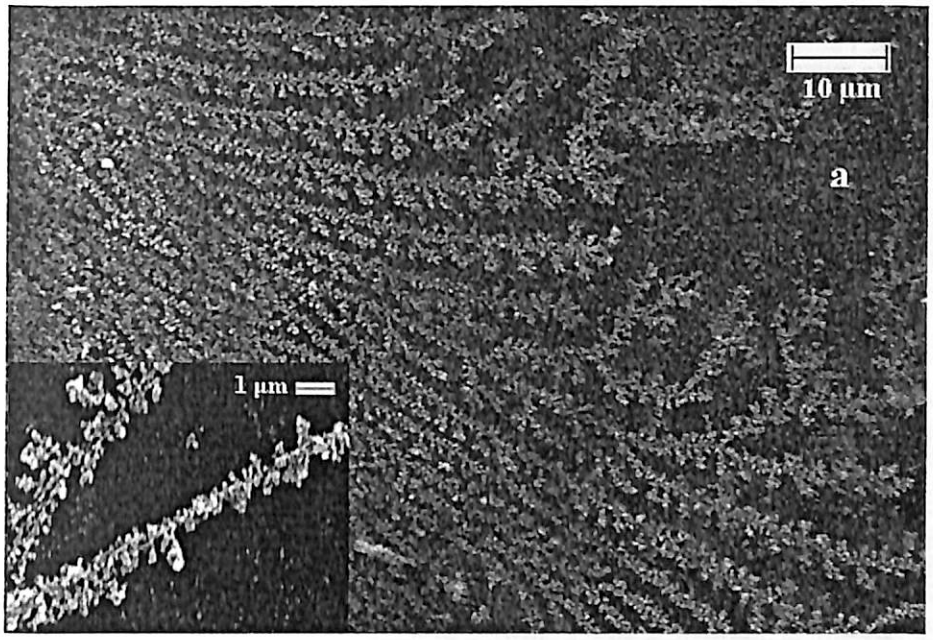

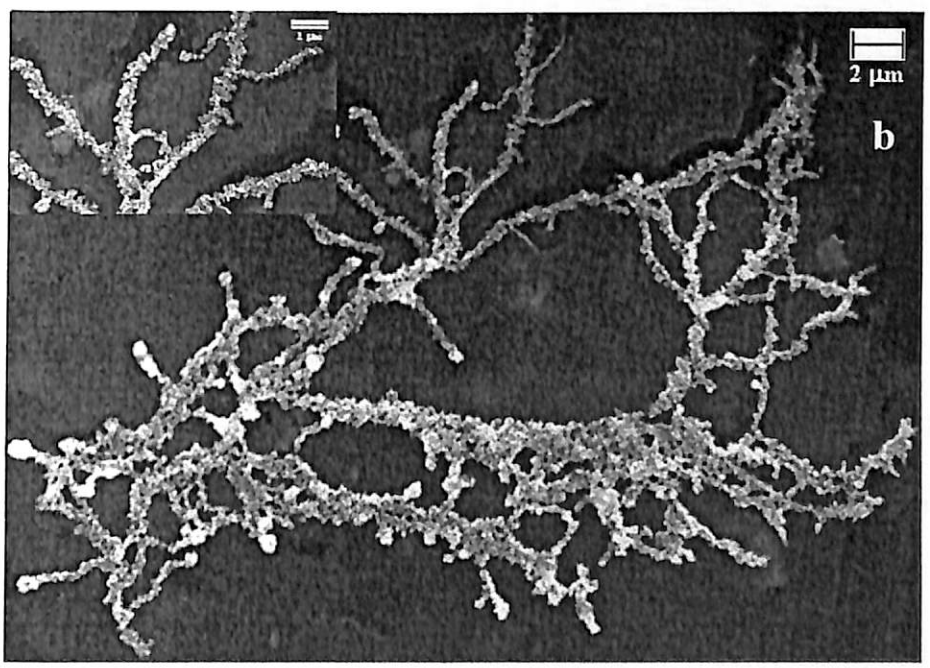

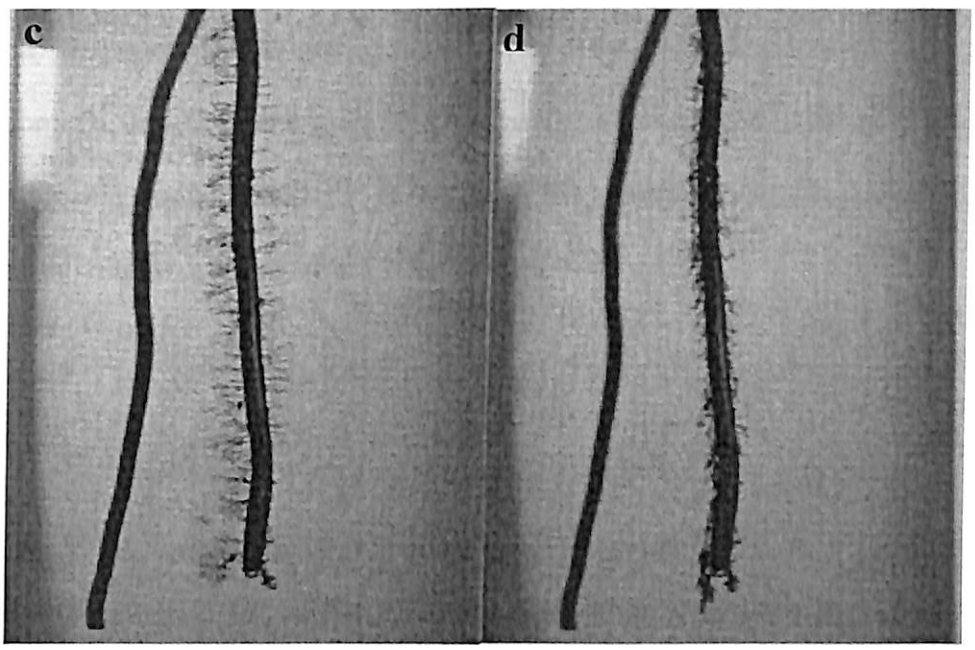

Figure 6.2 (**a**) Scanning electron micrograph of dendritic Cu grown on a glass slide with an expanded view in the inset. (**b**) Scanning electron micrograph of dendritic Cu grown in a regular electrochemical cell with an expanded view in the inset. (**c**) Actuation of fibers at the cathode with field on at 6.0 V and subsequent relaxation with the field off (**d**).

Turning off the voltage turned off the actuation (i.e. the fibers switched to relaxed position along the electrode). The actuation process was reversible as long as the time during the voltage 'off' position did not exceed typically 7 - 9 s. If the time exceeded this limit the fibrous dendritic structures agglomerated, which prevented further actuation in the next voltage "on" cycle. A typical on-off cycle of actuation is shown in Figures 6.2c and 6.2d.

Electrochemical deposition of dendritic metal fibers is known to occur at rather low electrolytic concentrations, where the reaction is diffusion controlled.[20] This occurs via preferential growth at the tip in comparison to stunted growth across

the length of the fiber due to kinetic factors. Thus, the fibers grow longer and assume dendritic structures at the cost of thickness of the deposited structures. Under these conditions the length of the growing fiber would act as a polarizable electrode where changes in interfacial tension, γ, is related to the changes in applied potential and to changes in solution composition[13, 20] and is governed by

$$d\gamma = -q_M dV - \frac{q_M}{z_j F} d\mu_j - \sum \Gamma_i d\mu_i \qquad (6.1)$$

where, $d\gamma$ is the differential interfacial tension at the polarizable electrode;

q_M is the charge density on the electrode given by,

$$q_M = \frac{\varepsilon}{4\pi d} V; \qquad (6.1a)$$

dV is the differential applied voltage

μ_j is the chemical potential of species j which are released at the electrodes

z_j is the charge on the species j

$d\mu_i$ is the chemical potential of species i which react on the unpolarizable electrode(s),

Γ_i is the surface excess of i^{th} species; $\Gamma_i = \frac{c_i}{A} - \frac{c_i^o}{A}$, c_i^o is bulk concentration of i, c_i is concentration of species i at the electrode and A is the cross sectional area of the electrode.

At constant composition, the second and third terms assume null values. Hence, equation (6.1) yields

$$d\gamma = -q_M dV \qquad (6.2)$$

Which is the Lippmann equation[20].

The solution leads to

$$\gamma = \gamma_{max} - \left(\frac{\varepsilon}{8\pi d} V^2\right) \qquad (6.2a)$$

where, $d = \chi^{-1}$ is the Debye separation of double layer for a plane electrode, at 25^0C,

$$\chi^{-1} = \sqrt{\frac{\varepsilon kT}{8\pi e_0^2 \sum n_i z_i^2}}$$

For 10^{-4} M $CuCl_2$ solution, χ^{-1} = 13.1 nm

10^{-6} M $CuCl_2$ solution, χ^{-1} = 131 nm

10^{-8} M $CuCl_2$ solution, χ^{-1} = 1310 nm

V = applied potential difference

ε = permittivity of bulk water = 6.9×10^{-10} C^2/Nm^2

or permittivity of structured water (at the electrode-electrolyte interface)[20]

= 5.31×10^{-11} C^2/Nm^2

γ_{max} for Cu = 0.03 N/m and is the potential when γ for copper electrode is maximum.

Thus $\Delta\gamma = \gamma - \gamma_{max} = -\left(\frac{\varepsilon}{8\pi d} V^2\right)$ (6.2b)

Thus the applied electrical potential would lead to changes in the interfacial tension which in turn would produce actuation of the fibers as explained below.

Actuation of the fiber could possibly be understood to occur in a manner similar to the wetting and de-wetting characteristics of a drop of liquid on a flat substrate surface. The drop spreads or recoils to minimize the surface free energy as governed by surface tension of the liquid drop, the surface tension of the substrate surface and the interfacial tension between the liquid and the substrate surface. In a

similar fashion when a microscopic fiber is subjected to different interfacial stresses the result will be the actuation of the fiber as it cannot move, being bound to the surface of the electrode.

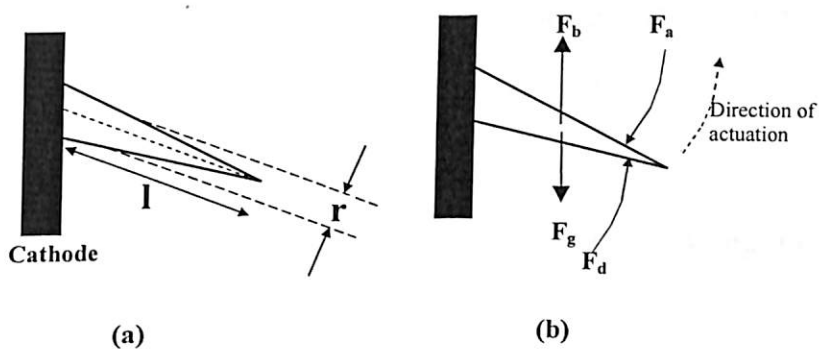

Figure 6.3 (**a**) A cone shaped nanofiber suspended at one of its end from the cathode of an electrochemical cell. (**b**) Qualitative representation of the forces acting on the fiber. F_b is the buoyancy force, F_g the gravitational force, F_d is the viscous drag force and F_a is the force required for actuation.

A model calculation shown below indicates that, when a small fiber attached to an electrode (in the present case Cu fiber on the cathode) is subjected to an applied voltage, in order to minimize the interfacial tension across the electrified interface the fiber will actuate and will tend to remain perpendicular to the electrode at a relatively high voltage. The extent of deflection would depend on the magnitude of the applied voltage, bulk solution ionic strength of an electrolyte and concentration of depositing species and shape and size of the fiber. However, this can happen only if the cations (in the present case) get continuously deposited at the tip of the fiber, while a kinetic barrier prevents the growth across the length of the fiber thus creating the situation of a polarizable electrode. For simplicity of calculation and to be in line with the above argument we consider the fiber to be conical in shape, with the base diameter fixed at

100 nm and the length at 1 cm. The fiber is considered to be made up of Cu metal deposited at the cathode from an aqueous solution of $CuCl_2$ and the copper anode. A pictorial representation of the fiber is shown in Figure 6.3a. The forces acting on the fiber are represented qualitatively in Figure 6.3b.

In order to have a typical result the following assumptions are made

the conical fiber, l = 1cm, and its base radius, r = 100 nm,

$\rho_{Cu} = 8230$ kg m^{-3} (same as that of bulk copper)

The fiber is polarizable along its length with deposition occurring at the tip only.

Gravitational force:

$$F_g = \pi r^2 l \rho_{Cu} \times 9.81 = 2.54 \times 10^{-11} N$$

Buoyancy force:

$$F_b = \pi r^2 l \rho_{H_2O} \times 9.81 = 3.08 \times 10^{-12} N$$

The viscous drag force acting on fiber during its movement is (using Stokes equation)

$$F = 3\pi\eta U d_e \kappa$$

where, κ = convection factor for a fiber of uniform cross section = 1.25 to 1.5

$$\eta_{H_2O} = 8.905 \times 10^{-2} Nm^{-2} s$$

$$d_e = \text{effective diameter} = \left(\frac{6}{\pi} \times \text{volume of fibre}\right)^{-\frac{1}{3}}$$

For the present fiber, $d_e = \left(\frac{6}{\pi} \times \pi\left(100 \times 10^{-9}\right)^2 \times 0.01\right)^{-\frac{1}{3}} = 8.4 \times 10^{-6} m$

The measured angular velocity of the fiber,

$$U = r\frac{d\theta}{dt} = 5.07 \times 10^{-4} m/s \text{ (Table 6.2)}$$

Table 6.2 Angular actuation velocity of a typical fiber

Concentration of electrolyte (M)	Applied voltage (V)	Length of the fiber (mm)	Angular deflection (degree)	Time required for the deflection (s)	Angular Velocity (m/s)
1.03×10^{-4}	6	5.0	45	7.0	5.61×10^{-4}
1.03×10^{-4}	6	5.0	45	7.5	5.23×10^{-4}
1.03×10^{-4}	6	5.0	45	9.0	4.36×10^{-4}
Mean angular velocity:					5.07×10^{-4} m/s

$\therefore F_d = 3.57 \times 10^{-9}$ N (when $\kappa = 1.25$)

At a constant composition of 1.0×10^{-4} M $CuCl_2$, the Debye length d = 13.1 nm and at an applied potential of V = 6.0 volts equation (6.2b) provides

$\Delta\gamma = 7.54 \times 10^{-2}$ N/m for bulk water; $\Delta\gamma = 5.80 \times 10^{-3}$ N/m for structured water

The force due to interfacial tension at the polarizable electrode = Electrocapillary force = Actuation force = F_a

$\therefore F_a = \Delta\gamma \times (\text{half circumference}) = \Delta\gamma \times \pi r$

where r is the radius of the fiber base.

$\therefore F_a = 0.0754 \times \pi r = 2.37 \times 10^{-8} N$, for bulk water

and $F_a = 1.82 \times 10^{-9} N$, for structured water.

From the above calculation of forces F_d, F_g and F_b, acting on the actuating fiber, it is imperatively clear that buoyancy and gravity forces are insignificant as compared to

the drag force. Moreover, coulombic interaction between two fibers, which are separated in the present case by millimeters, is too small (on the order of 10^{-17} N)[21] to make a meaningful contribution to actuation and hence discounted in the discussion altogether. Also, the magnitude of actuation force is on the order of the dominant drag force, and hence the actuation of fiber occurs due to interfacial tension at the polarizable electrode.

Further, we show here that actuation can be upwards or downwards depending on the original direction of orientation of the fiber during growth. Consider two orientations of the fiber in Figures 6.4a (initially pointing downward) and 6.4b (initially pointing upward). The fiber shown in Figure 6.4a would ideally remain attached to the cathode such that axis of the fiber (dotted line) is directed down along the cathode, i.e. $\theta_1 = 0^0$ when the applied voltage V = 0. When this fiber is actuated, it moves upward under the application of external voltage i.e. $\theta_1 > 0^0$ when V > 0. On the other hand the fiber shown in Figure 6.4b would ideally remain attached to the cathode such that axis of the fiber (dotted line) is directed up along the cathode, i.e. $\theta_1 = 0^0$ when the applied voltage V = 0. And the fiber would actuate and move downward under the application of external voltage i.e. $\theta_1 > 0^0$ when V > 0. The corresponding vector (force) diagrams are schematically shown in Figures 6.4c – 6.4f. The relation between interfacial tension (γ) and contact angle (θ) for the electrified interface formed by the fiber and the surrounding fluid layer is

$$\gamma = \frac{rhg\Delta\rho}{2\cos\theta} \qquad (6.3)$$

where, r = radius, h= height of fluid, $\Delta\rho$ = difference of densities between the copper fiber and the fluid forming the electrified interface, and g is the gravitational acceleration.

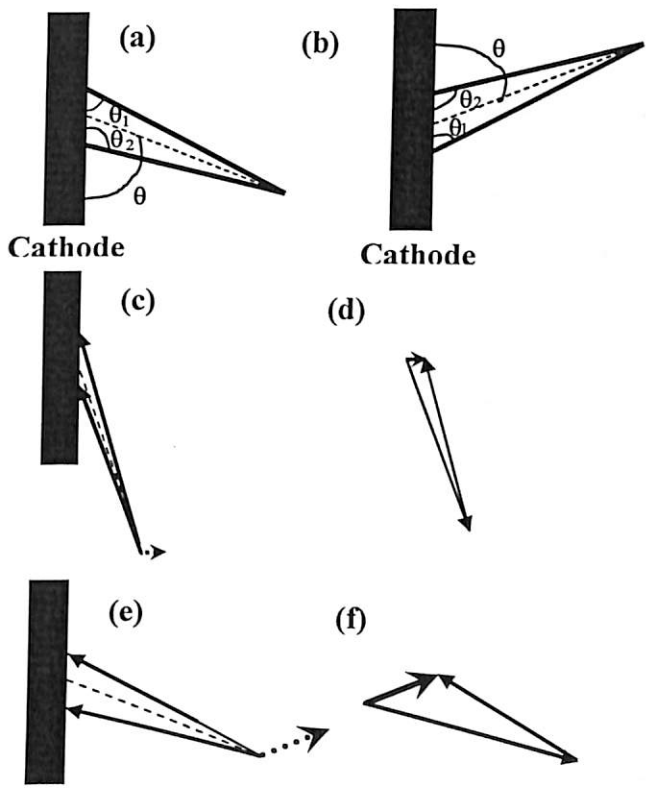

Figure 6.4 A schematic illustration of the orientation of fibers (**a** and **b**) with angles relative to the cathode. Schematic illustrations of the direction of actuation of fibers with corresponding vector diagrams (**c**, **d**, **e**, **f**).

In the present system assuming growth is slower than actuation, r, h, $\Delta\rho$ and g can be set constant, and hence, $\gamma \propto \frac{1}{Cos\theta}$

In both cases shown in Figure 3, $\theta_2 > \theta_1$, on two sides of the conical fiber such that average angle θ of actuation of the filament is:

$$\theta = \left(\frac{180^o + \theta_1 - \theta_2)}{2} \right)$$

In absence of an applied field the net actuation force is zero. This means the summation of γ_1 and γ_2 is equal to 0. This is possible when the fiber is relaxed, i.e. $\theta_1 = 0°$ and $\theta_2 = 180°$. So, $\gamma_1 = (rhg\Delta\rho/2)$ and $\gamma_2 = -(rhg\Delta\rho/2)$ and thus the resultant force $F_1+F_2 = 0$, cannot move the fiber away from main electrode. Thus the fiber remains relaxed.

On the other hand under the application of a potential the net force is non-zero and the actuation of fiber occurs, which is possible if $\Delta\gamma$ is non-zero when voltage is applied. When actuation occurs, then $\theta > 0°$, $\Delta\gamma$ is negative and the resultant force is in the direction of actuation, as explained with an example below:

Consider that $\theta_1 = 60^0$ and $\theta_2 = 110^0$, then $\theta = 65^0$ with the filament sloping downwards (Figure 4a). Then $\gamma_1 = 2.00$ x $(rhg\Delta\rho/2)$; $\gamma_2 = -2.92$ x $(rhg\Delta\rho/2)$ and R, the resultant force lifts the fiber during actuation (Figures 6.4e and 6.4f).

Similar arguments can be extended to a fiber which is originally directed upwards (Figure 4b) and it can be shown in that case also the fiber actuates in the direction of increasing θ. This is because in both cases we are assuming that the fiber has two half surfaces: lower and upper. Because of the symmetry of a fiber, the maximum actuation for any fiber occurs when the surface tension (hence contact angle) above and below the fiber are equal, i.e. 90°. During actuation more of the surface is

exposed (similar to spreading of the drop on a flat substrate due to the favoring of interfacial tension in the system). The copper metal is not a fluid, but is composed of assemblies of nanoparticles so it responds to this electrocapillary induced stress by actuation of the fiber at various possible junctions. When the voltage is turned off, $\gamma \approx \gamma_{max} \approx 0$ (for Cu) and hence the actuation force is zero and the fiber relaxes. However, when voltage is applied, then $\gamma < \gamma_{max}$ and fiber actuate as explained above.

The above model presents a simple yet realistic account for the actuation of a fiber by taking into account the driving and opposing forces of actuation. Additionally, the actuation of the branched dendritic structure observed in our study could be explained by the same model, whereby a fiber is attached in a branched fashion to the main fiber. The branched fiber actuates on the main fiber, in just the same way as the main fiber actuates on the cathode, upon the application of voltage. Further, the calculation of drag force for a branched fiber would be more involved. One can also extend the argument to the whole length of a long and flexible fiber by considering that it is composed of multiple small fibers of increasingly thinner average cross section from its base to its tip. The approximations involved are that the fibers are all of identical shapes and sizes. It is to be noted that the conical shape used in our model is a representative shape and is chosen just to demonstrate the various forces acting on the fiber. Similar conclusions can be obtained by choosing a differently shaped fiber as long as the fiber is polarizable along its length. Further, for simplifying the model formulation, interaction between the adjacent fibers is neglected and it is assumed that there is no growth of fiber during the measurement of actuation.

Does the total surface area of the fibre change during activation?

Factors affecting the actuation of fibers

We have studied in detail the dependence of actuation on various factors such voltage, concentration of electrolyte, concentration of other ions, etc. These are reported below.

Extent of deflection versus applied voltage

It was observed experimentally that the extent of deflection increased with applied voltage. The results in Figure 6.5 demonstrate such a trend for a single dendritic fiber of 2.0 mm length, initially grown at 12.0 V in a 1.0 x 10^{-4} M $CuCl_2$ electrolytic solution and then subjected to various applied voltages. Unfortunately, a relation between the angle of actuation and $d\gamma$ is not straightforward and depends on the exact growth conditions due to the reasons explained in preceding paragraphs. However, our results in Figure 6.5 are consistent with the Lippmann equation (equation 6.2). The plot of $1/\text{Cos}\theta$ is found to be proportional to the square of applied voltage (V^2), where θ is the experimentally observed angle of actuation, consistent with that predicted by Lippmann equation.

Parabolic ?

Validation of Lippmann Equation

The angle of actuation is dependent on the applied voltage, characteristic dimensions of the growing fiber and some other factors. The experimental results presented in Figure 6.5 are consistent with electrocapillary forces governed by Lippman equation as shown below.

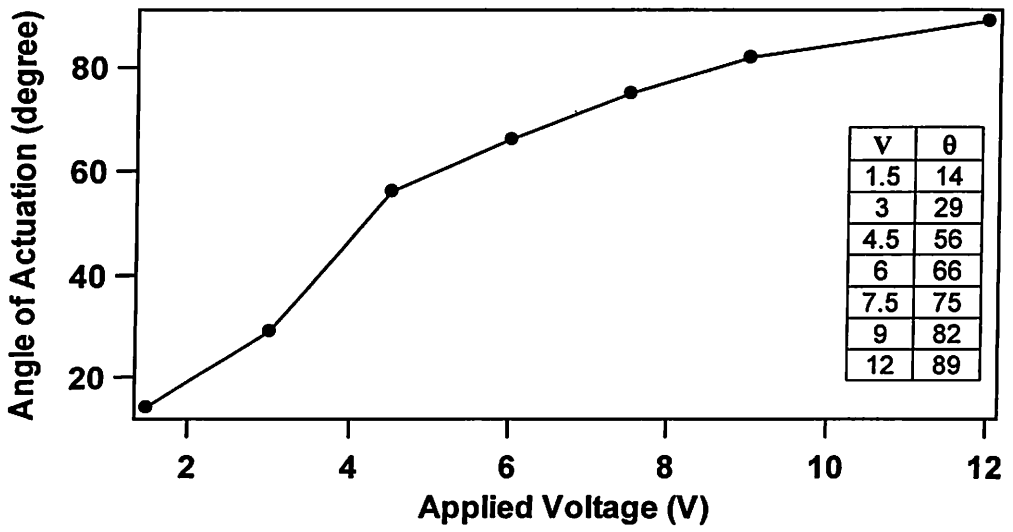

Figure 6.5 Plot of angle of actuation verses applied voltage. The applied voltages and the corresponding θ values are in the table (inset).

The change in interfacial tension across the electrified interface of the fibre is given by Lippman equation as,

$$\Delta\gamma = -\left(\frac{\varepsilon}{8\pi d}V^2\right) \qquad (6.4a)$$

$$\Delta\gamma = \gamma - \gamma_{max} \qquad (6.4b)$$

The relation between interfacial tension (γ) and contact angle (θ) for the electrified interface formed by the fiber and the surrounding fluid layer is

$$\gamma = \frac{rhg\Delta\rho}{2Cos\theta} \qquad (6.4c)$$

Is angle of actuation true contact angle ?

From above equations, γ is inversely proportional to $Cos\theta$ within limits of small actuation angle. Also, γ is proportional to V^2. Hence, $1/Cos\theta$ should vary linearly with V^2.

From the data given in Figure 6.5 we have,

Applied Voltage (V)	Angle of actuation θ *(rad)*	$Cos\theta$	$1/Cos\theta$
1.5	0.24	0.97	1.03
3.0	0.51	0.87	1.14
4.5	0.98	0.56	1.79
6.0	1.15	0.41	2.46
7.5	1.31	0.26	3.87

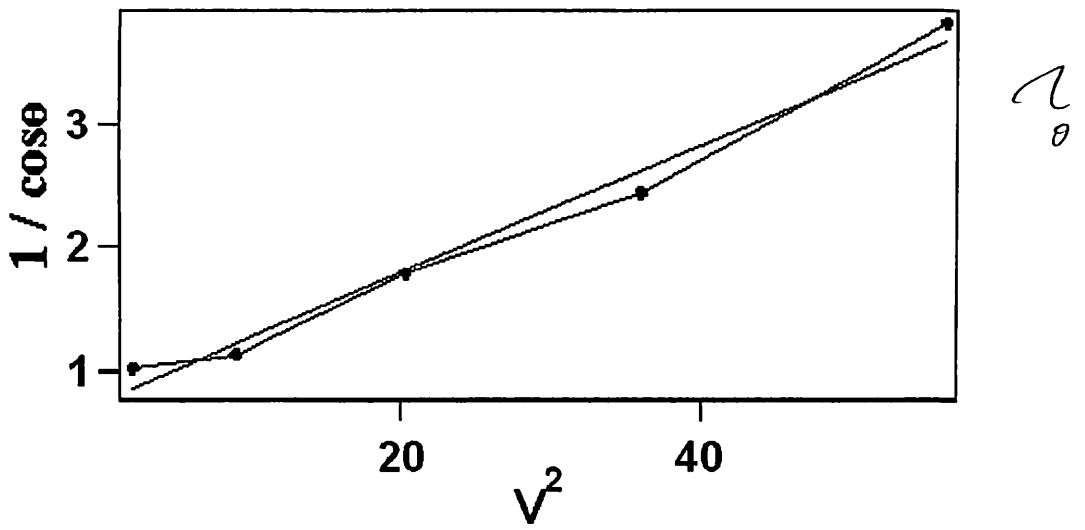

Figure 6.6 Variation of $1/Cos\theta$ with V^2.

Figure 6.6 demonstrates that $1/Cos\theta$ varied linearly with V^2 and hence consistent with Lippman equation within limits of small actuation angle.

Extent of actuation at a constant voltage versus concentration of $CuCl_2$

We found that the final actuation angle was higher when the concentration of $CuCl_2$ electrolyte was higher (Table 6.3). When 2.0 mm dendritic structures were grown at a $CuCl_2$ concentration of 5.00×10^{-5} M then an actuation of 90^0 could be observed at an applied voltage of 12.0 V. After this when the voltage was stepped down to 6 V the angle of actuation reduced to 14°. Upon gradual addition of a concentrated solution of $CuCl_2$ to the actuated system, the angle of actuation increased gradually and reached a value of 90^0 at a final concentration of 5.08×10^{-5} M of $CuCl_2$. The maximum actuation angle is as always 90°. For example, when a much higher concentration of $CuCl_2$ solution was used (1.00×10^{-4} M) at an applied voltage of 6.0 V

the angular deflection was still 90^0. Similar results were obtained when $CuSO_4$ was used as the electrolytic medium instead of $CuCl_2$.

When $CuCl_2$ is added at constant applied voltage, the condition of electro-neutrality reduces equation 1 to:[16]

$$d\gamma = -\Gamma_{-}\, d\mu \qquad (6.5)$$

Where Γ_{-} is surface excess of anions at the anode and $d\mu$ is the chemical potential change of the electrolyte. At higher $CuCl_2$ concentrations $d\mu$ is more positive as compared to when concentration of $CuCl_2$ is lower. Hence addition of $CuCl_2$ makes $d\gamma$ more negative. As a result, more actuation is observed with increasing concentration of $CuCl_2$ at constant applied voltage.

Unfortunately in this experiment, a relation between the angle of actuation and $d\gamma$ is not straightforward and depends on the exact growth of the fiber. There are additional issues, such as the extent of polarizability of the surface of the fibers and the rate of growth of the fiber tips, which need to be taken into account to quantify the effect. However, the above results could still be explained qualitatively within the limits of Lippman equation.

Table 6.3 Cu^{2+} concentration dependent actuation of the fiber

Concentration of $CuCl_2$ (M)	Applied voltage (V)	Angle of deflection (degree)
5.00×10^{-5}	6.0	14
5.02×10^{-5}	6.0	17
5.04×10^{-5}	6.0	56
5.06×10^{-5}	6.0	63
5.08×10^{-5}	6.0	90

Observed variation of concentration of Cu^{2+} ions in the solution as a function of time of electrodeposition

Concentration of Cu^{2+} was monitored by measuring the optical density of the copper ammine complex at 605 nm after addition of ammonia to a part of the electrolytic solution. The concentration of copper ion reduced with the time allowed for electrodeposition of the copper dendritic structures (Table 6.4 and Figure 6.7). When milli-Q water and no additional salt was used as the electrolyte along with copper anode, then the concentration of Cu^{2+} reached a steady state value of ~ 6.60×10^{-5} M

(after 50 min. of deposition at 12.0 V), which is close to the limiting concentration of 8.18×10^{-5} M achieved after a 134 min of deposition using $CuCl_2$ (Table 6.4).

Table 6.4 Tabulated data of concentration of Cu^{2+} with deposition time.

Time (min)	Concentration of Cu^{2+} (M)
0	4.21×10^{-4}
5	4.28×10^{-4}
10	3.82×10^{-4}
15	3.91×10^{-4}
20	3.49×10^{-4}
25	2.85×10^{-4}
30	3.12×10^{-4}
134	8.18×10^{-5}

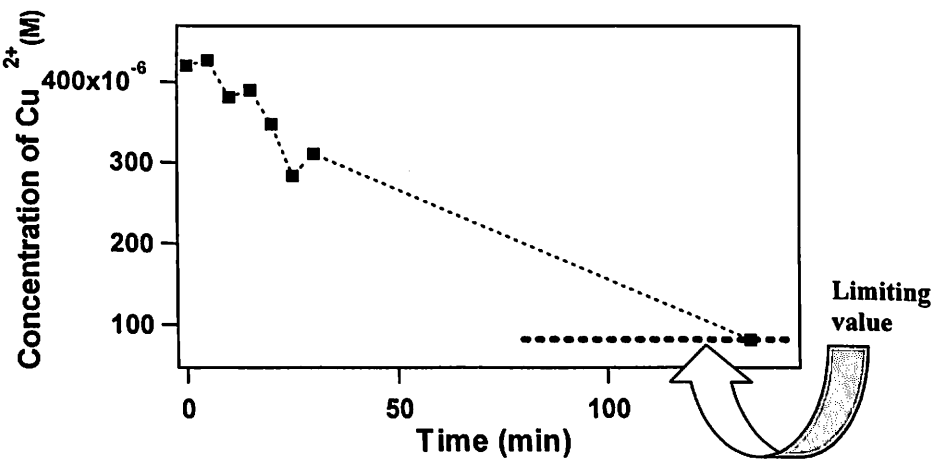

Figure 6.7 Graphical plot showing the approach to a steady state concentration of Cu^{2+}

The effect of addition of NaCl on the extent of actuation of fiber

We are also interested in finding the effect of ionic strength on the actuation of the fiber. When a few drops of concentrated NaCl was added to a growing and actuated (with 90^0 deflection) copper fiber electrolytic system (with 1.0 x 10^{-4} M $CuCl_2$ electrolytic solution and grown at 12.0 V till fibers were 1.5 mm long) the maximum angle of actuation dropped (Table 6.5). Similar results were obtained if Na_2SO_4 was added instead of NaCl.

Table 6.5 Effect of NaCl on the actuation of the fiber

Concentration of NaCl (M)	Applied voltage (V)	Angle of deflection (degree)
0	12 V	90
5.0 x 10^{-5} M	12 V	21
1.0 x 10^{-4} M	12 V	0

The decrease in actuation of fibers on addition of NaCl can be rationalized on the basis of ionic strength effects. Addition of a nonreactive salt at constant applied voltage implies that equation 1 simplifies to

$$d\gamma = -\frac{q_M}{z_j F} d\mu_j \qquad (6.6)$$

where, $z_j = +2$ for Cu^{2+} ions.

Initially the system is at a steady state with constant applied voltage V, prior to the addition of NaCl. So the composition is fixed and as per equation 6.1, $d\gamma$ is constant and the fiber remains actuated at a constant angle. The presence of additional non-reactive ions (NaCl or Na_2SO_4) increases the ionic strength (I) of the solution thus making $d\mu_{Cu^{2+}}$ more negative in equation 6.5. This leads to more positive $d\gamma$ and reduction of the net actuation force in presence of NaCl. Higher the concentration of NaCl lesser the actuation. Thus the observed results could again be explained within the limits of electrocapillarity.

Effect of anode material on growth of dendritic structure of copper nanofiber

We found that when the anode was made of metals other than copper, dendritic copper did not grow on the cathode, even when the electrolyte was a copper salt. Also, if after growing a copper fiber using copper anode we replaced the anode with any other metal, such as Ag or stainless steel; we found that the growth as well as the actuation stopped. This observation is important and suggests that the origin of actuation is not due to the applied potential drop as such across the two electrodes. On the other hand the continuous growth of the fiber was observed to be a prerequisite for actuation.

Herein we have been able to demonstrate electrochemical actuation of growing dendritic mono and bimetallic fibers with nanoscale structures in aqueous solutions. We have been able to account for the actuation based on electrocapillary forces (Lippmann equation), produced by changes in interfacial tension at the

electrified interfaces. An externally applied potential induces a gradient in interfacial tension on two opposite sides of the fiber resulting into its actuation. The actuation of fibers could also be controlled by controlling the applied potential and the concentration of electrolytes. This work is expected to propel further research work in the field of micro and nano electromechanical systems.

Reference and Notes

1. D. J Beebe, J. S. Moore, J. M. Bauer, Q.Yu, R. H. Liu, C. Devadoss, B-H. Jo *Nature* **2000**, 404, 588.
2. T. F. Otero, M. T. Cortes *Sens. Actuators B* **2003**, B96, 152.
3. R. H. Baughman et al. *Science* **1999**, 284, 1340.
4. G. Gu, et al. *Nature Mater.* **2003**, 2, 316.
5. Drexler, K. E.. *Engines of Creation: The Coming Era of Nanotechnology*. Fourth Estate, 1990.
6. Ratner, M.; Ratner, D. *Nanotechnology: A Gentle Introduction To The Next Big Idea*; Pearson Education India, 2003, pp 1-12
7. G. Che, S. A. Miller, E. R. Fisher, C. R. Martin *Analytical Chemistry* **1999**, 71, 3187
8. Q. Pei, O. Inganas *Advanced Materials* **1992**, 4, 277.
9. E. Smela, O. Inganas, I. Lundstrom *Science* **1995**, 268, 1735.
10. W. F. Paxton, A. Sen, T. E Mallouk *Chemistry--A European Journal* **2005**, 11, 6462.
11. J. C .Meyer, M. Paillet, S. Roth *Science* **2005**, 309, 1539.
12. E. W. Jager, E. Smela, O. Inganas *Science* **2000**, 290, 1540.
13. B. M. Le, Y. Chen, C. Crozatier, Z. L. Zhang *Microelectronic Engineering* **2005**, 78-79, 93.
14. R. F. Ismagilov, A. Schwartz, N. Bowden, G. M. Whitesides *Angew. Chem. Int. Ed.* **2002**, 41, 652.
15. P. A. Smith, C. D. Nordquist, T. N. Jackson, T. S. Mayer, B. R. Martin, J. Mbindyo, T. E. Mallouk *Appl. Phys. Lett.* **2000**, 77, 1399.
16. Y. J. Yuan, M. K. Andrews, B. K. Marlow *Appl. Phys. Lett.* **2004**, 85, 130.

17. Y. Huang, X. Duan, Q. Wei, C. M. Lieber *Science* **2001**, 291, 630.

18. C. Cheng, R. K. Gonela, Q. Gu, D. T. Haynie *Nano Lett.* **2005**, 5, 175.

19. A. Parfenov, I. Gryczynski, J. Malicka, C. D. Geddes, J. R. Lakowicz *J. Phys. Chem. B* **2003**, 107, 8829.

20. J O'M Bockris, A. K. N. Reddy in *Modern Electrochemistry*, 1st Ed., Plenum Publishing Corporation, New York, **1973**, Vol. 2, Chap. 7, p.702.

$\varepsilon = K \times \varepsilon_o$, where, K is the dielectric constant of the medium; ε is the permittivity of the medium and ε_o is the permittivity of vacuum where (a) K = 78 for bulk water and K = 6 for structured water; J O'M Bockris, A. K. N. Reddy, *Modern Electrochemistry*, 1st Ed. (Plenum Publishing Corporation, New York, **1973**), Vol. **2**, Chap. 7, p.757. and (b) ε_o = 8.85419 x 10^{-12} $C^2N^{-1}m^{-2}$; P. Atkins, J. Paula, *Physical Chemistry*, 7th edition (Oxford University Press).

21. The electrolytic cell is considered as a parallel plate capacitor, where the cathode and anode are separated by a distance (d) of 2.0 cm and the two consecutive fibers (that actuate) on the cathode are 1.0 mm apart (R). Under an applied potential (V) of 6.0 V, the charge density on the cathode, $\sigma = \frac{\varepsilon V}{d}$, where ε = permittivity of the medium between the two plates (electrodes) that is of water here. If one considers the radius of the fiber to be 100 nm and length 1 cm, then the charge on a fiber $q = \sigma \times 3.14 \times 10^{-9} C$. The electrostatic force between the two consecutive fibers is then

$F = \frac{q^2}{4\pi\varepsilon R^2} = 4.87x10^{-17} N$, for bulk water and $F = 3.74 \times 10^{-18} N$ for structured water.